SEISMIC SLOPE STABILITY FOR LANDSLIDES

A DISSERTATION

Submitted in partial fulfilment of the

requirements for the award of the degree

of

MASTER OF TECHNOLOGY

in

EARTHQUAKE ENGINEERING

(With Specialization in Soil Dynamics)

By

ANIRUDDHA BHADURI

DEPARTMENT OF EARTHQUAKE ENGINEERING

INDIAN INSTITUTE OF TECHNOLOGY ROORKEE

ROORKEE – 247 667 (INDIA)

MAY, 2016

CANDIDATE'S DECLARATION

I, Aniruddha Bhaduri, hereby declare that the work which is being presented in this dissertation entitled, **"SEISMIC SLOPE STABILTY FOR LANDSLIDES"**, in the partial fulfilment of the requirements for the award of the degree of **MASTER OF TECHNOLOGY** in **EARTHQUAKE ENGINEERING**, with specialization in **SOIL DYNAMICS**, submitted in the Department of Earthquake Engineering, Indian Institute of Technology Roorkee, is an authentic record of my own work carried out for a period from July 2015 to May 2016, under the supervision of **Dr. B. K. Maheshwari**, Professor, Department of Earthquake Engineering, Indian Institute of Technology Roorkee.

Aniruddha Bhaduri
M. Tech. (IInd year) Soil Dynamics
Department of Earthquake Engineering
Indian Institute of Technology, Roorkee

Place: Roorkee
Date: 31-05-2016

CERTIFICATE

This is to certify that the above statement made by the candidate is correct to the best of my knowledge.

Dr. B. K. Maheshwari
Professor
Department of Earthquake Engineering
Indian Institute of Technology, Roorkee
Roorkee – 247667 (India)

Place: Roorkee
Date: 31-05-2016

ACKNOWLEDGEMENT

I would like to express my solemn acknowledgement and gratitude to my guide **Dr. B. K. Maheshwari,** Professor, Department of Earthquake Engineering, I.I.T Roorkee, for his careful attention and constant motivation throughout the work. I wish to convey my deep sense of regard to him for motivating me continuously in completing this dissertation work. His co-operation in scrutinizing the manuscript and providing me with his valuable suggestions are highly appreciated.

I want to express my sincere thanks to all the other faculty members of the department who have helped and motivated me, both directly and indirectly, in successful completion of my dissertation work. I also convey my thanks to all the non-teaching staffs of the department for extending their helping hands when I needed it.

I am extremely grateful to all of my friends and well-wishers for supporting me and helping me unconditionally. I feel short of words to express my profound sense of regards to some of my best friends, whose endless encouragement and motivation helped me a lot in accomplishing the work successfully.

I am immensely thankful to my parents without whom I could never have reached to this position. It is beyond my literary capability to express my gratitude to them. Their blessings, motivation and inspiration guide me in the path of my life.

I deeply acknowledge the financial assistance provided by MHRD, Govt. of India, during the entire period of my post-graduation study. Last but never the least, I would like to thank almighty god for making me capable enough to complete the dissertation successfully.

Date: 31-05-2016 ----------

Place: Roorkee **(Aniruddha Bhaduri)**

ABSTRACT

Landslides are one of the major contributors of natural hazards due to ground failure. It occurs due to failure of a slope. Triggering mechanisms like excessive rainfall, earthquake or some man made activities (like production blast etc.) can cause a marginally to moderately stable slope to become unstable. Considering the fact that slope stability is a major reason behind landslide, it is necessary to analyse the stability of a slope before suggesting some remedial measures. As because analysing the stability of a slope is a large scale problem, so numerical simulation is the best technique to get a deeper understanding about the nature and behaviour of a slope. Mainly two types of slopes are analysed in this work. Natural hill slopes and rock slopes.

Two natural hill slopes of Uttarakhand state of India, in Mussoorie and Nainital, are analysed with the help of Geostudio 2012 software products. Two types of analysis have been done. Limit equilibrium analysis and finite element stress-deformation analysis. In the limit equilibrium analysis, static and pseudostatic factor of safety values have been calculated by different methods and a comparative study is done between them. LEM based software SLOPE/W is used. The finite element stress-deformation analysis is done by using SIGMA/W and QUAKE/W software for the static and dynamic cases respectively. The results are presented in the form of stress and displacement contours.

In the analysis of rock slopes, discontinuities possess a major role in its stability. Here, three types of analysis of rock slopes have been done. Slope under gravity loading, under excess rainfall condition and under seismic loading. In each of the analysis, parametric studies are carried out by considering different joint orientations. As distinct element method (DEM) is the best numerical technique for analysing a fractured rock mass, two dimensional DEM based software UDEC (Universal Distinct Element Code) 4.0 is used for all the analysis. The results are obtained in the form of factor of safety, displacements and block rotation. It has been found that out of plane joints are vulnerable towards sliding failure while in-plane joints are prone to toppling failure.

LIST OF CONTENTS

Candidate's Declaration **i**

Acknowledgement **ii**

Abstract **iii**

List of Contents **iv**

List of Figures **vii**

List of Tables **xi**

1. Introduction **1-4**

1.1 Background 1

1.2 Objectives 2

1.3 Scope of Dissertation 3

1.4 Organisation of Dissertation 4

2. Literature Review **5-14**

2.1 General 5

2.2 Limit Equilibrium Method (LEM) 5

2.3 Finite Element Method (FEM) 8

2.4 Distinct Element Method (DEM) 9

2.4.1 Case Studies 10

2.4.2 Mathematical Formulation 11

2.4.3 Dynamic Analysis 13

2.4.4 Boundary Conditions 14

2.5 Probabilistic Methods 15

3. Analysis of Soil Slope **16-35**

3.1 General 16

3.2 Material Properties 16

3.2.1 Material Properties from Literature 16
3.2.2 Material Properties Adopted for Analysis 18
3.3 Numerical Modelling 19
3.3.1 Modelling of Mussoorie Slope 19
3.3.2 Modelling of Nainital Slope 20
3.4 Limit Equilibrium Analysis 21
3.4.1 Methodology 22
3.4.2 Results and Analysis 23
3.5 Finite Element Analysis 27
3.5.1 Mussoorie Slope Analysis 28
3.5.2 Nainital Slope Analysis 32
3.6 Concluding Remarks 35

4. Analysis of Rock Slope 36-76
4.1 General 36
4.2 Geology of Jointed Rock Slope 36
4.2.1 Orientations of Discontinuities 36
4.2.2 Failure Patterns 37
4.3 UDEC Modelling 40
4.3.1 Mohr-Coulomb Model 41
4.3.2 Elastic Isotropic Model 44
4.4 Problem Description 45
4.4.1 Out of Plane Joints 45
4.4.2 Into the Plane Joints 46
4.5 Static Gravity Analysis 46
4.5.1 Joints Dipping Out of Plane 47
4.5.2 Joints Dipping Into the Plane 50
4.5.3 Results and Discussions 50

4.6 Slope under Excessive Rainfall 51
4.6.1 Joints Dipping Out of Plane 52
4.6.2 Joints Dipping Into the Plane 55
4.6.3 Observations and Discussions 58
4.7 Slope under Seismic Loading 59
4.7.1 Formulation of Harmonic Excitation 59
4.7.2 Joints Dipping Out of Plane 60
4.7.3 Joints Dipping Into the Plane 65
4.7.4 Slope with Two Perpendicular Joints 72
4.8 Concluding Remarks 76

5. Summary and Conclusions 78-80
5.1 Summary 78
5.2 Conclusions 79
5.3 Recommendations for Future Work 80
References 81

LIST OF FIGURES

Fig No.	Title	Page No.
2.1	Calculation cycle of DEM	11
2.2	Types of dynamic loading and boundary conditions in UDEC	15
3.1	Geometrical design of Mussoorie slope	20
3.2	Geometrical design of Nainital slope	21
3.3	Factor of safety versus lambda plot	22
3.4 (a)	Slip surface of the Mussoorie slope for static case	25
3.4 (b)	Slip surface of the Mussoorie slope for pseudostatic case	25
3.5 (a)	Slip surface of the Nainital slope for static case	27
3.5 (b)	Slip surface of the Nainital slope for pseudostatic case	27
3.6 (a)	Static vertical stress contours of Mussoorie slope	28
3.6 (b)	Static horizontal stress contours of Mussoorie slope	28
3.7	Time history of Sikkim earthquake (2011) used for dynamic analysis	29
3.8 (a)	Dynamic vertical stress contours of Mussoorie slope	30
3.8 (b)	Dynamic horizontal stress contours of Mussoorie slope	30
3.9 (a)	Dynamic vertical displacement contours of Mussoorie slope	31
3.9 (b)	Dynamic horizontal displacement contours of Mussoorie slope	31
3.10 (a)	Static vertical stress contours of Nainital slope	32
3.10 (b)	Static horizontal stress contours of Nainital slope	32
3.11 (a)	Dynamic vertical stress contours of Nainital slope	33
3.11 (b)	Dynamic horizontal stress contours of Nainital slope	33
3.12 (a)	Dynamic vertical displacement contours of Nainital slope	34
3.12 (b)	Dynamic horizontal stress contours of Nainital slope	34
4.1	Dip inclinations of different faults	37
4.2	Plane failure	38

4.3	Non-circular failure	38
4.4	Wedge failure	39
4.5	Toppling failure	40
4.6	Mohr-Coulomb failure criteria in UDEC	42
4.7	Basic slope geometry	45
4.8	Slope with out of plane joint set	46
4.9	Slope with into the plane joint set	46
4.10	Plot of strain contours with velocity vectors for ψ_p of 35° out of plane	48
4.11	Plot of strain contours with velocity vectors for ψ_p of 60° out of plane	49
4.12	Plot of strain contours with velocity vectors for ψ_p of 75° out of plane	49
4.13	Plot of strain contours with velocity vectors for ψ_p of 70° into the plane	50
4.14	Plot of strain contours with velocity vectors for jfric of 38° out of plane	52
4.15	Plot of strain contours with velocity vectors for jfric of 34° out of plane	53
4.16	Plot of strain contours with velocity vectors for jfric of 32° out of plane	53
4.17	Plot of strain contours with velocity vectors for jfric of 30° out of plane	54
4.18	Plot of strain contours with velocity vectors for jfric of 38° into the plane	55
4.19	Plot of strain contours with velocity vectors for jfric of 32° into the plane	56

4.20	Plot of strain contours with velocity vectors for jfric of 28° into the plane	56
4.21	Plot of strain contours with velocity vectors for jfric of 24° into the plane	57
4.22	Input sinusoidal shear stress waveform at the base of model	60
4.23	Displacement plot at gravity loading for out of plane joints	61
4.24	Displacement plot after 1 sec of seismic loading with joints dipping out of plane	61
4.25	Displacement plot after 3 sec of seismic loading with joints dipping out of plane	62
4.26	Displacement plot after 5 sec of seismic loading with joints dipping out of plane	62
4.27	Displacement plot after 7 sec of seismic loading with joints dipping out of plane	63
4.28	Displacement plot after 9 sec of seismic loading with joints dipping out of plane	63
4.29	Displacement plot after 11 sec of seismic loading with joints dipping out of plane	64
4.30	Displacement plot after 11.26 sec of seismic loading with joints dipping out of plane	64
4.31	Displacement plot at gravity loading for into the plane joints	66
4.32	Displacement plot after 1 sec of seismic loading with joints dipping into the plane	66
4.33	Displacement plot after 3 sec of seismic loading with joints dipping into the plane	67
4.34	Displacement plot after 5 sec of seismic loading with joints dipping into the plane	67

4.35	Displacement plot after 7 sec of seismic loading with joints dipping into the plane	68
4.36	Displacement plot after 9 sec of seismic loading with joints dipping into the plane	68
4.37	Displacement plot after 11 sec of seismic loading with joints dipping into the plane	69
4.38	Displacement plot after 13 sec of seismic loading with joints dipping into the plane	69
4.39	Displacement comparison between two joint orientations	71
4.40	Block rotation comparison between two joint orientations	71
4.41	Displacement plot at gravity loading for two joint sets	72
4.42	Displacement plot after 1 sec of seismic loading for two joint sets	73
4.43	Displacement plot after 3 sec of seismic loading for two joint sets	73
4.44	Displacement plot after 5 sec of seismic loading for two joint sets	74
4.45	Displacement plot after 7 sec of seismic loading for two joint sets	74
4.46	Displacement plot after 7.772 sec of seismic loading for two joint sets	75

LIST OF TABLES

Table No.	Title	Page No.
3.1	Shear wave velocity ranges of different soils	16
3.2	Typical values of Poisson's ratio	17
3.3	Typical values of E_s	17
3.4	Typical values of τ_0	17
3.5	Typical values of ϕ	18
3.6	Typical values of ρ	18
3.7	Typical values of material properties adopted for modelling and analysis	18
3.8	Shear wave velocity ranges of soil types	19
3.9	Location of field test sites in Mussoorie	19
3.10	Location of field test sites in Nainital	21
3.11	Factor of safety results for Mussoorie slope	24
3.12	Factor of safety results for Nainital slope	26
3.13	Summary of Mussoorie slope results	31
3.14	Summary of Nainital slope results	34
4.1	Material properties	47
4.2	Results of static analysis	51
4.3	Slope under rainfall with out of plane joint	54
4.4	Slope under rainfall with into the plane joint	57
4.5	Seismic results for one joint set dipping 70° out of plane	65
4.6	Seismic results for one joint set dipping 70° into the plane	70
4.7	Results of seismic loading for two perpendicular joint sets	75

CHAPTER – 1

INTRODUCTION

1.1 Background

Landslide is one of the major forms of ground failures around the world. It is actually a type of mass movement which ranges from rockfalls to deep slope failures and debris flow. Though gravity acts as a primary driving force behind a landslide, there are other factors that contribute to trigger it. The main triggering forces that can cause a landslide are earthquake, heavy rainfall or some man-made activities like production blast.

Since as early as 1789 B.C., landslides have been documented throughout the world. It has been observed that landslides can cause as much or more damage than all other seismic hazards combined and thus, it turned out to be a serious threat to mankind. Besides the adverse direct effects like high death toll and damages of properties, it has also a huge impact on the social and economic aspect. Keeping in mind these adverse effects of landslides, it is of utmost importance to lessen the adversity by advising remedial measures. But before doing that, the primary requirement is to understand the stability of slope. Thus it is necessary to analyse a slope to find out its proximity towards failure.

Since it is well known that landslide occurs due to failure of slopes, thus from the landslide perspective, evaluation of stability of slopes is one of the most important works for a geotechnical engineer. As slope stability is a large scale problem, it is not practical to rely solely on the field and lab tests to get a proper understanding about the slope. Also it is not possible to examine the behaviour of a slope with change in parameters. These problems can be overcome by numerical techniques. In numerical modelling techniques, a slope can be modelled efficiently by incorporating all the major aspects of it which is expected to be present in the field. Further parametric studies can also be done to get a deeper understanding about the nature and behaviour of slope by changing important parameters.

Stability of a slope can be analysed mainly in terms of safety (i.e. calculating a factor of safety) and serviceability aspect (i.e. by doing the stress-deformation analysis).

Limit equilibrium method is mainly used for calculating factor of safety while strength reduction method can also determine factor of safety in finite element or distinct element approach though this method is also based upon limit analysis. In the stress-deformation analysis, mainly continuum, discontinuum and hybrid modelling is used. It is expected that the user should be familiar with the numerical methods well enough before using any software. This is because, as all the numerical techniques are very powerful tools, caution must be taken before applying it. Or else, the tools will provide misleading results. Also all the methods have certain special features which suits certain problems. So a particular method should be applied according to the requirements.

1.2 Objectives

The main objective of this study is to investigate stability of soil and rock slopes and to perform parametric studies under different loading environments to get a complete understanding about the slopes and there failure mechanisms. The major focus is on the stability of rock slope and the effects of discontinuities on its failure pattern. The major objectives of the dissertation are twofold.

1. In the analyses of soil slopes, two natural soil slopes are investigated, Mussoorie and Nainital slope. In each of these cases, both limit equilibrium and finite element analyses are done.

   a) In the limit equilibrium analyses, static and pseudostatic factor of safety values have been calculated by five different methods. These are ordinary method of slices, Bishop's method, Janbu's method, Morgenstern-Price method and Spencer's method. A comparative study has been performed between these methods for a proper understanding about the methods.

   b) In the finite element analyses, static and dynamic stress deformation analyses have been done for both the slopes. In this case, static and dynamic stress contours and dynamic displacement contours for the slopes are generated. Depending upon these contours, the behaviour of the slopes are investigated.
2. In the analyses of rock slopes, a rock slope of which the data are available in literature, is investigated under different joint orientations and also under different loading environments. Mainly two types of joints are considered. One set of joints dipping out of the plane of the slope and other dipping into the plane of the slopes.

The occurrence of different failure patterns (like planar failure, rotational sliding failure, wedge failure, toppling failure etc.) are investigated depending upon the orientations of joints. The behaviour of the slopes are investigated under three different loading environments. These are, gravity loading, slope under excessive rainfall and under seismic loading. In the seismic case, the behaviour of the slope having two perpendicular joint sets are also investigated.

1.3 Scope of Dissertation

The scope of the dissertation lies in fulfilling the objectives of the work. These are as follows.

1. a) Limit equilibrium method (LEM) based software SLOPE/W of GEOSTUDIO 2012, is used for calculating the static and pseudostactic factor of safety values for natural soil slopes. To make a conclusion about which of these methods is most appropriate, a comparison of these methods have been done by analysing the results.

   b) Two finite element method (FEM) based software of GEOSTUDIO 2012, SIGMA/W and QUAKE/W are used for doing stress deformation analysis of those slopes for the static and dynamic cases respectively.
2. For the analyses of rock slope distinct element method (DEM) based software UDEC 4.0 is used. As UDEC can model a discontinuous rock mass more efficiently than others, therefor it has been found to be more suitable for use. In the analyses, factor of safety values have been calculated under different joint alignment conditions for static gravity loading. For simulating rainfall conditions, factor of safety and shear displacements have been calculated for different joint friction angles under different joint alignments. Seismic conditions have been simulated for three different joint alignments for the rock slope. The maximum total displacement, maximum shear displacement and the block rotation are the parameters which have been investigated for every cases.

1.4 Organisation of Dissertation

The organisation of the dissertation work is given below:

1. This dissertation is divided into five chapters, this is the chapter containing the background of the work, scope and objectives of the dissertation and organisation of the report.
2. Chapter 2 represents the literature review regarding various methods for slope stability analysis.
3. Chapter 3 deals with the analysis of soil slope. GEOSTUDIO 2012 software product SLOPE/W is used for doing limit equilibrium analysis and FEM based software SIGMA/W and QUAKE/W have been used for doing static and dynamic stress-deformation analysis, respectively.
4. Chapter 4 deals with the analysis of rock slope by using UDEC 4.0 software. A 260 m high rock slope is analysed. Gravity analysis, rainfall condition and seismic loading has been considered. Effects of joint orientations on the stability of the slope for each loading condition is analysed.
5. Chapter 5 is the last chapter which contains summary and conclusions.

CHAPTER – 2

LITERATURE REVIEW

2.1 General

The evaluation of stability of a slope has begun since early in the 20th century. With time and with the advent of modern computers various forms of analysing techniques have been developed. In the deterministic approach, generally 3 parameters define the stability of a slope. Factor of safety is the most common of all. Limit Equilibrium method is the most common method to determine the factor of safety of a slope. Besides this, Shear Strength Reduction (SSR) also computes factor of safety. This method reduces the shear strength of the slip surface or failure envelope by the factor of safety term until the convergence of the solution. But the factor of safety term does not provide all the necessary information regarding a slope failure. It does not give us any idea about how much deformation is taking place or how much stress is generated in the slope. Therefore, Stress-deformation analysis is done to check this aspects of a slope. In today's time different numerical methods are extensively used for the doing stress deformation analysis of a slope. These methods can incorporate the complex boundary conditions and material properties which better represents the actual scenario of the field. FEM and DEM are the most popular methods under this category. Probabilistic methods are still in its early days of development. This chapter briefly describes these methods and also talks about the advantages and limitations with respect to each other.

2.2 Limit Equilibrium Method (LEM)

Limit equilibrium approach generally assess the shear stress generated along a failure surface and then compares it with the shear strength available for the stability of the slope. The factor of safety (FOS) value is nothing but the ratio of the shear strength to the shear stress for the slope. When the FOS value becomes greater than 1, the slope is considered to be stable, when it becomes equal to 1, the slope becomes critical and when it becomes less than 1, it is considered to be unstable.

The methods of determining the factor of safety values have been evolved since a very long time. Many researchers have modified the evaluation methods of determining the FOS. Some of those methods are ordinary or Felleinus (1936) method, Janbu's (1954) method, Bishop's method, Morgenstern-Price (1965) method, Spencer (1967) method. The major difference between these methods lies on what kind of interslice forces have been considered by each method. Depending upon this criteria, some method satisfies moment equilibrium, some satisfies force equilibrium and some methods satisfy both. According to this, two types of factor of safety values are calculated. FOS with respect to moment equilibrium (F_m) and with respect to force equilibrium (F_f). In SLOPE/W, all of these methods have been incorporated. Fredlund and Krahn (1977). A general formulation of the limit equilibrium method was proposed which encompasses all the compulsory elements of all the methods. Two general formulae of FOS has been proposed. One satisfies moment and other satisfies force equilibrium.

The factor of safety satisfying moment equilibrium is given below.

$$\boldsymbol{F_m} = \frac{\Sigma(c'\beta R+(N-u\beta)R\ tan\phi')}{\Sigma Wx-\Sigma Nf\pm\Sigma Dd} \tag{2.1}$$

The factor of safety satisfying force equilibrium is given below.

$$\boldsymbol{F_f} = \frac{\Sigma(c'\beta\ cos\alpha+(N-u\beta)tan\phi'\ cos\alpha)}{\Sigma N\ sin\alpha-\Sigma D\ cos\omega} \tag{2.2}$$

Where,

c' = effective cohesion

ϕ' = effective angle of internal friction

u = pore-water pressure

N = slice base normal force

W = slice weight

D = concentrated point load

$\beta, R, x, f, d, \omega$ = geometric parameters

α = inclination of slice base

The formulae mentioned above are for static case. For pseudostatic case, the effects of earthquake can be incorporated into the model by adding horizontal (F_h) and vertical (F_v) forces into the equations. The forces can be defined as follows:

$$\boldsymbol{F_h} = \frac{a_h W}{g} = k_h W \tag{2.3}$$

$$\boldsymbol{F_v} = \frac{a_v W}{g} = k_v W \tag{2.4}$$

Where,

a_h= pseudostatic acceleration in horizontal direction

a_v= pseudostatic acceleration in vertical direction

g = gravity constant

W = weight of the slice

The terms $'k'$ in the above equations are dimensionless terms as it represents the ratio of a/g. The horizontal pseudostatic force tends to reduce the factor of safety value as it increases the driving force. While the vertical pseudostatic force has less impact on the value of factor of safety.

The main advantage of LEM is that nowadays, a vast number of software are available based on this method. So it is quite easy for the user to use it. Also the FOS value can be found quite easily and for that, there is no need to go through some rigorous modelling practices. Again, the FOS value can provide us a rough estimate about the stability of a slope thus in today's time, LEM based analysis has become a routine process before going into any numerical analysis.

There are a number of limitations of LEM which should be addressed. The main disadvantage arises from the point that this method does not talk about strain-displacement compatibility of a slope. As a result, it provides us with no information about the instability mechanism of a slope. Moreover, the FOS value which it gives, is an overall FOS of the slope. The change in local FOS throughout the slope and the realistic stress distribution are missing here. This is because no LEM is designed on the basis of a stress-strain constitutive relationship. Because of this drawback, LEM sometimes produces unrealistic results.

As LEM cannot recognises a lot of serious issues about a slope failure that is why, instead of having an easier and user friendly approach, one cannot fully trust on the outcomes of this method. Thus numerical modelling techniques have emerged in the scenario. Various modelling techniques have been developed over the years depending upon different methods. These techniques can be broadly categorised as serviceability aspect. Finite element method (FEM), distinct element method (DEM) and probabilistic methods come under this category.

2.3 Finite Element Method (FEM)

Since the very inception, finite element method is considered to be a very powerful computational tool in engineering. The main advantage of this method is that it can simulate complex behaviour of a problem without simplifying it and produce more accurate results. The advantage of FEM over LEM is that it can satisfy the equilibrium condition in a local domain as well as in a global domain. While LEM only satisfies global moment or force equilibrium condition of the sliding mass in a slope. Also a number of linear and non-linear stress-strain constitutive laws are included in this method which can provide results about the generation of stress and displacements in a soil mass. These advantages makes it a better choice for a user over LEM.

In SIGMA/W, two dimensional plane strain and axisymmetric problems can be solved by finite element analysis. For a 2D plain strain problem, the software considers unit thickness for each element and provides the following FE equation for a particular time increment:

$$t\int_A [B]^T [C][B]dA\,\{a\} = bt\int_A < N >^T dA + pt\int_L < N >^T dL \qquad (2.5)$$

Where,

t = Constant element thickness,

$[B]$ = Strain-displacement matrix,

$[C]$ = Constitutive matrix,

$\{a\}$ = Column vector of nodal incremental x- and y- displacements,

$< N >$ = Row vector of interpolating functions,

A = Area along the boundary of an element,

b = Unit body force intensity,

p = incremental surface pressure,

L = Length of the element along boundary.

In short, the FE equation can be written as,

$$[K]\{a\} = \{F\} = \{F_b\} + \{F_s\} + \{F_n\} \qquad (2.6)$$

Where,

$[K]$ = Stiffness matrix,

$\{a\}$ = nodal incremental displacements,

$\{F\}$ = Total nodal incremental force,

$\{F_b\}$ = Incremental body force,

$\{F_s\}$ = Force due to surface boundary incremental pressures,

$\{F_n\}$ = Concentrated nodal incremental force.

If $\{\sigma\}$ is the stress vector and $\{\varepsilon\}$ is the strain vector, the relationship between them is given as follows:

$$\{\sigma\} = [C]\{\varepsilon\} \tag{2.7}$$

Where, $[C]$ is the constitutive matrix.

In QUAKE/W, the governing equation for the dynamic response is given by,

$$[M]\{\ddot{a}\} + [D]\{\dot{a}\} + [K]\{a\} = \{F\} \tag{2.8}$$

Where,

$[M]$ = Mass matrix,

$[D]$ = Damping matrix,

$[K]$ = Stiffness matrix,

$\{\ddot{a}\}$ = Nodal acceleration vector,

$\{\dot{a}\}$ = Nodal velocity vector,

$\{a\}$ = Nodal displacement vector.

Though the FEM have a vast advantage to model complex boundary conditions and effects of pore pressure, creep/deformation or dynamic loading, still it has got certain limitations. FEM cannot properly simulate of the effects of a highly jointed rock mass. Also if the number of discontinuities are larger, then the code may break down. Distinct Element Method is the most appropriate one to take care the effects of discontinuities and that is why, it is more appropriate to model a system having discontinuities.

2.4 Distinct Element Method (DEM)

Distinct element method is developed by Cundall (1971) and it is further modified by Cundall & Strak (1979), Walton et al. (1988) and other researchers for using it in different field of researches. It is a type of discontinuous analysis technique. The method developed by Cundall (1971) is generally a discontinuum approach which represents any section of a system as an assemblage of discrete blocks. The discontinuities present in the body is considered as interface elements between the blocks. The major advantage of this method is that it allows deformation of blocks and movement of blocks relative to each other. The basic characteristic of the

numerical modelling of a discontinuous system is that it represents two type of mechanical behaviours. 1) The behaviour of the discontinuities and 2) the behaviour of the solid material. This particular characteristic differentiates it from other numerical techniques. The use of distinct element method in jointed and fractured rock masses has been explored by many researchers. Universal Distinct Element Code (UDEC) was first developed by Cundall (1980) and Lemos et al. (1985) for the formulations of discontinuous rigid and deformable bodies. The mathematical formulation of the code is discussed in the section 2.4.2.

2.4.1 Case Studies

A number of case studies have been done about rockslides due to seismic activity or excessive rainfall. Some of them are presented below.

a) 700 m High Rock Slope in Norway (Bhasin and Kaynia., 2004): The static and dynamic stability analysis was done in a 700 m high rock slope in Western-Norway. The main objective of the study is to have some profound insights about the failure mechanism of the slope and to assess the volume of rock mass which is vulnerable to sliding in static and dynamic cases. Distinct element code UDEC is used for the simulation.

b) 178 m High Gotvand Dam in Iran (Noorzad et al., 2008): Gotvand dam is one of the largest dams in Iran. It has been observed that the right abutment of the dam has potentially unstable rock mass and is prone to failure under dynamic loading. Also the right abutment of the dam is consisted of a number of joint sets which can cause sliding failure of the dam under earthquake condition. In this case, the stability of rock mass subjected to dynamic loading has been simulated by using UDEC software.

c) Surabhi Resort Landslide in Mussoorie (Pal et al., 2012): Surabhi resort landslide has been an unstable slope which has caused landslide triggered due to excess rainfall in the past. The main objective of the study is to identify the most vulnerable part of the landslide and study the behaviour of it. The zone of detachment has found out to be the most unstable region of the slope and the assessment of the total volume of unstable mass has been identified. The study has been done by using UDEC software.

d) 100 m High Mahabaleshwar Road Cut Hill Slope (Kainthola et al., 2012): In this study, the analysis of a 100 m high hill slope has been analysed under both dry

and saturated condition. The analysis shows that the slope is marginally stable under dry condition whereas it fails under saturated condition. Distinct element software UDEC has been used in this case.

2.4.2 Mathematical Formulation

In DEM, the calculation is performed by alternate application of force-displacement law applied at all the contacts and Newton's second law of motion applied at all the blocks. Newton's second law provides the movement of the blocks resulting from known forces and then when the force-displacement law is applied, it determines the contact forces from the known displacements. If the blocks are deformable, then the displacements are calculated at the grid point of the triangular finite-strain elements and then from that displacement, the stress generated in the elements are calculated. The following figure describes the calculation cycle for DEM.

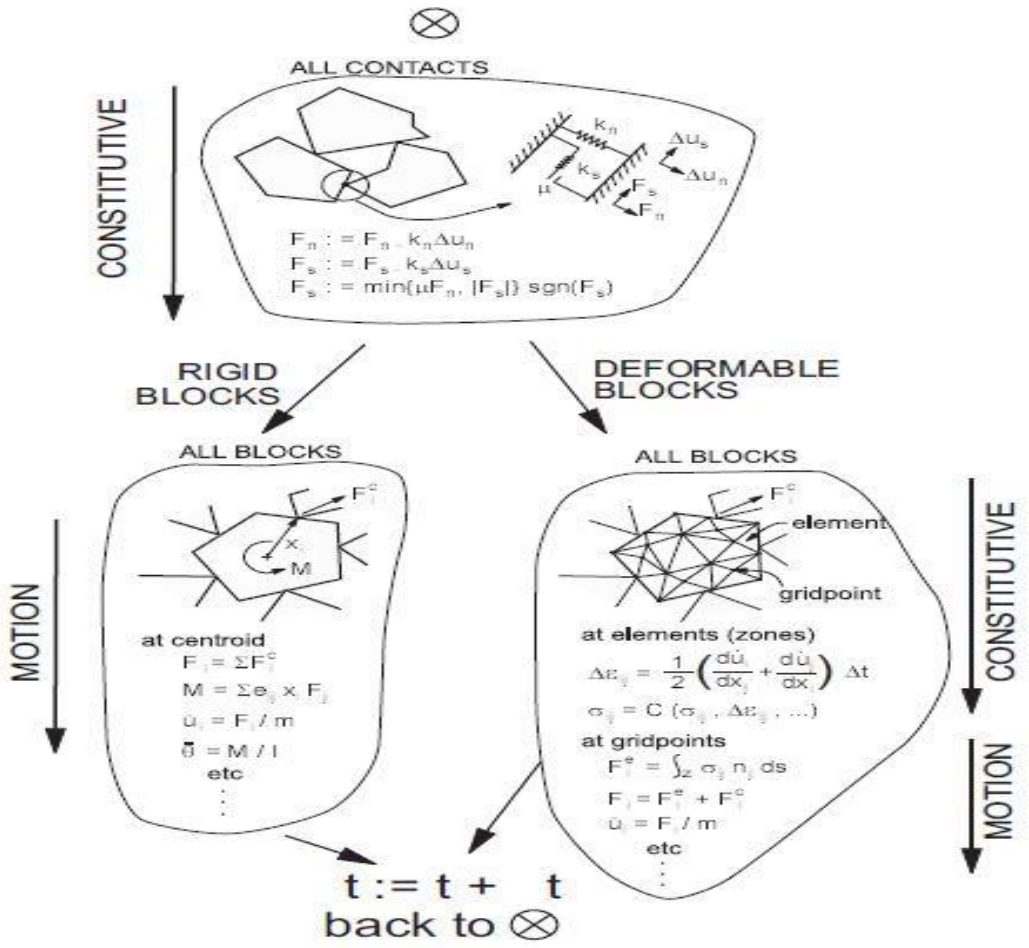

Fig 2.1 Calculation cycle of DEM

[Itasca C. G Inc., Universal Distinct Element Code (UDEC) User's Manual]

For rotation and translation, the equation of motion of the block can be written as,

$$m_{(x)}\ddot{x} = \boldsymbol{\Sigma} F_{(x)} \tag{2.9}$$

$$l_{(x)}\ddot{\theta} = \Sigma M_{(x)} \tag{2.10}$$

Where, $F_{(x)}$ is the unbalanced force on element x, $M_{(x)}$ is the resultant moment that is acting on element x, $m_{(x)}$ is the mass of the element, $l_{(x)}$ is the moment of inertia of the element, $\ddot{x}$ and $\ddot{\theta}$ are the linear and angular acceleration of the element. If we take the two accelerations constant over the time step Δt, by numerical integration, the above two equations leads to the following equations for velocities.

$$(\dot{x})_{(t+\frac{\Delta t}{2})} = (\dot{x})_{(t-\frac{\Delta t}{2})} + [\frac{\Sigma F_{(x)i}}{m_{(x)}}]_t \Delta t \tag{2.11}$$

$$(\dot{\theta})_{(t+\frac{\Delta t}{2})} = (\dot{\theta})_{(t-\frac{\Delta t}{2})} + [\frac{\Sigma M_{(x)}}{I_{(x)}}]_t \Delta t \tag{2.12}$$

If gravity forces has to be taken into account, then the equation modifies as follows,

$$(\dot{x}_i)_{(t+\frac{\Delta t}{2})} = (\dot{x}_i)_{(t-\frac{\Delta t}{2})} + [\frac{\Sigma F_{(x)i}}{m_{(x)}} + g_i]_t \Delta t \tag{2.13}$$

$$(\dot{\theta}_{(x)})_{(t+\frac{\Delta t}{2})} = (\dot{\theta}_{(x)})_{(t-\frac{\Delta t}{2})} + [\frac{\Sigma M_{(x)}}{I_{(x)}}]_t \Delta t \tag{2.14}$$

These values are then used to find the new displacements. This cycle is repeated for new time increments.

$$(x)_{(t+\frac{\Delta t}{2})} = (x)_{(t-\frac{\Delta t}{2})} + (\dot{x})_{(t+\frac{\Delta t}{2})} \Delta t \tag{2.15}$$

$$(\theta_{(x)})_{(t+\frac{\Delta t}{2})} = (\theta_{(x)})_{(t-\frac{\Delta t}{2})} + (\dot{\theta}_{(x)})_{(t+\frac{\Delta t}{2})} \Delta t \tag{2.16}$$

Force displacement law directly relates the normal forces to the amount of normal displacement like below,

$$(\Delta F_n) = k_n \Delta_n \tag{2.17}$$

$$(\Delta F_s) = k_s \Delta_s \tag{2.18}$$

Finally, at each time step the incremental forces are added into the sum of all the force increments F_n and F_s determined from the previous time step.

$$(F_n)_t = (F_n)_{t-\Delta t} + \Delta F_n \tag{2.19}$$

$$(F_s)_t = (F_s)_{t-\Delta t} + \Delta F_s \tag{2.20}$$

A coulomb-type friction law is incorporated as follows. The magnitude of the shear force found from the above equation which is checked against the maximum value which is defined as below,

$$(F_s)_{max} = F_n tan\phi_\mu + C \tag{2.21}$$

If $(F_s)_t$ is greater than the above maximum value, then $(F_s)_t$ is set equal to$(F_s)_{max}$. Now, for contacts no tension is permitted. Therefor normal force should be greater than zero i.e. F_n>0. When this condition is violated then joint opens and that contact is deleted and new contact is made.

For dynamic analysis, the equation of motion for block is written as,

$$m_{(x)}\ddot{x}_{i(t)} + C\dot{x}_{i(t)} = \Sigma F_{(x)i} + m_{(x)}g_i \tag{2.22}$$

Where, C is the viscous damping constant.

$$C = \alpha m_{(x)} \tag{2.23}$$

Solving the above two equations, we get,

$$(\dot{x})_{(t+\frac{\Delta t}{2})} = \{(\dot{x})_{\left(t-\frac{\Delta t}{2}\right)}P + \left[\frac{\Sigma F_{(x)i}}{m_{(x)}} + g_i\right]_t \Delta t\}R \tag{2.24}$$

Where,

$$P = [1 - \frac{C}{m_{(x)}}\frac{\Delta t}{2}]$$

$$R = \frac{1}{[1+\frac{C}{m_{(x)}}\frac{\Delta t}{2}]}$$

2.4.3 Dynamic Analysis

DEM is a powerful tool for modelling rock slope subjected to dynamic loading such as earthquake loading or blasting. There are three main components which consists of the dynamic model in DEM. They are: boundary conditions, mechanical damping and dynamic loading. Boundaries for the problem domain can be chosen to permit energy radiation and to limit reflection of outward propagating waves through the use of dashpot as viscous damping. To account for the natural damping of vibration energy and energy losses that exists in real system, mechanical damping (e.g. Rayleigh damping consisting of both mass and stiffness proportional component) is then added to the model. Lastly dynamic loading is added to the model in the form of an upward propagating stress wave originating from the bottom boundary of the model.

Here, in the dynamic analysis, we use the lumped mass matrix and diagonal mass matrix and the critical time step is calculated as,

$$\Delta t_\beta = \{\frac{2}{\omega_{max}}\}(\sqrt{1+\lambda^2} - \lambda) \tag{2.25}$$

$$\omega_{max} = \frac{2}{\Delta t_d} \tag{2.26}$$

$$\lambda = \frac{0.4\beta}{\Delta t_d} \tag{2.27}$$

$$\beta = \frac{\xi_{min}}{\omega_{min}} \tag{2.28}$$

Where, ω_{max} is the highest eigen frequency of the system and λ is the fraction of critical damping at this frequency.

ξ_{min} and ω_{min} are the damping fraction and angular frequency specified for Rayleigh damping and Δt_d is the time step for dynamic runs when no stiffness-proportional damping is used. The resulting value of Δt_β is used as dynamic time step if stiffness-proportional damping is in operation.

2.4.4 Boundary Conditions

In DEM, two types of boundary conditions are used for dynamic analysis. Viscous and free field boundary.

The viscous boundary is based on the use of independent dashpots attached to the model boundary in normal and shear directions which provides viscous normal tractions to cancel the reflected waves and given by,

$$t_n = -\rho c_p v_n \tag{2.29}$$

$$t_s = -\rho c_s v_s \tag{2.30}$$

Where, v_n and v_s are the normal and shear component of velocity at boundary, c_p and c_s are the P and S-wave velocities and ρ is the mass density.

The free field boundary is used to account for the free field motion which would exist in the absence of the structure. The lateral boundaries are coupled to the free field grid by the viscous dashpots to simulate a quite boundary and unbalanced forces from free field are applied to deformable block boundary at boundary grid points.

Dynamic input can also be applied for rigid block models in the form of velocity history. Velocity input cannot be applied along the viscous boundary. Thus dynamic input is applied to viscous boundary in the form of stress histories. The velocity histories can be converted to stress histories using the following formulae.

$$\sigma_n = -2(\rho c_p) v_n \tag{2.31}$$

$$\sigma_s = -2(\rho c_s) v_s \tag{2.32}$$

Where, σ_n and σ_s are applied normal and shear stress.

Fig. 2.2 simulates the different types of boundary conditions used in UDEC.

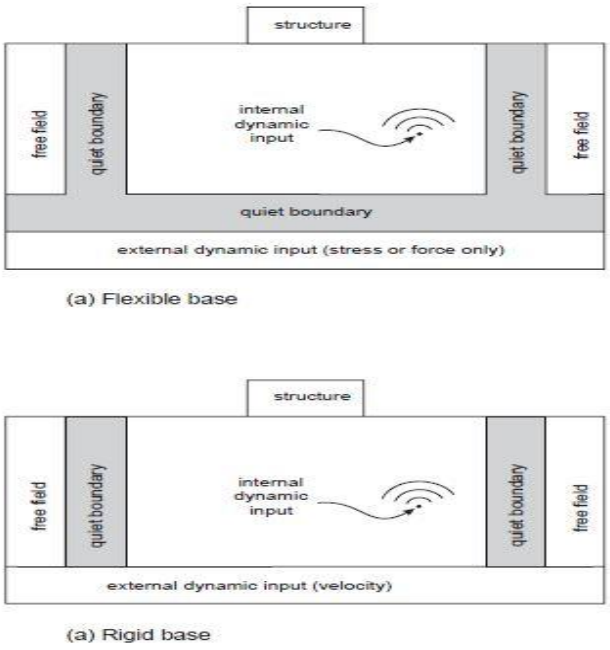

Fig 2.2 Types of dynamic loading and boundary conditions in UDEC
[Itasca C. G Inc., Universal Distinct Element Code (UDEC) User's Manual]

2.5 Probabilistic Methods

Over the years, a number of researchers have proposed a number of sliding displacement predictive models, to account for the uncertainties in the ground motions, in the displacement analysis, empirically. The magnitude of the sliding displacement is strongly affected by the characteristics of the earthquake ground motion (i.e. intensity, frequency content and duration). Thus a number of models have been proposed as a function of different ground motion parameters (e.g. PGA, Arias Intensity etc.) and site/slope parameters (e.g. Yield Acceleration, Site Period). Bray et al. (1998) model, Watson – Lamprey and Abrahamson (2006) model, Jibson (2007) model, Bray and Travasarou (2007) model, Rathje and Saygili (2009) model, Saygili and Rathje (2008) model are some examples of predictive displacement models. Kaynia et al. (2011) showcases how these models can be used in the probabilistic approach to determine the probable displacements. The Campania region in Italy has been studied in this paper. This region is selected due to its proximity towards the Irpania earthquake (1980). The usage of shakemaps and further development of slidemaps and how these maps can be used in landslide-risk assessment is noteworthy.

CHAPTER – 3

ANALYSIS OF SOIL SLOPE

3.1 General

This chapter deals with the modelling and analysis of two natural slopes in Uttarakhand namely Mussoorie and Nainital slopes. The modelling of the slopes have been done with the help of previously available soil profiling data. Two types of analysis have been carried out i.e., limit equilibrium analysis and stress-deformation analysis. SLOPE/W software has been used for the limit equilibrium analysis of the slopes while SIGMA/W and QUAKE/W software products have been used for the static and dynamic finite element stress-deformation analysis respectively.

3.2 Material Properties

For the analysis of a soil slope, the material properties and other parameters which are important are Poisson's ratio, modulus of elasticity and shear modulus. Further strength parameters can be represented in terms of cohesion and angle of internal friction.

3.2.1 Material Properties from Literature

1) Shear wave velocity (V_s)

Table 3.1: Shear wave velocity ranges of different soils (After Borcherdt 1994)

Description	Minimum velocity (m/s)	Average velocity (m/s)	Maximum velocity (m/s)
Hard rock	1400	1620	1840
Firm to hard rock	700	1050	1400
Gravel to firm rock	375	540	700
Sandy soil	200	290	375
Soft soil	100	150	200
Very soft soil	50	75	100

2) Poisson's ratio (μ)

Table 3.2: Typical values of Poisson's ratio (APPC appendix-C table C.4)

Type of soil	**μ**
Clay (Saturated)	0.4 – 0.5
Clay (Unsaturated)	0.1 – 0.3
Sandy clay	0.2 – 0.3
Sand (dense)	0.3 – 0.35
Rock	0.1 – 0.3

3) Modulus of Elasticity (E_S)

Table 3.3: Typical values of E_S (APPC appendix-C table C.2)

Type of soil	**E_S (MPa)**
Very soft clay	2-15
Soft clay	5-25
Medium clay	15-50
Hard clay	50-100
Sandy clay	25-250
Silty clay	7-21
Loose sand	10-24
Dense sand	48-81
Sand and Gravel	48-192
Shale	144-14400

4) Cohesive strength (τ_0)

Table 3.4: Typical values of τ_0 [Some useful numbers on the engineering properties of materials (Geologic and otherwise) GEOL 615]

Type of soil	**τ_0 (kPa)**
Rock	10,000
Silt	75
Very soft clay	0 – 48
Medium clay	96 – 192
Stiff clay	192 – 384
Very stiff clay	384-766

5) Angle of internal friction (ϕ)

Table 3.5: Typical values of ϕ [Some useful numbers on the engineering properties of materials (Geologic and otherwise) GEOL 615]

Type of soil	**Φ (degree)**
Rock	45
Clay	20
Loose sand	30 – 35
Medium sand	35 – 40
Dense sand	40 – 45
Gravel with some sand	34 – 48
Silt	26 - 35

6) Density (ρ)

Table 3.6: Typical values of ρ [Some useful numbers on the engineering properties of materials (Geologic and otherwise) GEOL 615]

Type of soil	**ρ (kg/m^3)**
Sandy soil	1800
Gravel soil	2000
Silty soil	2100
Clay soil	1900
Igneous rock	2700 - 3000
Metamorphic rock	2700

7) Shear Modulus (G)

$$\mathbf{G = \rho\, V_S^2} \tag{3.1}$$

Where,

ρ = Density of soil,

V_S = Shear wave velocity

3.2.2 Material Properties Adopted for Analysis

Table 3.7: Typical values of material properties adopted for Modelling and Analysis

Material Property	**c-ϕ soil**	**Sandy soil**	**Gravel**	**Bedrock**
Density (kg/m^3)	1850	1900	2000	2700
Cohesive strength (kPa)	40	0	200	10,000
Angle of internal friction (ϕ)	35	40	43	45
Modulus of elasticity (MPa)	20	70	150	500
Poisson's ratio (μ)	0.35	0.3	0.25	0.2
Shear Modulus (MPa)	7.41	26.92	60	208.33

3.3 Numerical Modelling

For modelling of the slopes, it is necessary to know the soil profiles of the region. First the work area is identified by locating the longitudes and latitudes of the area where field test need to be conducted. Second, the soil profile of the test area is carried out by conducting MASW (Multichannel Analysis of Surface Wave) test. The modelling of the Mussoorie and Nainital slopes has been done based on these soil profiles. The geometries of the slopes has been made with the help of GPS coordinates and cross sectional data available in the literature. Also it is to be noted that depending upon the shear wave velocity ranges, the depth of the soil layers is determined. The velocity ranges of each soil type, available in the literature, based on which the soil profiling is made is shown in Table 3.8.

Table 3.8: Shear wave velocity ranges of soil types (Hunter and Motezedian 2006)

Soil Type	Minimum V_S (m/s)	Maximum V_S (m/s)
c-ϕ Soil	100	180
Sandy Soil	150	360
Gravel	350	760
Rock	750	Inf.

3.3.1 Modelling of Mussoorie Slope

The location of the areas in Mussoorie, where MASW tests has been conducted are shown in Table 3.9. For the geometrical modelling, the depth of each soil layers has been taken based on the soil profiles of the sites A_1, A_2 and A_3 as discussed earlier and with the help of the ranges of the shear wave velocities of different soil types.

Table 3.9: Location of field test sites in Mussoorie (After Singh 2014)

	Latitude	Longitude	Elevation (m)	Milestone
Site A_1	N 30°27′27.1″	E 78°04′34.4″	2011	Dalmia house near ropeway, Mussoorie
Site A_2	N 30°27′36″	E 78°15′01″	1791	Ghananand school Mussoorie-Dehradun road
Site A_3	N 30°24′36″	E 78°04′12″	1181	Kolukhet villege Mussoorie-Dehradun road

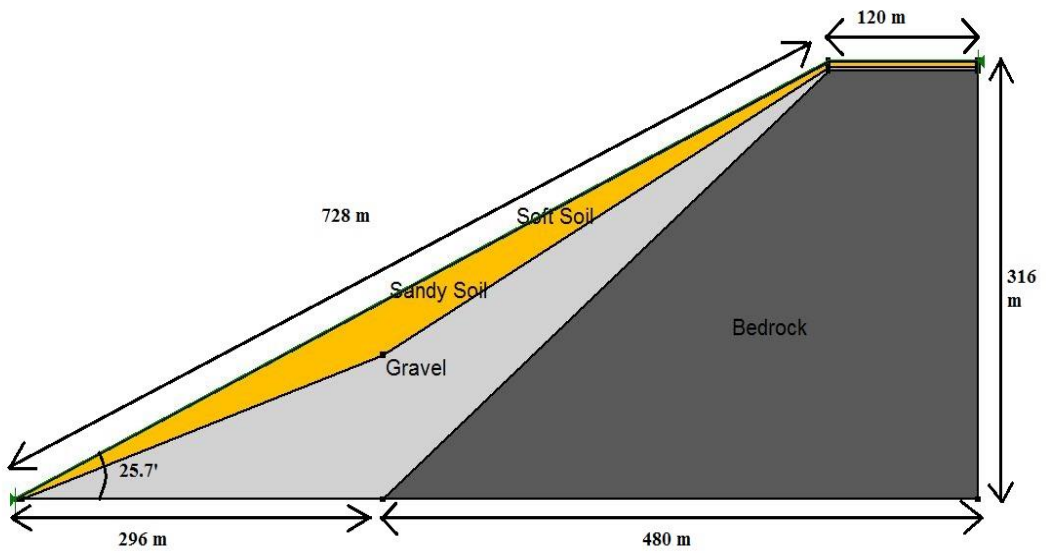

Fig. 3.1 Geometrical Design of Mussoorie Slope

Fig. 3.1 shows the geometrical modelling of Mussoorie slope. The major cross-sectional parameters of the slope (i.e. the length, height and dip angle of the slope face) has been done according to Singh (2014). The depth of different types of soils in the slope has been incorporated in the model with the help of the data of the soil profiles collected by Singh (2014) by conducting MASW test and in accordance with the shear wave velocity ranges of different soils described in table 3.8.

3.3.2 Modelling of Nainital Slope

Like the previous, the modelling of the Nainital slope has been done in the similar manner. The location of the areas in Nainital, where MASW tests has been conducted are shown in table 3.10. For the geometrical modelling, the depth of each soil layers has been taken based on the soil profiles of the sites B_1, B_2, B_3 and B_4 and with the help of the ranges of the shear wave velocities of different soil types.

Table 3.10: Location of field test sites in Nainital (After Singh 2014)

	Latitude	Longitude	Elevation (m)	Milestone
Site B_1	N 29°23′44.58″	E 79°27′44.70″	2374	Ground on top of ropeway, Nainital
Site B_2	N 29°23′26.10″	E 79°27′19.08″	2084	Cricket ground near mall road, Nainital
Site B_3	N 29°22.459′	E 79°27.925′	2071	Rahis hotel, Nainital
Site B_4	N 29°22.450′	E 79°27.822′	2189	Government girls inter collage, Nainital

Fig. 3.2 shows the geometrical modelling of Nainital slope. The procedure of making the model is same as described in the previous case.

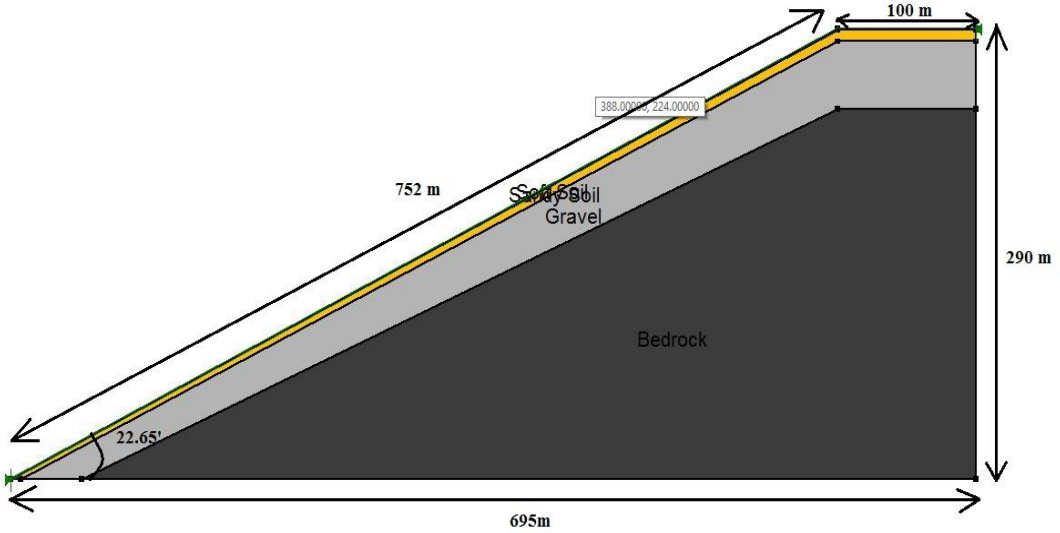

Fig. 3.2: Geometrical Design of Nainital Slope

3.4 Limit Equilibrium Analysis

Limit equilibrium analysis of the slopes has been done by using SLOPE/W software. In SLOPE/W, a number of methods have been incorporated to find the factor of safety value. Here, both static and pseudostatic factor of safety values have been calculated for both the slopes by using five methods. They are ordinary or Felleinus method, Bishop's simplified method, Janbu's method, Spencer's method, Morgenstern-Price method. The brief discussions of different methods has given below.

3.4.1 Methodology

Ordinary or Felleinus method: This method, given by Fellenius (1936), ignores all the interslice shear and normal forces. The weight of the slices are resolved into base shear and normal forces at the slice base. As this method generates extremely poor force polygon closure which indicates the non-equilibrium of forces, thus it gives unrealistic factor of safety value.

All the other methods considers either interslice shear or normal forces or both. Because of this, the methods either satisfies force equilibrium or moment equilibrium. The general limit equilibrium (GLE) formulation was developed in the 1970s (Fredlund and Krahn 1977), to incorporate these interslice forces more rigorously in the formulation of factor of safety values. In the GLE formulation, two types of factor of safety values are calculated, moment and force factor of safety. Bishop's method calculates the moment factor of safety (F_m) while the Janbu's method calculates the force factor of safety (F_f). The spencer's and Morgenstern-Price method calculates both the factor of safety values and F_m=F_f. The relation between the interslice shear and normal forces is given by Morgenstern and Price (1965) and the equation is given below:

$$X = E\,\lambda\,f(x) \tag{3.2}$$

Where, $f(x)$ is a function, λ is the percentage of the function used, X is the interslice shear force and E is the interslice normal force. Fig. 3.3 shows the factor of safety-lambda plot which properly describes all the methods in a nutshell.

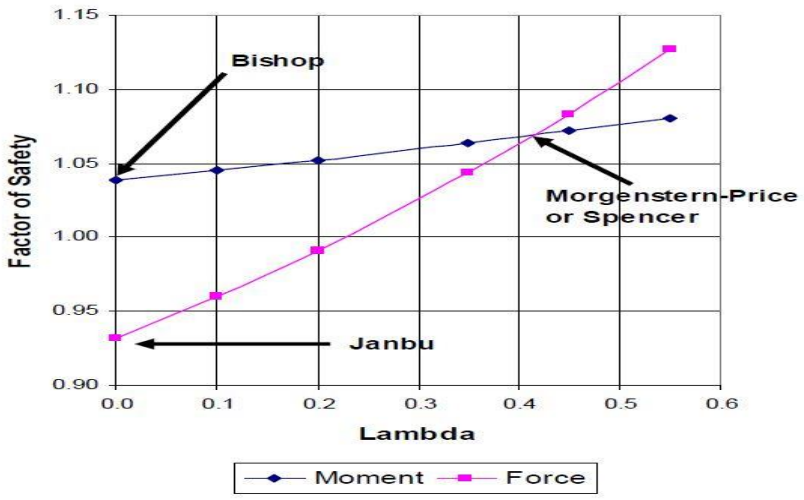

Fig. 3.3: Factor of safety versus lambda plot [GEO-SLOPE International Ltd.]

Bishop's simplified method: This method, given by Bishop (1955), includes interslice normal forces but ignores the interslice shear forces. The interslice normal forces act at the base of the slice. The expression for the factor of safety equation is a non-linear one and thus iterations are required. The force polygon closure is comparatively good than the previous one. This method satisfies moment equilibrium but not force equilibrium.

Janbu's method: This method, given by Janbu (1954), takes into account the interslice normal force but ignores the shear component. It satisfies the horizontal force equilibrium. The force polygon closure is better than the Bishop's method but as this method does not satisfies the moment equilibrium, the factor of safety value is very low.

Spencer's method: This method, given by Spencer (1967), satisfies both the moment and force equilibrium as it considers both the interslice normal and shear force. This method adopts a constant relationship between the interslice normal and shear forces and with each equation, the ratio between the interslice normal and shear forces changes until the factor of safety values calculated by moment and shear equilibriums, become equal. The force polygon closure is very good in this case.

Morgenstern-Price method: This method, given by Morgenstern-Price (1965), considers both the interslice shear and normal functions and also satisfies both the moment and force equilibriums. A number of interslice functions have been defined by this method. This provides a lower factor of safety than Bishop's method as Bishop's method ignores the interslice shear force which sometimes can err on the unsafe side. Thus considering both interslice forces gives more realistic result.

Fig.3.3 clearly shows that as Bishop's method calculates F_m, it lies on the moment curve and similarly, as Janbu's method calculates F_f, it lies on the force curve. As the Morgenstern-Price and the Spencer's method satisfies both F_m and F_f, it reside where the moment and the force curve meets.

3.4.2 Results and Analysis

The factor of safety values have been calculated for both the slopes in both static and pseudostatic cases. Sikkim earthquake (2011) data is considered for doing the pseudostatic analysis. For that case, a horizontal seismic coefficient of 0.15g has been

considered. As the vertical seismic coefficient has no significant effects on determining the factor of safety value, it has been ignored. Factor of safety values have been calculated for all the methods. A comparison of these methods have been done thereafter. Mohr-Coulomb soil model is idealised here.

Mussoorie Slope

Table 3.11 shows the factor of safety for static and pseudostatic cases, calculated for Mussoorie slope by different methods.

Table 3.11: Factor of Safety Results for Mussoorie Slope

Methods	Static FOS	Pseudostatic FOS
Ordinary	1.798	1.277
Bishop	1.849	1.320
Janbu's Simplified	1.798	1.278
Morgenstern-Price	1.849	1.324
Spencer	1.849	1.324

As we know that the Bishop's and Janbu's simplified method, both ignores the interslice shear forces, obviously a comparison arises between the two methods. We know that the Bishop's method satisfies the moment equilibrium and the Janbu's simplified method satisfies the force equilibrium and also from the factor of safety-lambda plot, it is expected that the fos produced by the Bishop's method should be greater than the Janbu's simplified method. In case of Mussoorie slope, from Table 3.11, we can see that the static and the pseudostatic fos values generated by Bishop's method are 1.849 and 1.32 respectively while the same produced by Janbu's simplified method are 1.798 and 1.278 which is lesser than the previous values.

The other two methods, which are Morgenstern-Price and Spencer's method, both takes into account the interslice shear and normal forces and satisfies both the moment and force equilibrium. The factor of safety-lambda plot also shows the same. Also it is to be noted that in the Spencer's method, there is a constant relationship between the interslice normal and shear force. Where, the Morgenstern-Price method can assume a number of relationships (like constant, half-sine, clipped-sine, trapezoidal,

data point specified) between the interslice shear and normal forces and it can only match the Spencer's method if the constant relationship between the interslice shear and normal forces are assumed. In our analysis for the Mussoorie slope, the static and pseudostatic fos values by Morgenstern-Price method are, 1.849 and 1.324 respectively which is exactly the same calculated by Spencer's method. This occurs because a constant relationship has been assumed for the Morgenstern-Price method of analysis. The slip surfaces of Mussoorie slope is shown in Fig 3.4 for both static and pseudostatic cases. In this case, Morgenstern-Price method is applied.

Fig. 3.4 (a): Slip surfaces for the Mussoorie slope for static case

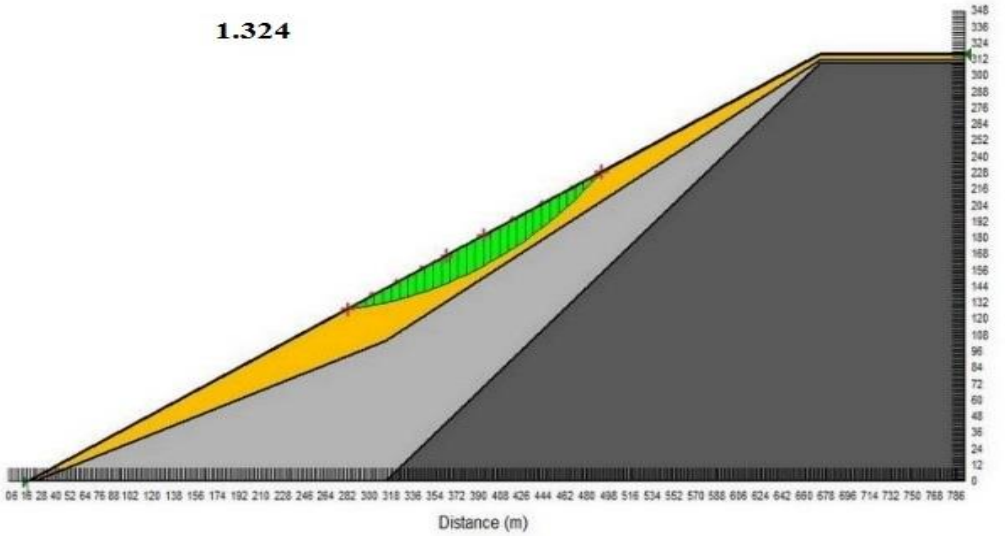

Fig. 3.4 (b): Slip surfaces for the Mussoorie slope for pseudostatic case

Nainital Slope

Table 3.12 shows the factor of safety for static and pseudostatic cases, calculated for Mussoorie slope by different methods.

Table 3.12: Factor of Safety Results for Nainital Slope

Methods	Static FOS	Pseudostatic FOS
Ordinary	1.781	1.268
Bishop	1.784	1.271
Janbu's Simplified	1.782	1.269
Morgenstern-Price	1.784	1.271
Spencer	1.782	1.268

From Table 3.12, we can say that the same relationship can be observed between the Bishop's and the Janbu's simplified method as discussed previously for the case of Mussoorie slope. The fos produced by the Bishop's method should be greater than that produced by the Janbu's simplified method. The fos values for static and pseudostatic cases for the slope by Bishop's method are 1.784 and 1.271 and the same values generated by Janbu's simplified method are 1.782 and 1.269 respectively.

As we know that Spencer's method takes into account a constant relationship between the interslice normal and shear force. So if the Morgenstern-Price method does not consider a constant relationship between the two forces and rather if it takes some other relations like half-sine etc. the factor of safety calculated by the two method will be different. For Nainital slope, a half-sine function has been assumed for the Morgenstern-Price method and that is why there is a slight difference noticed from Table 3.12, between the values calculated with Spencer's method. The fos values for both static and pseudostatic cases calculated by Morgenstern-Price method are 1.784 and 1.271 respectively while the same calculated by Spencer's method are 1.782 and 1.268, which is slightly on the lower side. Fig. 3.5 shows the slip surfaces determined by Morgenstern-Price method for static and pseudostatic cases.

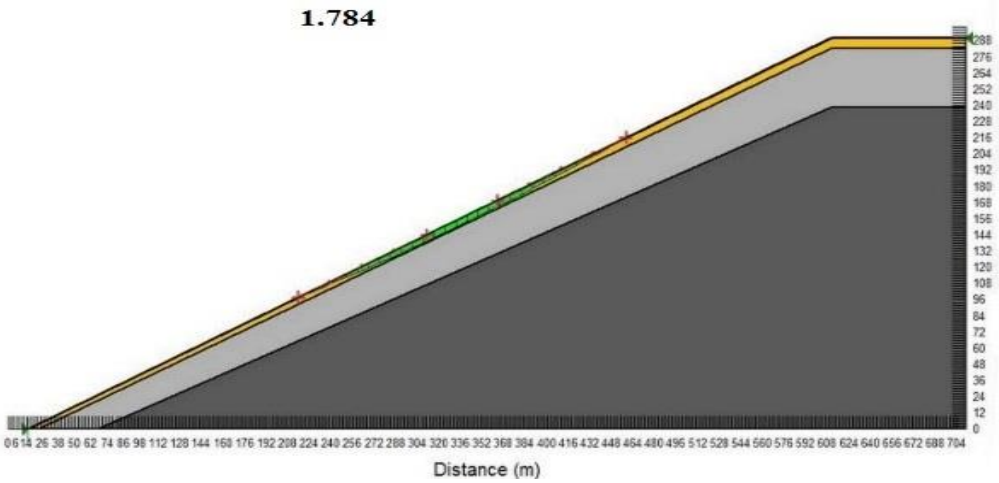

Fig. 3.5 (a): Slip surfaces for the Nainital slope for Static case

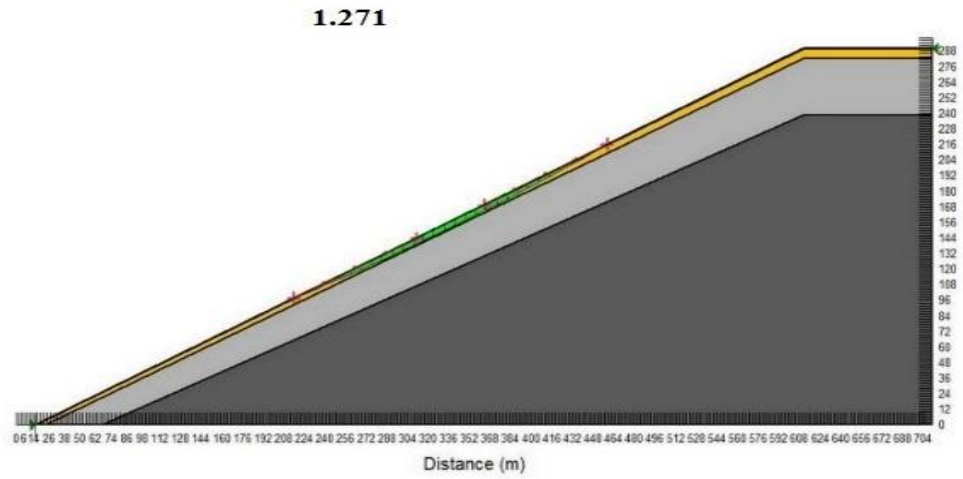

Fig. 3.5 (b): Slip surfaces for the Nainital slope for pseudostatic case

3.5 Finite Element Analysis

As we have already discussed that by only calculating factor of safety, one cannot get the overall idea about the stability of a slope. Also it says nothing about the strain induced to a slope due to earthquake or displacements due to a seismic event. There comes the importance of finite element modelling. Here the stress deformation analysis is performed by using FEM based software SIGMA/W, for static case and QUAKE/W for dynamic case. In both the cases, the horizontal model boundaries are fixed in both the directions and the horizontal movement of the vertical boundaries are fixed.

3.5.1 Mussoorie Slope Analysis

Static Analysis

In the static case, SIGMA/W software is used for obtaining the horizontal and vertical stress contour of the slope. Linear elastic soil model is assumed and the soil materials are taken as Mohr-Coulomb material. The bottom boundaries are considered to be fixed in both x and y directions while the vertical boundaries are considered to be fixed in horizontal direction.

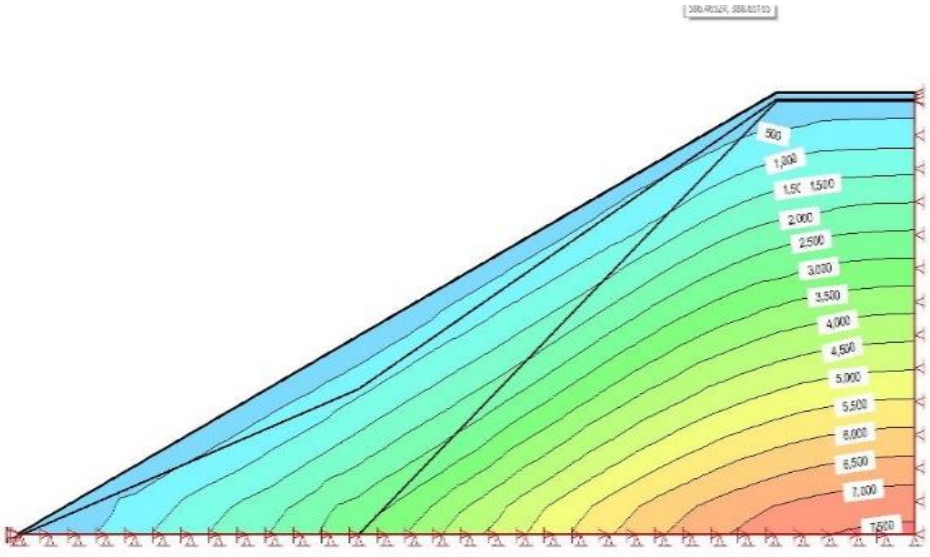

Fig. 3.6 (a): Static vertical stress contours of Mussoorie slope

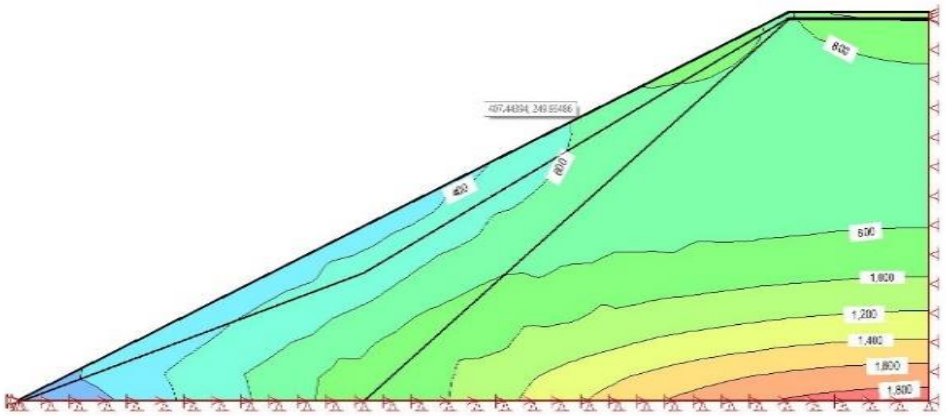

Fig. 3.6 (b): Static horizontal stress contours of Mussoorie slope

Fig. 3.6 shows the stress contours in both the directions. The vertical stress ranges from 9.33 kPa to 7618.5 kPa and the horizontal stress ranges from 56.745 kPa to 1904.4 kPa.

Dynamic Analysis

For doing the dynamic analysis, the time-history record of Sikkim earthquake (2011) data is incorporated into the model. The modified peak acceleration of the earthquake is 0.15g and the duration 194.29 seconds. Fig. 3.7 shows the time history record of the Sikkim Earthquake (2011)

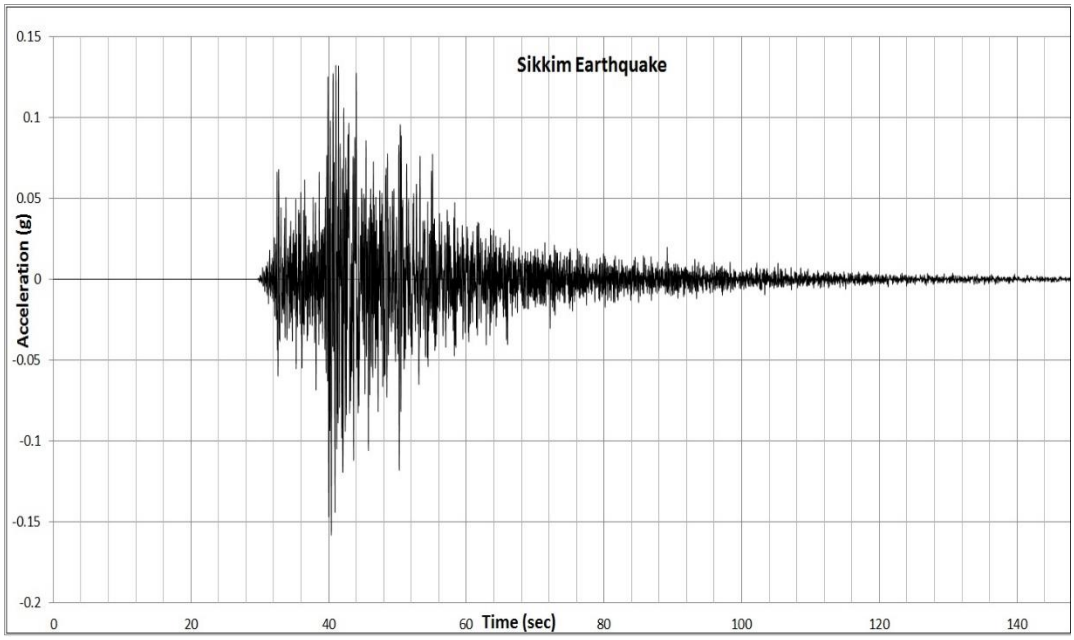

Fig. 3.7. Time history of Sikkim Earthquake (2011) Used for dynamic analysis

Fig. 3.8 shows the dynamic stresses generated in the slope and fig. 3.9 shows the displacements occurred in the slope because of the seismic effect. The dynamic stress-deformation analysis is done by using QUAKE/W software. The Mohr-Coulomb soil model is idealised in this case. Here, first the initial static loading condition is incorporated in the model by using Liner Elastic model and after that, the dynamic scenario has been incorporate in the model by taking an Equivalent Linear model. The vertical side boundary has been made fixed in the X direction and the horizontal bottom boundary has been made fixed in both X and Y directions.

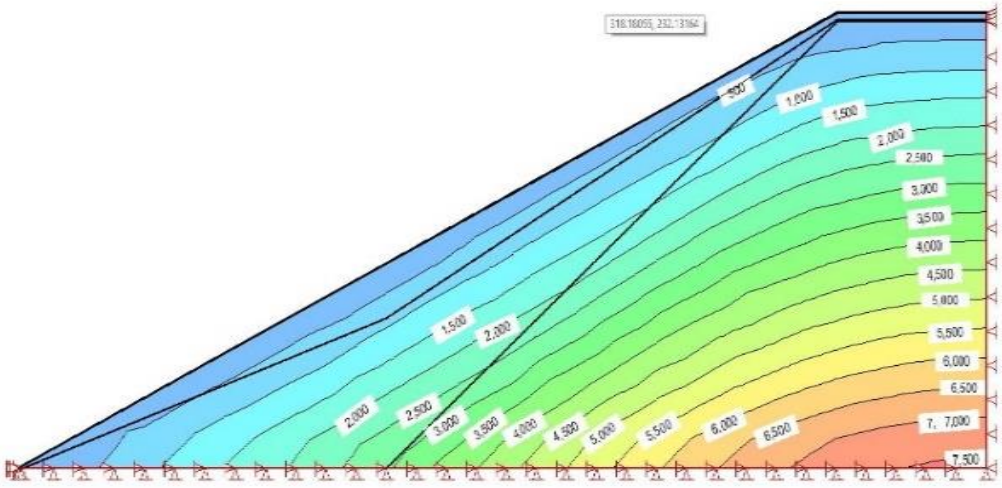

Fig. 3.8 (a): Dynamic vertical stress contours of Mussoorie slope

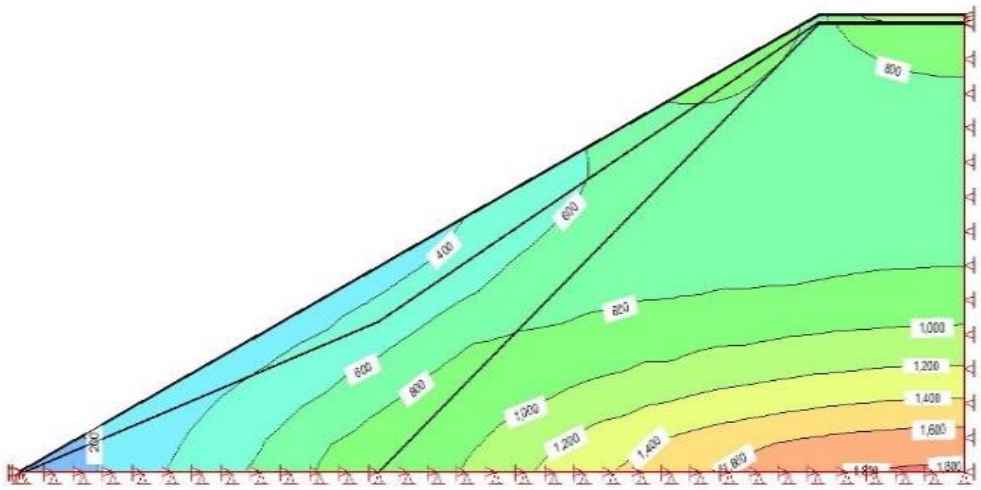

Fig. 3.8 (b): Dynamic horizontal stress contours of Mussoorie slope

The dynamic vertical and horizontal stress varies from 5.81 kPa to 7597.3 kPa and 44.228 kPa to 1834.1 kPa respectively. It can be observed that with respect to the static case, the maximum stresses in both the directions have been reduced.

Fig. 3.9 shows the dynamic displacement contours that have been taken place in the slope.

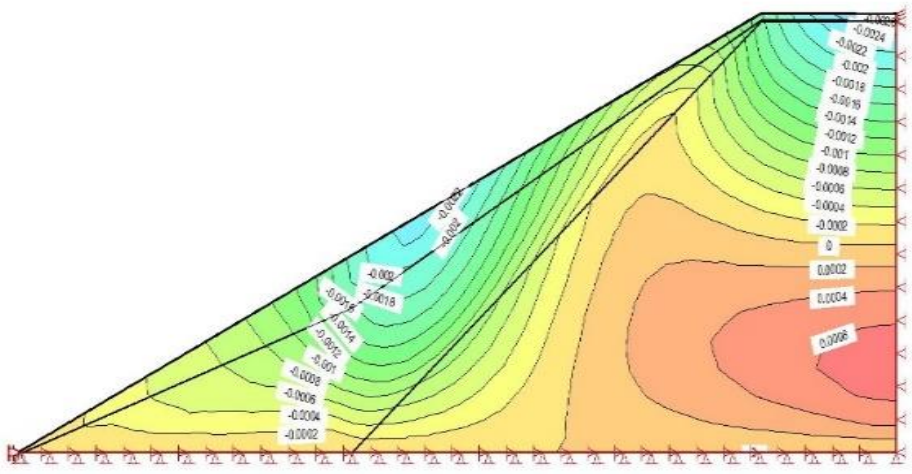

Fig. 3.9 (a): Dynamic vertical displacement contours of Mussoorie slope

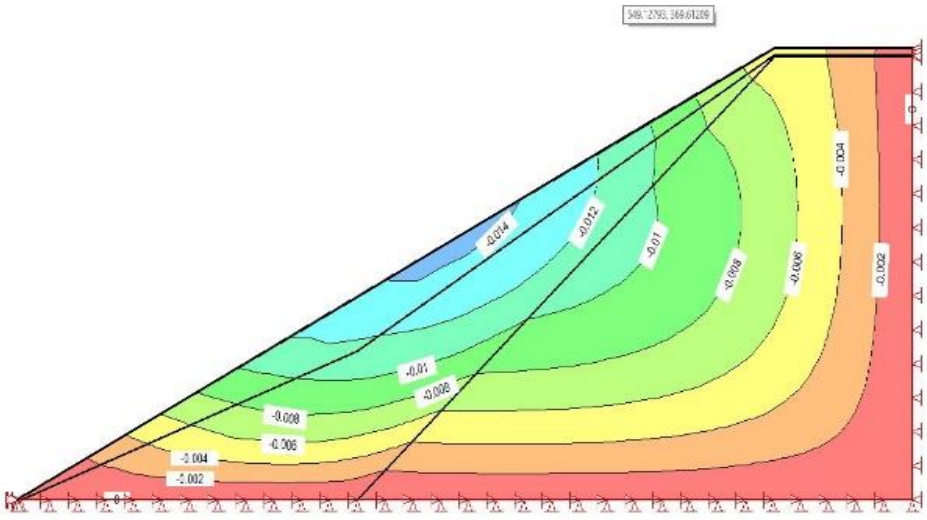

Fig. 3.9 (b): Dynamic horizontal displacement contours of Mussoorie slope

The results of the stress-displacement analysis of the Mussoorie slope in both the static and dynamic cases have been summarised in table 3.13.

Table 3.13: Summary of Mussoorie slope results

	Static	**Dynamic**
Max. Vertical Stress (kPa)	7618.5	7597.3
Max. Horizontal Stress (kPa)	1904.4	1834.1
Max. Vertical Displacement (mm)	0	2.7264
Max. Horizontal Displacement (mm)	0	14.605

3.5.2 Nainital Slope Analysis

Static Analysis

Static analysis is done by using SIGMA/W software like the previous one. The static horizontal and vertical stress contours of the slope is shown in fig. 3.10

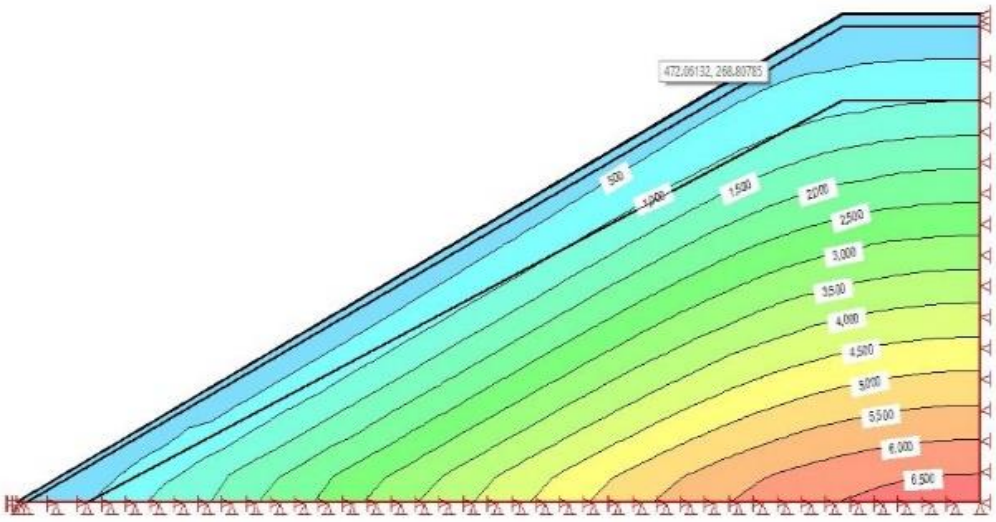

Fig. 3.10 (a): Static vertical stress contours of Nainital slope

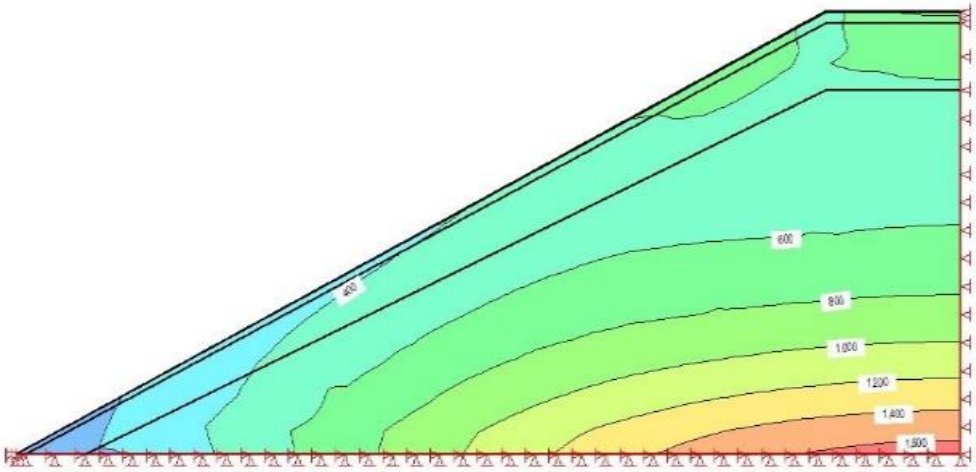

Fig. 3.10 (b): Static horizontal stress contours of Nainital slope

In fig. 3.10, linear elastic soil model is assumed and the soil materials are taken as Mohr-Coulomb material. The boundary conditions are taken to be the same as previous. The stress contour ranges from 8.2035 kPa to 6743.6 kPa and 43.894 kPa to 1685.9 kPa for the vertical and horizontal cases respectively.

Dynamic Analysis

In the dynamic analysis, the same dynamic loading of Sikkim earthquake (2011) has been incorporated. Fig. 3.7 shows the time-history plot of the earthquake. The analysis is done following the same manner as done for the case of Mussoorie slope. Fig. 3.11 shows the dynamic stress contours of the slope under earthquake excitation.

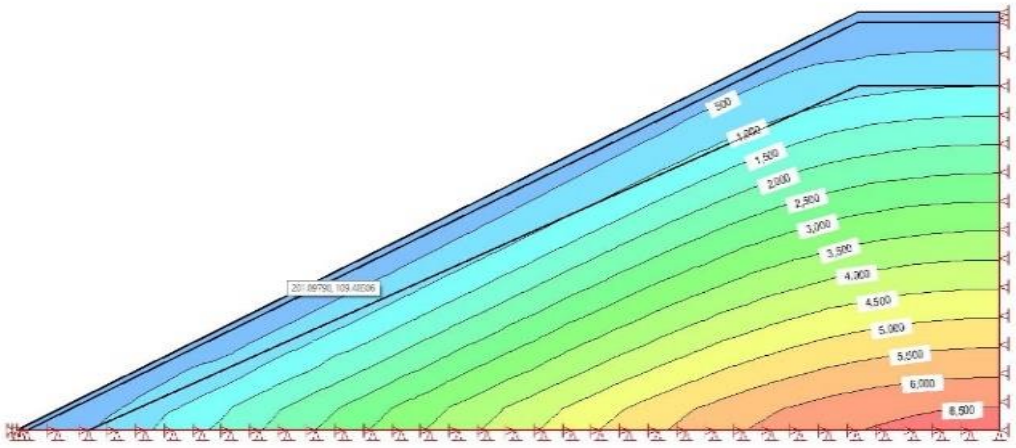

Fig. 3.11 (a): Dynamic vertical stress contours of Nainital slope

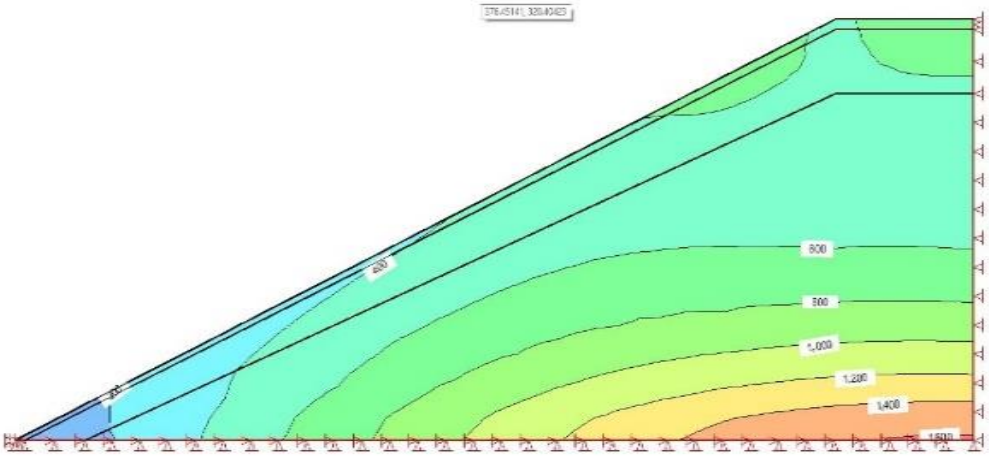

Fig. 3.11 (b): Dynamic horizontal stress contours of Nainital slope

The dynamic stresses in the vertical and horizontal direction ranges from 3.692 kPa to 6702.4 kPa and 31.706 kPa to 1625 kPa respectively. It can be observed that in comparison to the static stresses, the maximum stresses has been decreased in the dynamic case.

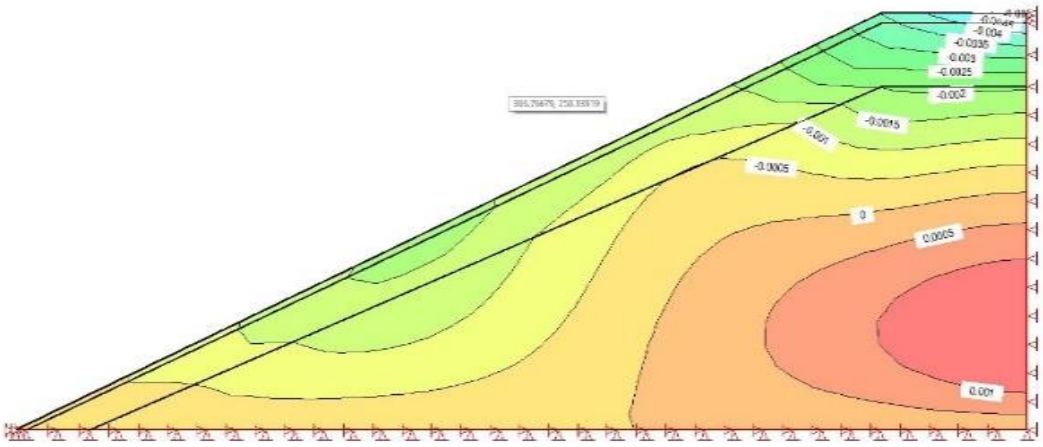

Fig. 3.12 (a): Dynamic vertical displacement contours of Nainital slope

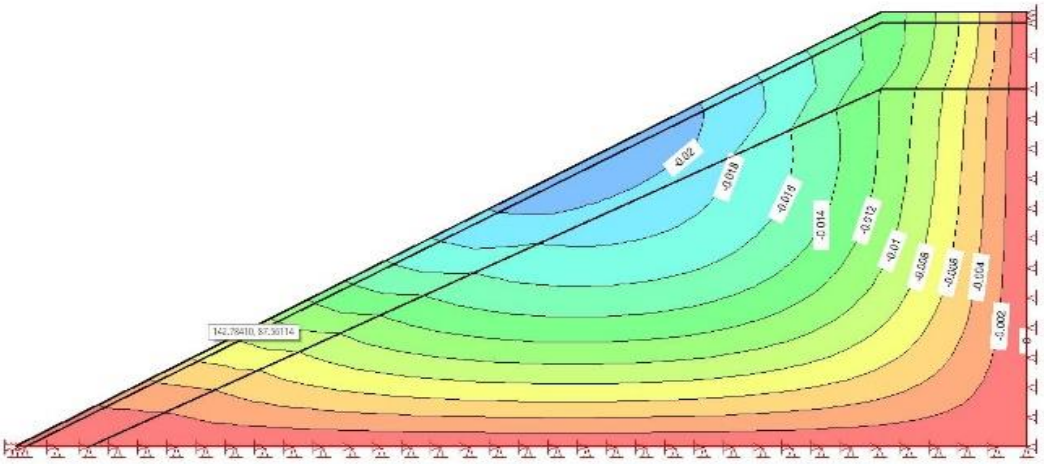

Fig. 3.12 (b): Dynamic horizontal displacement contours of Nainital slope

Fig. 3.12 shows the displacement contours of the slope where the displacements have increased compare to the static case.

Table 3.14 shows the summary of the static and dynamic results for the nainital slope.

Table 3.14: Summary of Nainital slope results

	Static	**Dynamic**
Max. Vertical Stress (kPa)	6743.6	6702.4
Max. Horizontal Stress (kPa)	1685.9	1625
Max. Vertical Displacement (mm)	0	5.0875
Max. Horizontal Displacement (mm)	0	21.593

3.6 Concluding Remarks

1. In all the cases, it has been observed that the pseudostatic factor of safety values have been reduced from the respective static factor of safety values. This observation confirms that soil stability decreases, as a result of increase in the driving forces, under seismic conditions.
2. As the ordinary method ignores both the interslice forces, depending solely on this method to determine factor of safety is not a good practice. The factor of safety produced by Bishop's method is greater than that of Janbu's simplified method.
3. The factor of safety values given by the Moregenstern-Price method and the Spencer's are found to be equal only when the Morgenstern-Price method takes a constant functional relationship between the interslice normal and shear force. If it takes any other function other than a constant function, the values will be different.
4. In the finite element static and dynamic analysis of the slopes, both the horizontal and the vertical displacements have been increased where in the static case, the displacements were absent in both the directions.. The horizontal displacements for the Mussoorie and Nainital slopes are 14.605 and 21.593 mm while the vertical displacements for the slopes are 2.726 and 5.087 mm respectively.
5. The stresses for dynamic case are decreased from the static ones as there are displacements due to earthquake loading. In both the slopes, this condition can be observed.

CHAPTER – 4

ANALYSIS OF ROCK SLOPE

4.1 General

In hilly areas, rockslides are a common phenomenon. Triggering mechanisms like occurrence of earthquakes or heavy rainfall often cause rockslides. If the rock slope consists of discontinuities or fractures, then the slope becomes vulnerable to failure. So understanding the behaviour of slopes having one or more sets of discontinuities is necessary. This chapter deals with the effects of joint patterns on the behaviour of a jointed rock slope under different loading environments and triggering conditions. Three types of triggering conditions have been considered here. Gravity loading, excessive rainfall condition and seismic environment.

4.2 Geology of Jointed Rock Slope

As it is evident that discontinuities possess a major role in deciding the failure of a rock slope, it is necessary to know about some of the major features of a jointed rock slope. Also it should be noted that the failure pattern of a rock slope depends on the orientations and alignment of its discontinuities.

4.2.1 Orientation of Discontinuities

The stability of a jointed rock slope hugely depends on the number and alignment of the discontinuities present in it. The basic terminology which defines the orientation of the discontinuities are dip or dip inclination (ψ_p). This is defined as, the maximum inclination of the discontinuity measured from the horizontal. Fig. 4.1 shows faults with different dip angles.

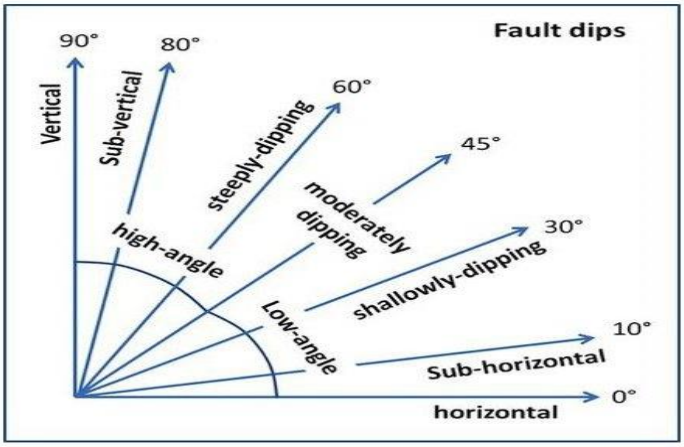

Fig. 4.1: Dip inclinations of different faults (after Sorkhabi R. 2012)

4.2.2 Failure Patterns

As joint orientation is the prime geologic factor of a discontinuous rock slope, the failure pattern of a jointed rock slope depends heavily on that. In a broader perspective, a jointed slope can fail in two ways, by sliding and by toppling. Sliding of rock masses can be divided further into 3 categories. Plane failure, rotational sliding failure and wedge failure. This section describes these failure patterns in brief.

Plane failure: Plane failure in a discontinuous rock mass occurs when the unstable rock mass slides down in a plane failure surface. There are certain conditions which defines a plane failure.

1) The dip of the slope face is denoted by ψ_f. The sliding plane on which failure takes place must be parallel or sub-parallel to the slope face.

2) The dip of the slope face (ψ_f) should be greater than the dip of the plane on which sliding occurs (ψ_p). I.e. $\psi_f > \psi_p$.

3) The dip inclination of the sliding plane must be greater than the joint friction angle of the discontinuity. I.e. $\psi_p > \phi$.

4) The upper portion of the discontinuity must intersects the upper slope.

Fig. 4.2 shows a schematic representation of plane failure

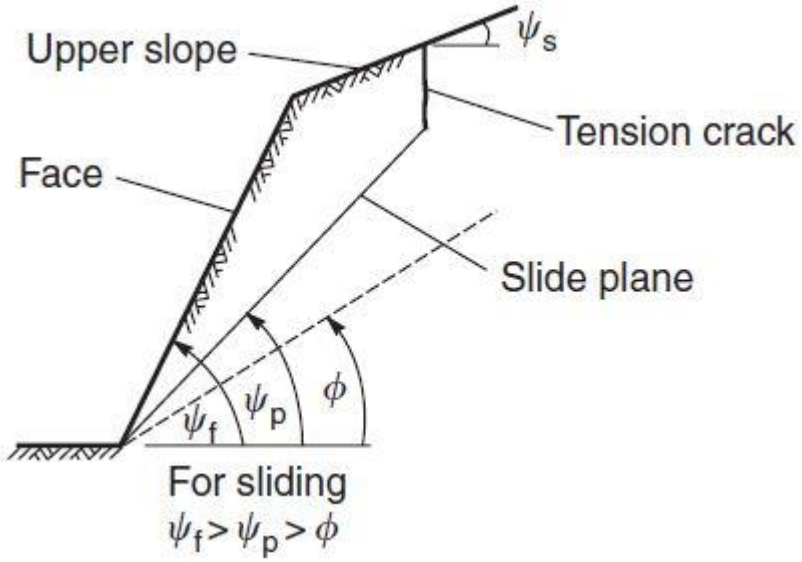

Fig. 4.2: Plane failure (after Duncan and Mah 2004)

Rotational Sliding failure: Rotational sliding failure in a discontinuous rock mass occurs when the unstable rock mass slides down along a curved surface. Two types of failure generally comes under this category. Circular and non-circular sliding. The conditions which favours this type of failure is listed below.

1) When the rock mass is densely fractured, then it becomes difficult to find a suitable failure pattern. Then the slope fails along the line of least resistance and it generally takes the shape of a circle. In this way, circular failure occurs.

2) If the rock mass becomes highly weathered and fragmented, then generally it takes non-circular failure pattern.

Fig. 4.3 shows a non-circular sliding failure pattern.

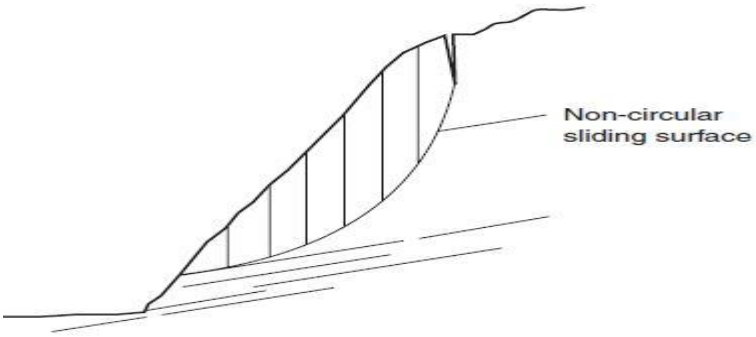

Fig. 4.3: Non-circular failure (after Duncan and Mah 2004)

Wedge failure: wedge failure generally occurs when two intersecting sets of discontinuities form a wedge shaped block along which sliding can take place. The main conditions that define a wedge failure is described below.

1) For a wedge type failure to occur, the dip of the line of intersection of the two sets of discontinuities (ψ_i) should be more than the average angle of internal friction of the two sliding surfaces (ϕ) and should be less than the dip of the slope face (ψ_f).

2) The line of intersection of the two sets of discontinuities should be aligned in the out of face direction with respect to the slope face.

Fig. 4.4 shows a schematic view of wedge type failure.

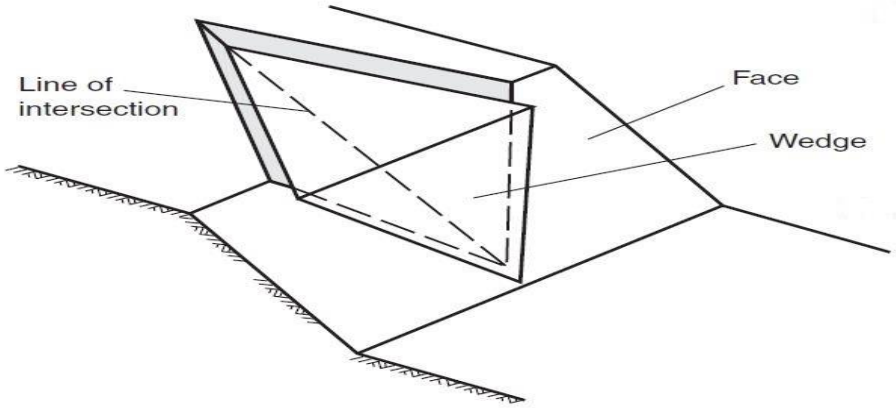

Fig. 4.4: Wedge failure (after Duncan and Mah 2004)

Toppling failure: The previous modes of failures possess sliding of rocks. In this mode, the unstable blocks of rocks rotates with respect to a fixed base. Primarily toppling failure can occur in three different ways. Block toppling, flexural toppling and block-flexural toppling. The general conditions which favours toppling mode of failure are discussed below.

1) The centre of gravity of the column slab of block must lie outside the base of the column block so that rotation takes place.

2) In the jointed rock mass, the alignment of the discontinuity should be dipping into the face and going away from the face.

3) The dip inclination of the joint sets should be steep and they should be closely spaced.

Fig 4.5 describes a typical schematic representation of a toppling failure.

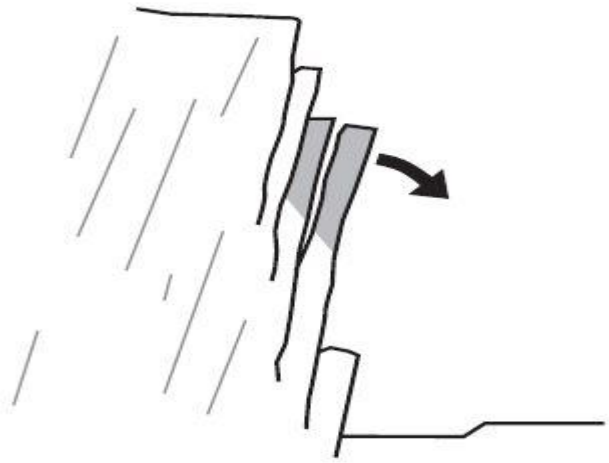

Fig. 4.5: Toppling failure (after Duncan and Mah 2004)

4.3 UDEC Modelling

Universal Distinct Element Code (UDEC) is the most popular code when it comes to modelling of rock materials. It is highly effective in simulating jointed rock slopes subjected to static and dynamic loading. The model can assume a rock block as both rigid and deformable. The discontinuities between the blocks are treated as interface elements. Generally two dimensional plain strain condition is assumed for the analysis.

In UDEC there are seven constitutive built-in material models for deformable blocks. The models are,

1) Null model: A null material model is used to represent material that is excavated or removed.

2) Elastic, isotropic model: The elastic isotropic model provides the simplest representation of material behaviour. This model is valid for homogeneous, isotropic, continuous material that exhibit linear stress-strain behaviour with no hysteresis on unloading.

3) Drucker-Prager model: the Drucker-Prager plasticity model is useful to model soft clays with low friction angles. However, this model is not generally recommended for application to geologic material. It is included here mainly to permit comparison with other numerical programmes.

4) Mohr-Coulomb model: This is the conventional model used to represent shear failure in soils and rocks.

5) Ubiquitous-joint model: This is an anisotropic plasticity model that includes weak planes of specific orientation embedded in a Mohr-Coulomb solid.

6) Strain-softening/hardening model: This model allows representation of non-linear material softening and hardening behaviour based on prescribed variations of the Mohr-Coulomb model properties (cohesion, friction, dilation, tensile strength) as functions of the deviator plastic strain.

7) Double-yield model: This model is intended to represent materials in which there may be significant irreversible compaction in addition to shear yielding.

The explicit solution algorithm in UDEC generally permits either static or dynamic analysis. For dynamic calculations, the dynamic loading can be incorporated directly into the model by either velocity or stress waves as an exterior or interior boundary condition. For reducing and absorbing the reflections of the waves into the model, free-field and non-reflecting viscous boundary conditions are applied.

Out of these seven constitutive models, Mohr-Coulomb model and elastic, isotropic model has been discussed in detail.

4.3.1 Mohr-Coulomb Model

This model comes under the plastic model group defined in UDEC. This model is applied for deformable blocks. It follows the Mohr-Coulomb yield criteria. In this model, the shear and tensile flow are non-associated and associated, respectively. The basic equation of a Mohr-Coulomb model is given below.

$$\tau = C + \sigma \, tan\phi \tag{4.1}$$

Where,

τ = Shear stress,

C = Cohesion,

σ = Normal stress,

ϕ = Friction angle.

a) Incremental elastic law

In UDEC, while implying this model, σ_1, σ_2, σ_3 are the principle stresses which have been used and the out of plane stress $\sigma_{zz}$is recognised as one among them. The principle stress and the principle directions are computed from the stress tensor components so that

$$\sigma_1 \leq \sigma_2 \leq \sigma_3 \tag{4.2}$$

The corresponding principle strain increments are Δe_1, Δe_2, Δe_3 and decomposed as,

$$\Delta e_i = \Delta e_i^e + \Delta e_i^p \qquad i = 1 \text{ to } 3 \tag{4.3}$$

Where the first and second term in eq. 4.3 denotes the elastic and plastic parts respectively. When the strain exceeds the elastic component, then only plastic flow takes place. The incremental stresses in terms of principle stresses and strains by Hooke's law is obtained as follows.

$$\Delta\sigma_1 = \alpha_1 \Delta e_1^e + \alpha_2(\Delta e_2^e + \Delta e_3^e) \tag{4.4}$$

$$\Delta\sigma_2 = \alpha_1 \Delta e_2^e + \alpha_2(\Delta e_1^e + \Delta e_3^e) \tag{4.5}$$

$$\Delta\sigma_3 = \alpha_1 \Delta e_3^e + \alpha_2(\Delta e_1^e + \Delta e_2^e) \tag{4.6}$$

Where, $\alpha_1 = K + {}^{4G}/_{3}$ and $\alpha_2 = K - {}^{2G}/_{3}$

b) Yield and potential functions:

The failure criteria may be represented in the plane (σ_1, σ_3) as shown in Fig. 4.6.

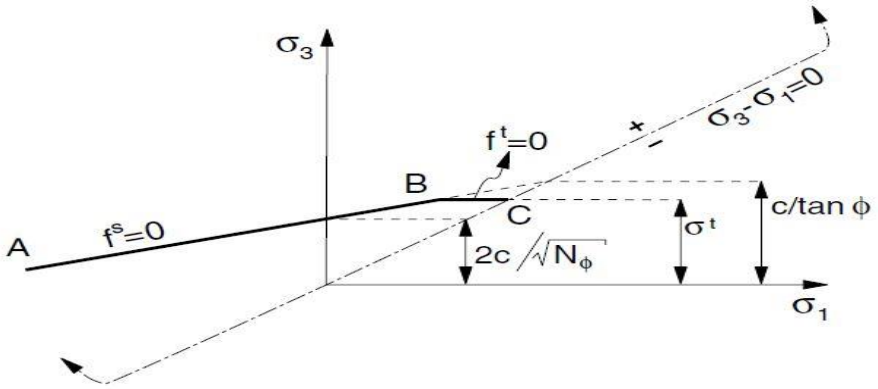

Fig. 4.6: Mohr-Coulomb failure criteria in UDEC
[Itasca C. G Inc., Universal Distinct Element Code (UDEC) User's Manual]

The failure envelope which is defined from point A to B by the Mohr-Coulomb yield function

$$f^s = \sigma_1 - \sigma_3 N_\phi + 2C\sqrt{N_\phi} \tag{4.7}$$

And from B to C by a tension yield function of the form

$$f^t = \sigma^t - \sigma_3 \tag{4.8}$$

Where ϕ is the friction angle, c is the cohesion and σ^t is the tensile strength and

$$N_\phi = \frac{1+\sin\phi}{1-\sin\phi} \tag{4.9}$$

It is to be noted that in the shear yield formulation only the major and minor principle stresses are active. There is no effect of the intermediate principle stress. For a material with friction $\phi = 0$ and the tensile strength of the material cannot exceed the value σ^t_{max} given by,

$$\sigma^t_{max} = \frac{C}{\tan\phi} \tag{4.10}$$

The shear potential function which corresponds to a non-associated flow rule is given by,

$$g^s = \sigma_1 - \sigma_3 N_\psi \tag{4.11}$$

Where, ψ is the dilation angle

$$N_\psi = \frac{1+\sin\psi}{1-\sin\psi} \tag{4.12}$$

The associated flow rule for tensile failure is derived from the potential function g^t with

$$g^t = -\sigma_3 \tag{4.13}$$

The flow rule for this model is given as,

$$h = \sigma_3 - \sigma^t + \alpha^p(\sigma_1 - \sigma^p) \tag{4.14}$$

Where the function $h(\sigma_1, \sigma_3) = 0$, is defined as the function represented by the diagonal between the functions $f^s = 0$ and $f^t = 0$ in the (σ_1, σ_3) plane. α^p and σ^p are constants which can be defined as,

$$\alpha^p = \sqrt{1 + N_\phi^2} + N_\phi \tag{4.15}$$

and

$$\sigma^p = \sigma^t N_\phi - 2C\sqrt{N_\phi} \tag{4.16}$$

4.3.2 Elastic Isotropic Model

Materials which are homogeneous, isotropic and continuous and which shows linear stress-strain behaviour can be modelled as an elastic, isotropic material. In this model, the relation of stress-strain can be expressed in incremental form assuming a plane strain case as,

$$\Delta\sigma_{11} = \alpha_1 \Delta e_{11} + \alpha_2 \Delta e_{22} \tag{4.17}$$

$$\Delta\sigma_{22} = \alpha_2 \Delta e_{11} + \alpha_1 \Delta e_{22} \tag{4.18}$$

$$\Delta\sigma_{12} = 2G\Delta e_{12} \qquad (\Delta\sigma_{12} = \Delta\sigma_{21})$$

$$\Delta\sigma_{33} = \alpha_2(\Delta e_{11} + \Delta e_{22}) \tag{4.19}$$

Where, $\alpha_1 = K + (4/3)G$;

$\alpha_2 = K - (2/3)G$;

K = bulk modulus; and

G = shear modulus.

$$\Delta e_{ij} = \frac{1}{2}\left[\frac{\partial \dot{u}_i}{\partial x_j} + \frac{\partial \dot{u}_j}{\partial x_i}\right]\Delta t \tag{4.20}$$

Where,

Δe_{ij} = incremental strain tensor;

$\dot{u}_i$ = displacement rate; and

Δt = time step.

4.4 Problem Description

The stability of a 260 m high slope has been simulated. The geometry of the slope is taken from Hammah et al. (2007) and also given by Wyllie and Mah (2004). The main objective of the study is to investigate the effects of discontinuities and their orientations on the stability of the slope and their failure patterns under different loading environments. All the work has been done by using UDEC 4.0 software. Three types of analysis has been done to investigate the behaviour of the slope. They are

1) Static gravity analysis assuming Mohr-Coulomb plasticity model.

2) Analysis of the slope under excessive rainfall assuming Mohr-Coulomb plasticity model.

3) Analysis of the slope under seismic loading assuming elastic, isotropic model.

Fig 4.7 shows the basic geometry of the slope

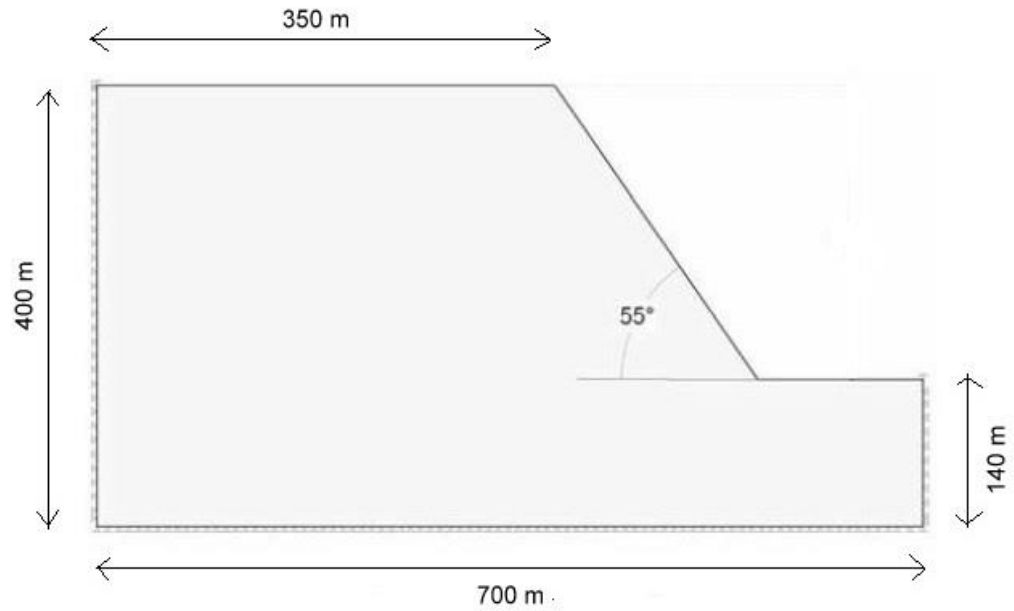

Fig. 4.7: Basic slope geometry

Joints may be oriented in two ways. Those are discussed in the following sub-sections.

4.4.1 Out of Plane Joints

In Fig. 4.8, the slope is having an out of plane joint set having a dip inclination of 35°. The spacing of the joint set is 20 m. For gravity loading purpose, the bottom boundary is made fixed in both the directions while the side boundaries are restrained against movement is the horizontal direction.

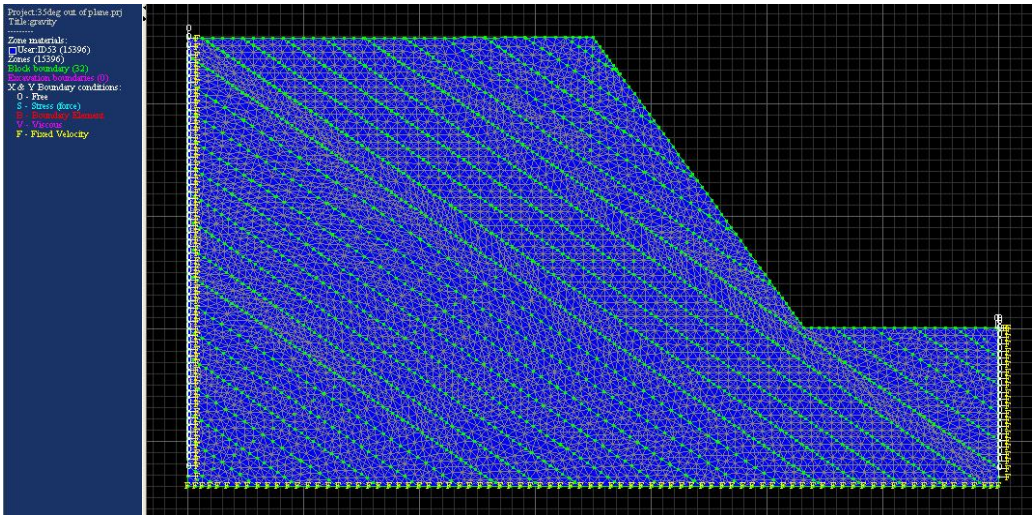

Fig. 4.8: Slope with out of plane joint set

4.4.2 Into the Plane Joints

Fig, 4.9 shows the slope having an into the plane joint set. Here the dip inclination of the joint set is 70° with a spacing of 20 m. The boundary condition is the same as previous, for gravity loading.

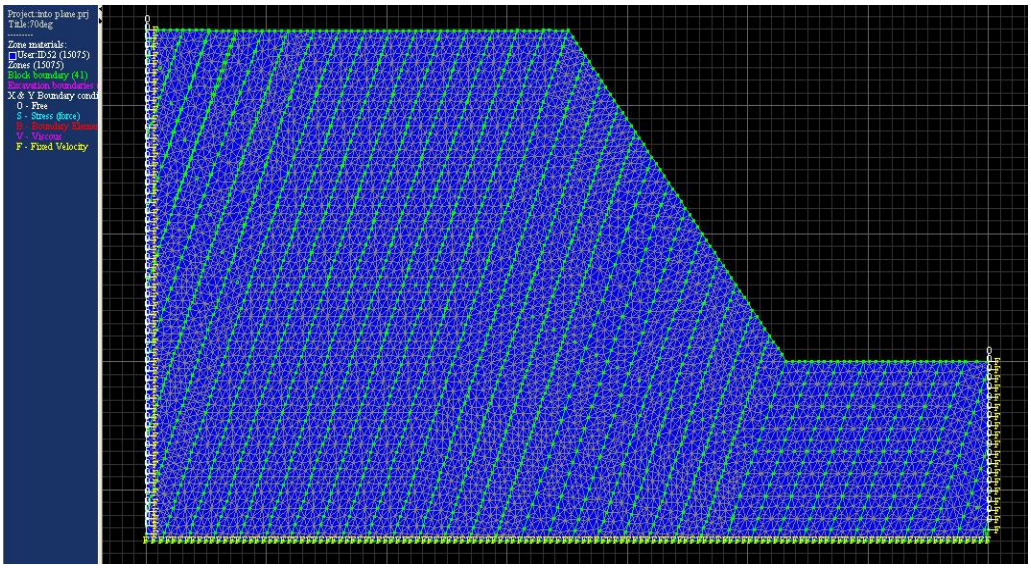

Fig. 4.9: Slope with into the plane joint set

4.5. Static Gravity Analysis

In this case, the 260 m high rock slope having a dip inclination of the slope face (ψ_f) of 55° has been investigated under static gravity loading. Mohr-Coulomb plasticity model has been taken for the material. The slope has been analysed under four different joint alignment conditions. The four cases are summarised below.

a) Slope having one joint set with a dip inclination (ψ_p) of 35° out of the plane.

b) Slope having one joint set with a dip inclination (ψ_p) of 60° out of the plane.

c) Slope having one joint set with a dip inclination (ψ_p) of 75° out of the plane.

d) Slope having one joint set with a dip inclination (ψ_p) of 70° into the plane.

In all the cases same joint spacing is considered. The properties of the rock mass and the discontinuities which have been considered for all the cases, have been given in table 4.1.

Table 4.1: Material Properties

Rock Mass	**Discontinuities**
Density = 2610 kg/m^3	Joint Normal Stiffness (Jk_n) = 100 GPa
Angle of Internal Friction = 43°	Joint Shear Stiffness (Jk_s) = 10 GPa
Poisson's ratio = 0.26	Cohesion = 0.1 MPa
Cohesion = 0.675 MPa	Joint Friction Angle (jfric) = 40°
Bulk Modulus = 9.072 GPa	Joint Spacing = 20 m
Shear Modulus = 5.184 GPa	---
Tensile Strength = 0 MPa	---

In the following sections, all the four cases have been analysed. The cases have been classified into two types depending upon the alignment of the joint sets. First type is having 3 cases of out of plane joints and the second case is having one case of into the plane joint sets.

4.5.1 Joints Dipping Out of Plane

a) Case 1: The basic geometry of the slope is given in fig. 4.7. In this case, the dip inclination of the joint sets (ψ_p) is 35° out of the plane. The bottom boundary is taken as fixed in both horizontal and vertical directions. The side boundaries have been restrained against movement in the horizontal direction. Here, the factor of safety is calculated and it comes out to be 1.32 which is in good agreement with the factor of safety calculated by Wyllie and Mah (2004) for the slope i.e. 1.27. Fig. 4.8 shows the plot of strain contours along with shear displacement and velocity vectors under gravity loading.

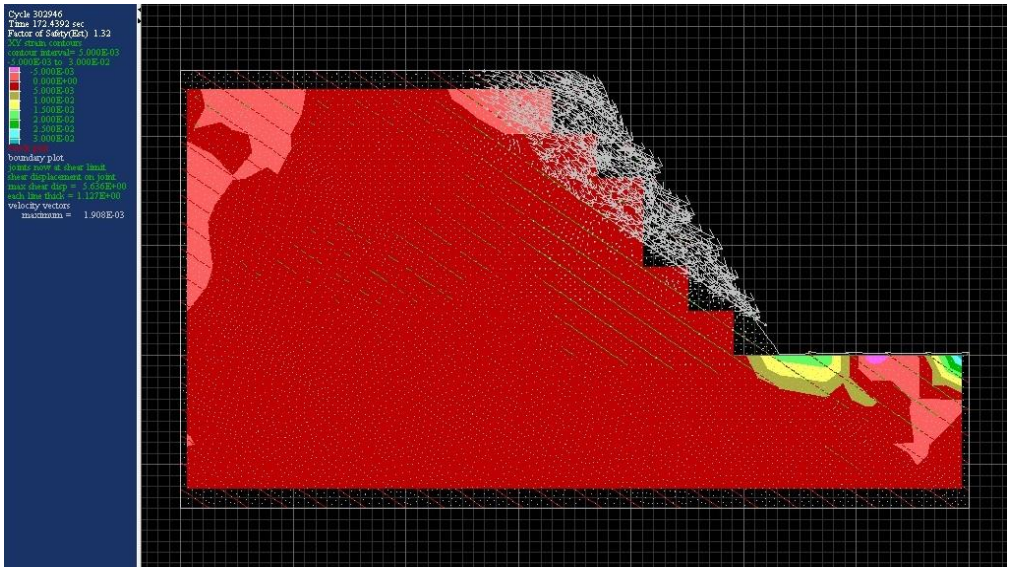

Fig. 4.10 Plot of strain contours with velocity vectors for ψ_p of 35° out of plane

From fig. 4.10 it can be clearly observed that the failure pattern is plane failure. There are a few reasons which support the failure pattern. Firstly, here the joint set is sub-parallel to the slope face. Secondly, the dip of the failure plane (ψ_p) is 35° and the dip of the slope face (ψ_f) is 55°. This means that the value of ψ_p is less than ψ_f. Thirdly, the dip of the failure plane is within a range of 20° variation with the dip of the slope face (i.e. ψ_f). These conditions favour the plane failure pattern.

b) Case 2: In this case, the dip of joint set (ψ_p) is 60°. The boundary conditions are the same as previous. Here, the factor of safety has been observed to be increased from the 1st case. This shows that as ψ_p increases, the slope becomes more stable. Non-circular sliding failure is observed here. It has been shown that the average shear strain has been decreased from the previous one. Fig. 4.11 shows the plot of strain contours along with shear displacement and velocity vectors under gravity loading.

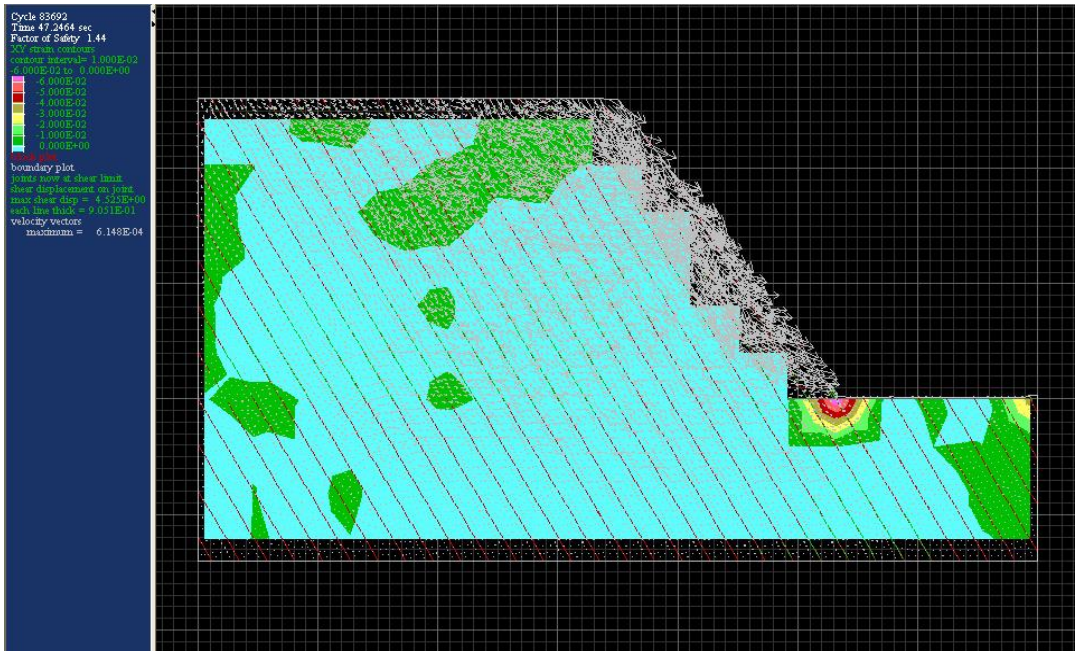

Fig. 4.11: Plot of strain contours with velocity vectors for ψ_p of 60° out of plane

c) Case 3: Here, the dip of joint set (ψ_p) is 75° out of plane. Boundary conditions are same as previous cases. As ψ_p is greater than ψ_f and inclinations of both the plane and face are out of the plane, circular sliding failure takes place rather than plane failure. Also it is observed from the strain contour that the average strain is decreased. The factor of safety is increased from the last two cases. These observations denote that the slope has become more stable. Fig. 4.12 shows the plot of strain contours along with shear displacement and velocity vectors.

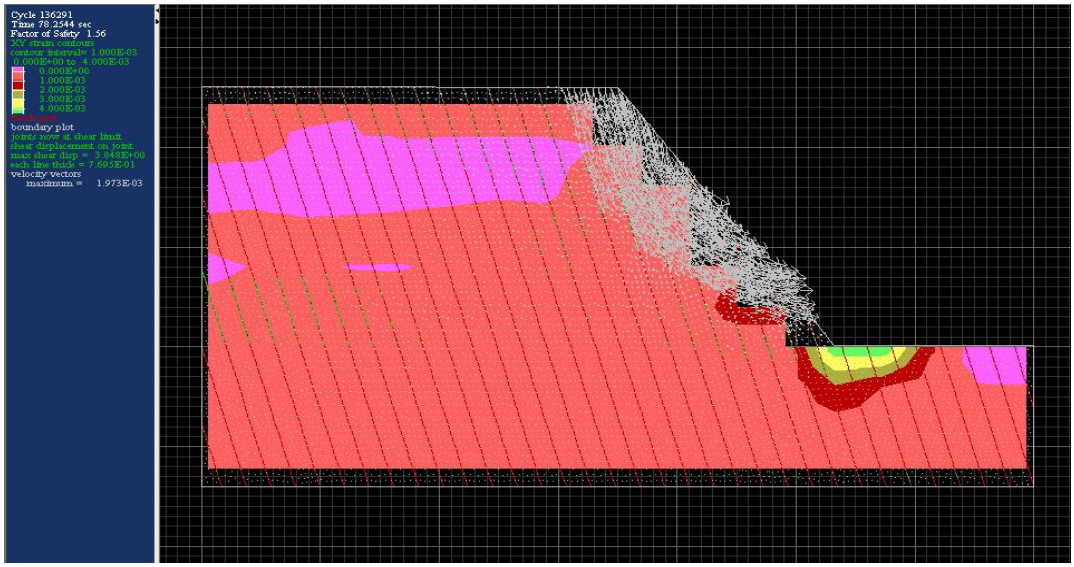

Fig. 4.12: Plot of strain contours with velocity vectors for ψ_p of 75° out of plane

4.5.2 Joints Dipping Into the Plane

In this category, one case is considered where the joint set is dipping 70° into the plane. Boundary conditions are same as the previous cases. Fig. 4.13 shows the plot of strain contours along with shear displacement and velocity vectors.

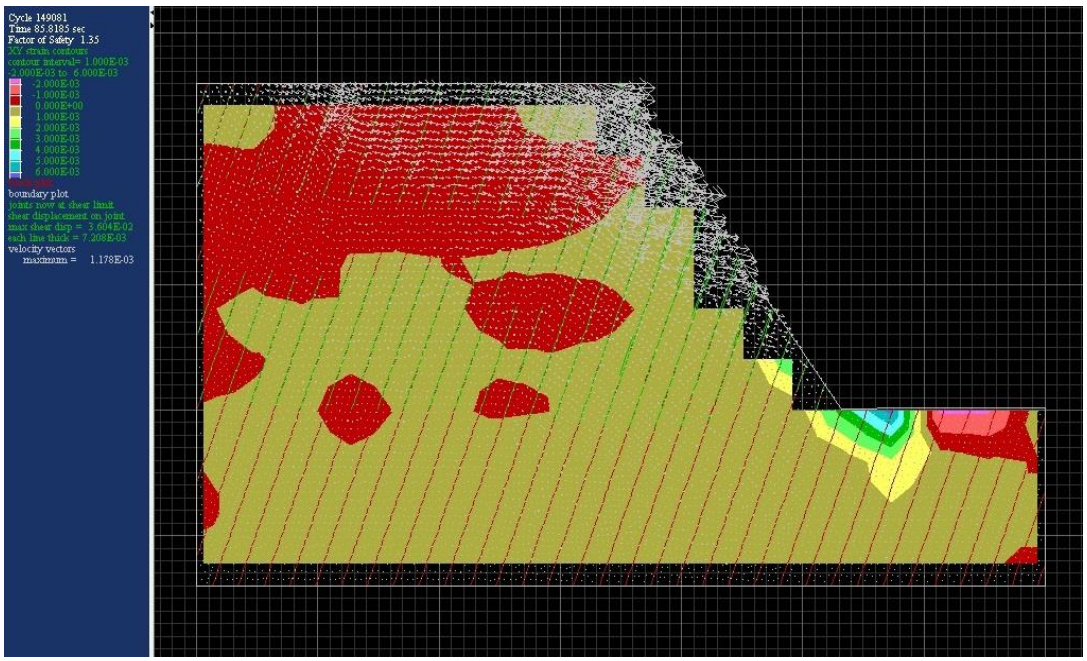

Fig. 4.13: Plot of strain contours with velocity vectors for ψ_p of 70° into the plane

From fig. 4.13, it has been noted that the shear strain and the maximum shear displacement is very much low in comparison with the previous cases while the factor of safety value is in accordance with others. This low value of shear displacement indicates that the slope does not undergo sliding failure. This observation indicates a toppling mode of failure. There are a few reasons which support this conclusion. Firstly, in this case the centre of gravity of each blocks lie outside the base of the blocks. Secondly, the joint sets are dipping into the face. Thirdly, the joints are closely spaced and going away from the slope face. These conditions favour the toppling failure mode.

4.5.3 Results and Discussion

In the above two sections, four cases of the slope with different joint orientations and joint alignments have been investigated. The results of this study is given in table 4.2. Also a brief discussion about the effects of joints on the behaviour of the slope has been given in this section.

Table 4.2: Results of static analysis

Orientation	Cases	Dip Angle (°)	F.O.S	Shear disp. (m)
Out of the plane	1st Case	35	1.32	5.636
	2nd Case	60	1.44	4.525
	3rd Case	75	1.56	3.848
Into the plane	---	70	1.35	0.036

From the results, the following observations can be made.

1) In section 4.5.1 slopes are orientated in out of plane direction. When dip of the joint (ψ_p) is 35° the factor of safety value is 1.32. As ψ_p is increased to 60° and 75°, the factor of safety values have increased to 1.44 and 1.56 respectively. From this observation it can be concluded that slopes having out of plane joints become more stable as ψ_p increases.

2) The maximum shear displacements in the first three cases are 5.636m, 4.525m and 3.848m respectively. These observations show that maximum shear displacement got reduced as ψ_p increases. Also from the plots of the strain contours in Fig. 4.10, Fig. 4.11 and Fig. 4.12, it has been observed that the average shear strains in these cases are approximately 0.5%, 0.2% and 0.08% respectively. These two observations again conclude that as the dip inclination of the out of the plane joints become steeper, the slope becomes more stable.

3) In the case where joint set is dipping into the plane, it can be observed that the maximum shear displacement is very low in comparison to the cases where joint set is dipping out of the plane. In the case described in section 4.5.2, the maximum shear displacement is 0.036 m while in the 3rd case, the maximum shear displacement is 3.848 m which is 100 times more than other case. This drastic reduction indicates that the failure pattern is neither sliding nor plane failure.

4.6 Slope under Excessive Rainfall

Rainfall is one of the major triggering mechanisms due to which rock slide can occur. As the water infiltrates and percolates through the joints, it reduces the friction angle of the joints thus making it more prone to failure. Two cases have been considered here.

1) In the 1st case, a joint set is dipping 35° out of plane.

2) In the 2nd case, a joint set is dipping 70° into the plane.

The initial joint friction angle (jfric) is 40°. To incorporate the rainfall effects, parametric studies has been done by reducing joint friction angle (jfric) in a step-by-step manner. Mohr-Coulomb plasticity model have been assumed for the material. The other rock and discontinuity properties have been considered as per table 4.1.

4.6.1 Joints Dipping Out of Plane

In this case, the dip inclination of the joint set (ψ_p) is 35° out of the plane. Firstly, jfric has been taken as 40°. The condition of the slope at joint friction angle 40° has already been simulated previously in case 1 under section 4.5.1. To simulate the rainfall effects, the jfric value is reduced in a step by step manner. Jfric has been taken as 38°and 34° and for the purpose of doing further parametric studies, jfric has been further reduced to 32° and 30°. The behaviour of the slope at different joint friction angle has been simulated in this section.

a) Jfric 38°: Here the joint friction angle has been taken as 38°. The plot of the shear strain contours along with shear displacement and velocity vectors has been shown in Fig. 4.14.

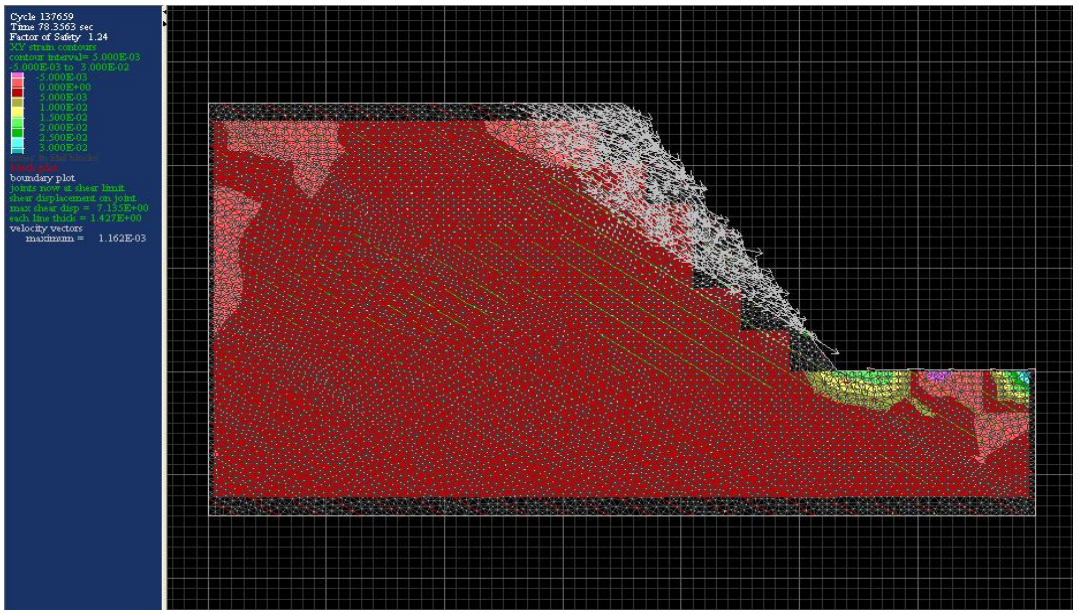

Fig. 4.14: Plot of strain contours with velocity vectors for jfric of 38° out of the plane

It has been observed that the factor of safety value has been reduced from the case with joint friction angle of 40° and the maximum shear displacement has also increased.

b) Jfric 34°: Here the joint friction angle is 34°. The plot of the shear strain contours along with shear displacement and velocity vectors has been shown in Fig. 4.15.

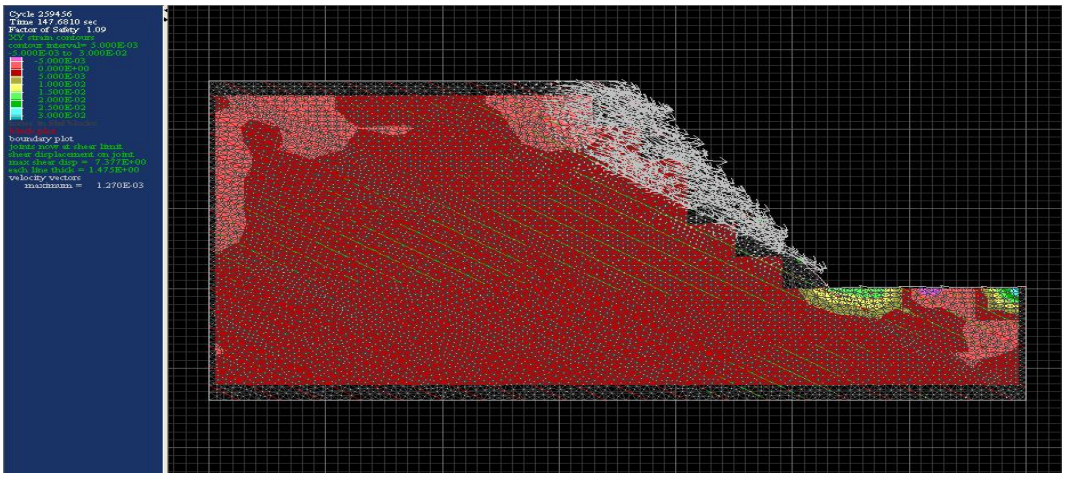

Fig. 4.15: Plot of strain contours with velocity vectors for jfric of 34° out of the plane

It has been observed that the joint friction angle is further reduced and the maximum shear displacement has increased. From the plot it has also been observed that the average shear strain has also increased.

c) Jfric 32°: Here the joint friction angle is 32°. The plot of the shear strain contours along with shear displacement and velocity vectors has been shown in Fig. 4.16.

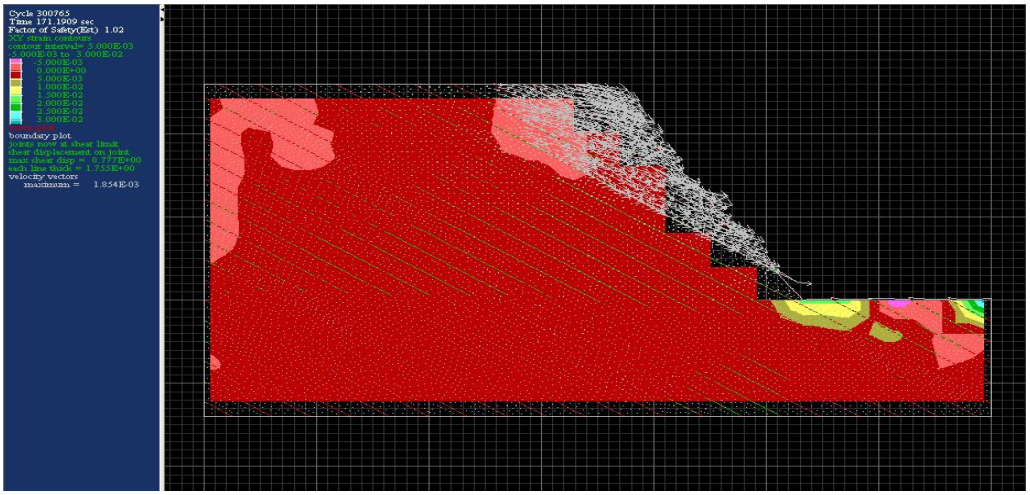

Fig. 4.16: Plot of strain contours with velocity vectors for jfric of 32° out of the plane

It has been observed that as the joint friction angle is less than the dip inclination of the joint (ψ_p), the slope becomes marginally stable. The factor of safety has also been reduced and the shear displacement has increased as well. In this case, the slope reaches at the verge of failure.

d) Jfric 30°: Here the joint friction angle is 30°. The plot of the shear strain contours along with shear displacement and velocity vectors has been shown in Fig. 4.17.

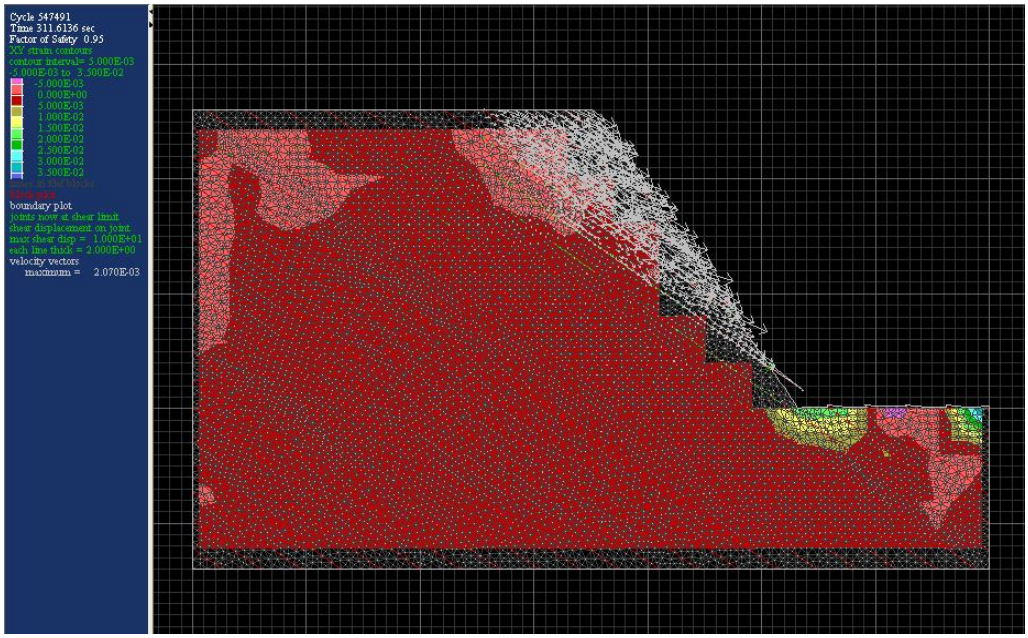

Fig. 4.17: Plot of strain contours with velocity vectors for jfric of 30° out of the plane

In this case, the factor of safety becomes less than 1 which means the slope fails. Here, it can be observed from fig. 4.15 that as the jfric is less than (ψ_p), plane failure is observed. The shear strain has increased and the maximum shear displacement has also increased. The results of the analysis has been shown in table 4.3.

Table 4.3: Slope under rainfall with out of plane joint

Joint Friction Angle (°)	F.O.S	Shear Disp. (m)
40	1.32	5.636
38	1.24	7.135
34	1.09	7.377
32	1.02	8.377
30	0.95	10.00

Table 4.3 shows that as the joint friction angle is reduced, the maximum shear displacement of the slope has increased and the factor of safety value has been reduced. Thus the slope tends towards failure. Also as we know that the dip of the joint set (ψ_p) is 35° so the failure of the slope occurs at jfric 30° which is less than ψ_p. Plane failure is observed in this case.

4.6.2 Joints Dipping Into the Plane

In this case, the dip inclination of the joint set (ψ_p) is 70° into the plane. Firstly, jfric has been taken as 40°. The condition of the slope at joint friction angle 40° has already been simulated previously under section 4.5.2. To simulate the rainfall effects, the jfric value is reduced in a step by step manner. Jfric has been taken as 38°and 32° and for the purpose of doing further parametric studies, jfric has been further reduced to 28° and 24°. The behaviour of the slope at different joint friction angle has been simulated in this section.

a) Jfric 38°: Here the joint friction angle has been taken as 38°. The plot of the shear strain contours along with shear displacement and velocity vectors has been shown in Fig. 4.18.

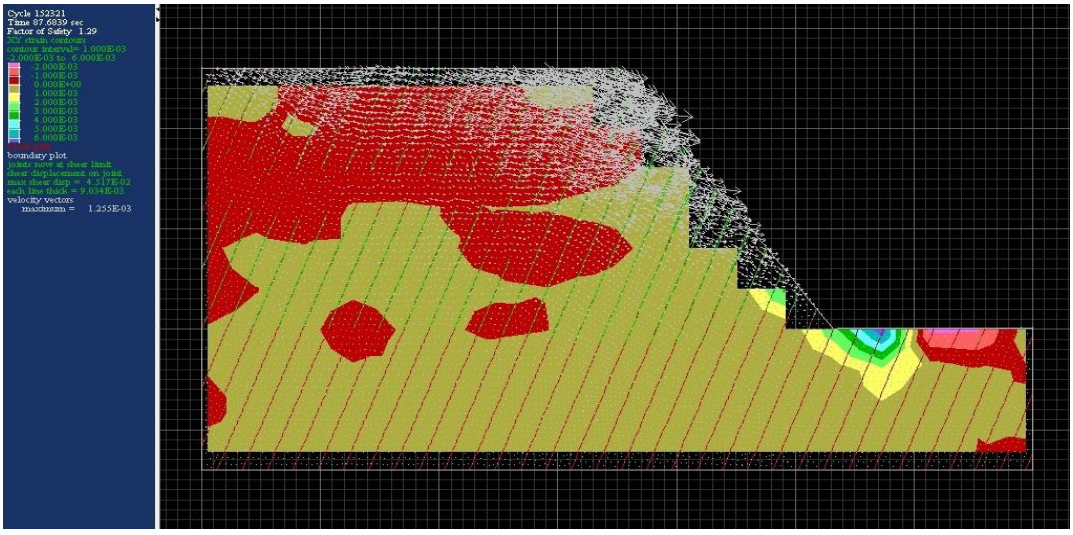

Fig. 4.18: Plot of strain contours with velocity vectors for jfric of 38° into the plane

It can be observed that the factor of safety value has been decreased from the case where jfric was 40°. Also it has been observed that the maximum shear displacement has increased. But it can be observed that the shear displacement is very low in comparison with the slope having (ψ_p) of 35° out of the plane, with jfric 38°. This difference shows that plane failure does not occur in this case.

b) Jfric 32°: Here the joint friction angle has been taken as 32°. The plot of the shear strain contours along with shear displacement and velocity vectors has been shown in Fig. 4.19.

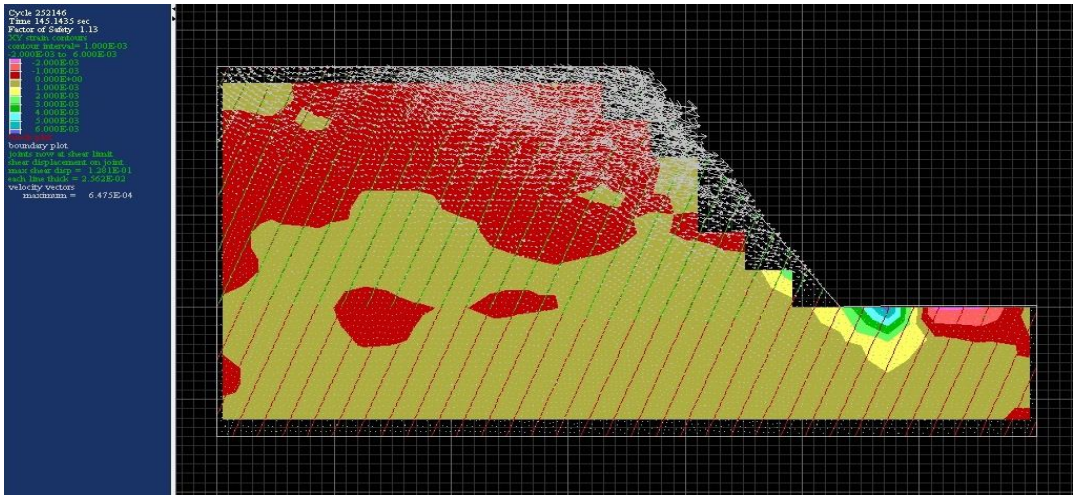

Fig. 4.19: Plot of strain contours with velocity vectors for jfric of 32° into the plane

In this case, as jfric reduces, the slope becomes more unstable. The reduction of factor of safety value and the increase in the maximum shear displacement, establishes this fact. Similarly the maximum shear displacement is observed to be very low in comparison with the case 'c' under section 4.6.1. This difference denotes that the slope does not undergo a sliding or plane failure.

c) Jfric 28°: Here the joint friction angle has been taken as 28°. The plot of the shear strain contours along with shear displacement and velocity vectors has been shown in Fig. 4.20.

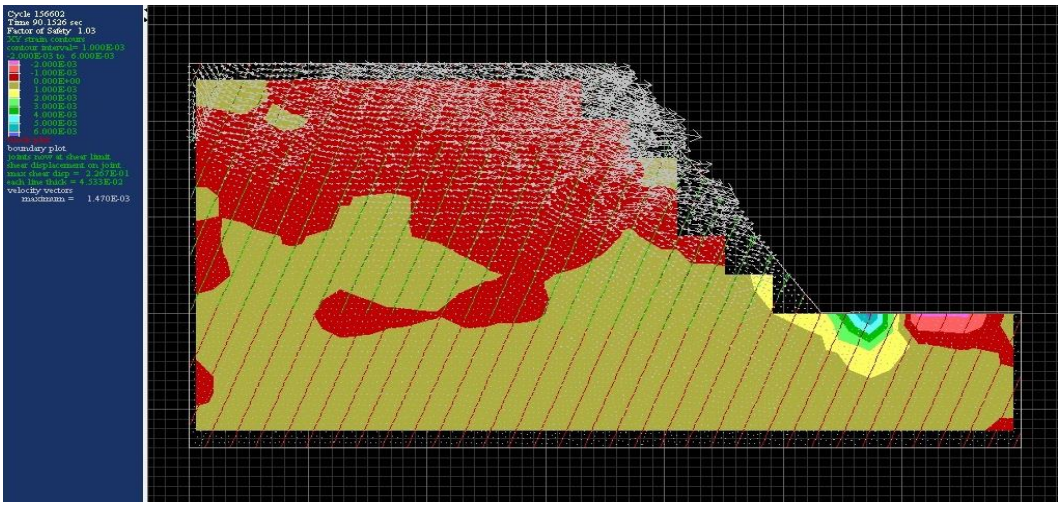

Fig. 4.20: Plot of strain contours with velocity vectors for jfric of 28° into the plane

In this case, as the jfric value reduces, the slope becomes more unstable. The factor of safety value reduces and the maximum shear displacement increases. But as the value of the shear displacement is not significant, plane or sliding failure does not take place. Also as the closely spaced joint set is dipping into the plane, toppling is the likely mode of failure.

d) Jfric 24°: Here the joint friction angle has been taken as 24°. The plot of the shear strain contours along with shear displacement and velocity vectors has been shown in Fig. 4.21.

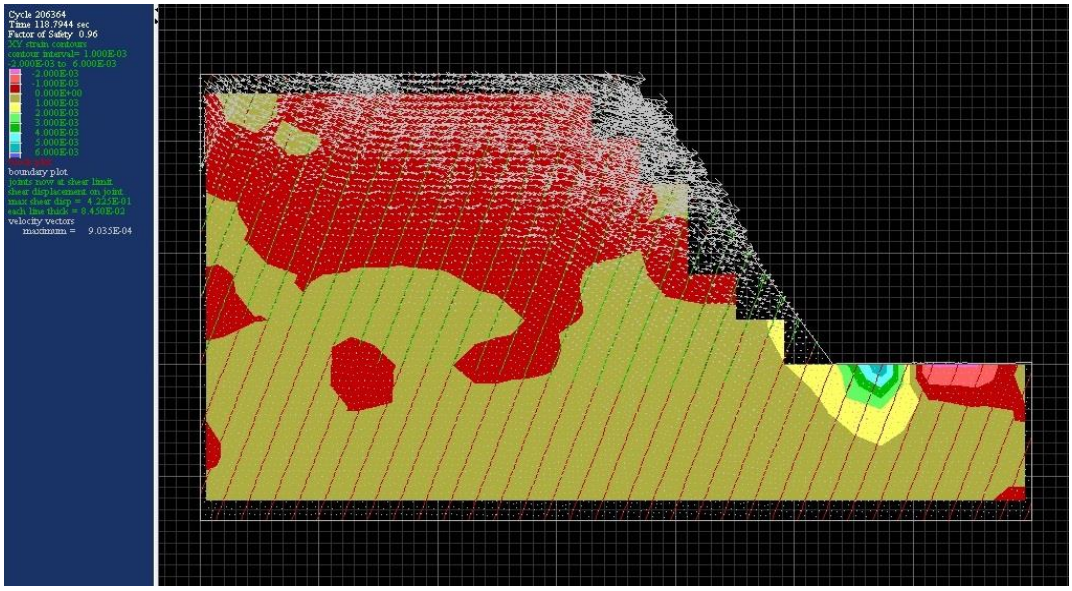

Fig. 4.21: Plot of strain contours with velocity vectors for jfric of 24° into the plane

In Fig. 4.21, it has been observed that the factor of safety value has become less than 1. This means that the slope has failed. But the shear displacement is very low in comparison to case'd' under section 4.6.1. This observation again establish the fact that the failure is not due to sliding or shear displacement. The results of the analysis has been shown in Table 4.4.

Table 4.4: Slope under rainfall with into the plane joint

Joint Friction Angle (°)	F.O.S	Shear Disp. (m)
40	1.35	0.036
38	1.29	0.045
32	1.13	0.128
28	1.03	0.227
24	0.96	0.422

Table 4.4 shows that as the joint friction angle has been reduced, the factor of safety has also been reduced and the shear displacement has increased in a step-by-step approach. But it can also be observed that the shear displacement is very low.

4.6.3 Observations and Discussions

The following observations and discussions can be made out of the above analysis of slopes under excessive rainfall.

1) To simulate the rainfall effects, the joint friction angle is reduced gradually. It has been observed from both the cases that as jfric got reduced, the slope becomes less stable.

2) In the first case, when the joint sets are dipping out of the plane, as the jfric value reduced in each step, the factor of safety value also reduced and the maximum shear displacement values got increased. Also the plots of the shear strain contours with velocity vectors (Fig. 14 to Fig. 17) shows a plane failure occurs.

3) In the second case, when the joint sets are dipping into the plane, as the jfric value reduced in each step, though the factor of safety value has reduced, but the increase in the maximum shear displacement is not a prominent one. The plots of the shear strain contours with velocity vectors (Fig. 18 to Fig. 21) shows that a plane or sliding failure is unlikely to occur. This proves that sliding is not the failure mode when joint sets dip into the plane.

4) If we compare this case under section 4.6.1 with the case described in section 4.6.2, we can see that there is a large difference between the shear displacements. In the previous case, when the slope fails at a jfric of 30°, the factor of safety was 0.95 and the shear displacement was 10 m. But in case 4.6.2, when the slope fails at a jfric of 24°, the factor of safety was also found out to be nearly equal, i.e., 0.95, but the shear displacement is 0.422 m which is very less in compare to the other. This observation indicates that, in slopes where joint set dips into the plane, the slope becomes more stable against sliding failure and becomes prone to toppling failure.

4.7 Slope under Seismic Loading

Seismic loading is one of the major triggering mechanism which causes landslides in rock slopes. Slopes behave differently depending upon the number of joint sets and the alignment of them, under seismic condition. Three cases have been considered in this case.

1) Slope having one joint set dipping 70° out of the plane
2) Slope having one joint set dipping 70° into the plane.
3) Slope having two perpendicular joint sets.

In the seismic analysis, elastic, isotropic constitutive model has been taken for the material. For each cases, first the static in-situ analysis has been done and then the seismic loading has been applied into the model. The seismic loading has been applied as a sinusoidal stress history at the base of the model. The stress history represents the seismic loading of Uttarkashi earthquake of October 20, 1991. The sinusoidal shear wave which has been applied at the base of the model has a frequency of 3 Hz for a period of 3 sec and PGA of 0.3g. When the sinusoidal loading is applied, the boundary condition has been changed to free field/viscous boundary at the base and in the sides of the model. The viscous boundary conditions are applied to absorb the incoming waves hitting the boundaries. It prevents the reflection of the waves back into the model.

4.7.1 Formulation of Harmonic Excitation

The material properties considered for the analysis is given in table 4.1 except the cohesion for the rock mass is considered to be zero according to the elastic, isotropic model and the joint spacing is variable for the different cases. The specific joint spacing is given in the appropriate sections where the three cases are described. The sinusoidal shear wave is applied at the base of the model. It is applied to propagate in the upward direction. The amplitude of the shear wave is calculated as given below:

$$\tau = v_s \rho v_{max} \tag{4.21}$$

$$v_s = \sqrt{(G/\rho)} \tag{4.22}$$

Where, v_s = shear wave velocity = 1410 m/s,

ρ = mass density of the rock,

v_{max}= peak ground velocity (0.162 m/s).

This is calculated to correspond to the PGA as observed in the Uttarkashi earthquake record of October 20, 1991.

The shear stress calculated as per equation 4.19 is,

$\tau = 1410 * 2610 * 0.162 = 0.596$ MPa

For the simplicity, it is assumed that isotropic conditions prevail. Therefor the shear stress calculated according to equation 4.19 is multiplied by 2. The amplitude of the sinusoidal shear wave is calculated as 1.2 MPa. The sinusoidal shear wave, which is applied at the base of the model is shown in Fig. 4.22.

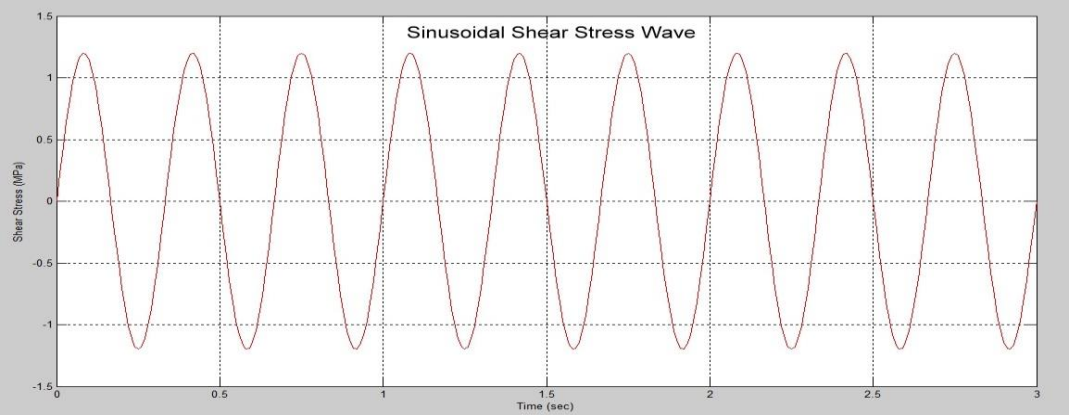

Fig. 4.22: Input sinusoidal shear stress waveform at the base of the model

4.7.2 Joints Dipping Out of Plane

In this case, one joint set is considered. The joint set is having a dip inclination (ψ_p) of 70° out of the plane with 20 m spacing. First the static in-situ analysis is done. After that the sinusoidal shear stress wave is applied at the base of the model. The boundary conditions have been changed to free-field/viscous boundary to absorb the reflection of the wave into the model. The loading is applied gradually with time. Response of the slope has been measured until it fails. The following total displacement plots show the mechanism of failure. Total displacement is denoted by 'd' and incremental displacement is denoted by 'Δd'.

a) Under gravity loading:

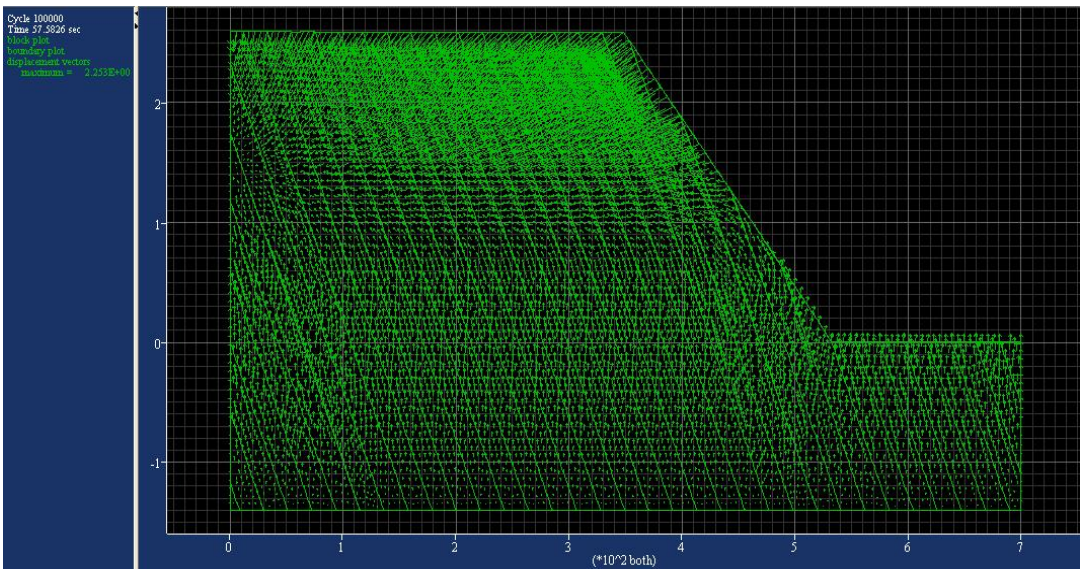

Fig. 4.23: Displacement plot at gravity loading for out of plane joints

Fig. 4.23 shows the plot of displacement vectors of the model under gravity loading. The maximum displacement under gravity loading is 2.253 m.

b) After 1 sec of seismic loading:

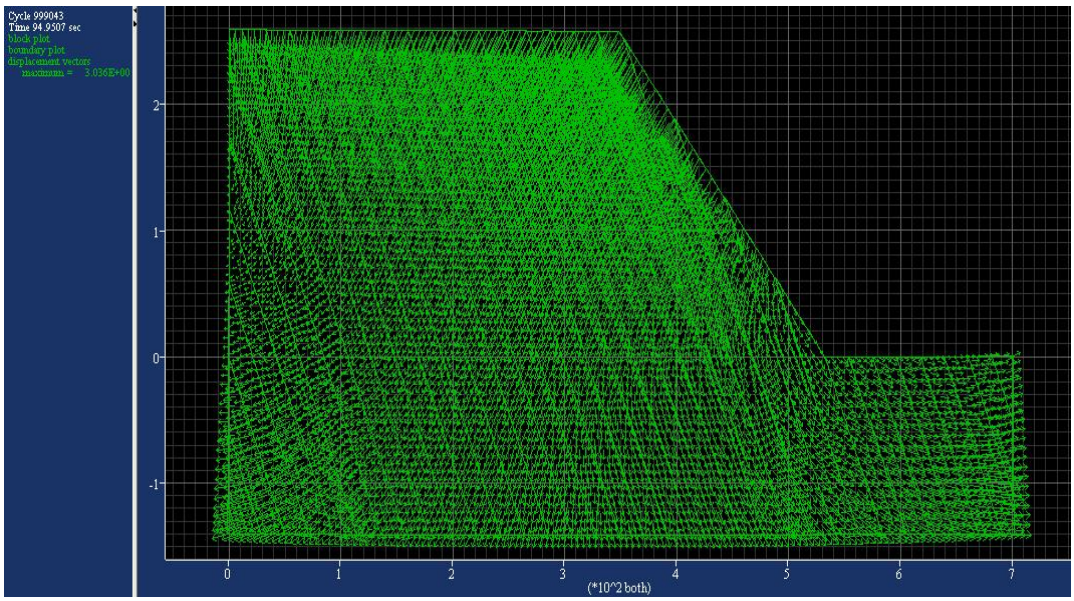

Fig. 4.24: displacement plot after 1 sec of seismic loading with joints dipping out of the plane

Fig. 4.24 shows the displacement plot of the slope after 1 second of seismic loading. The maximum displacement has found out to be 3.036 m while the increase in displacement (Δd) from the previous case is 0.783 m.

c) After 3 sec of seismic loading:

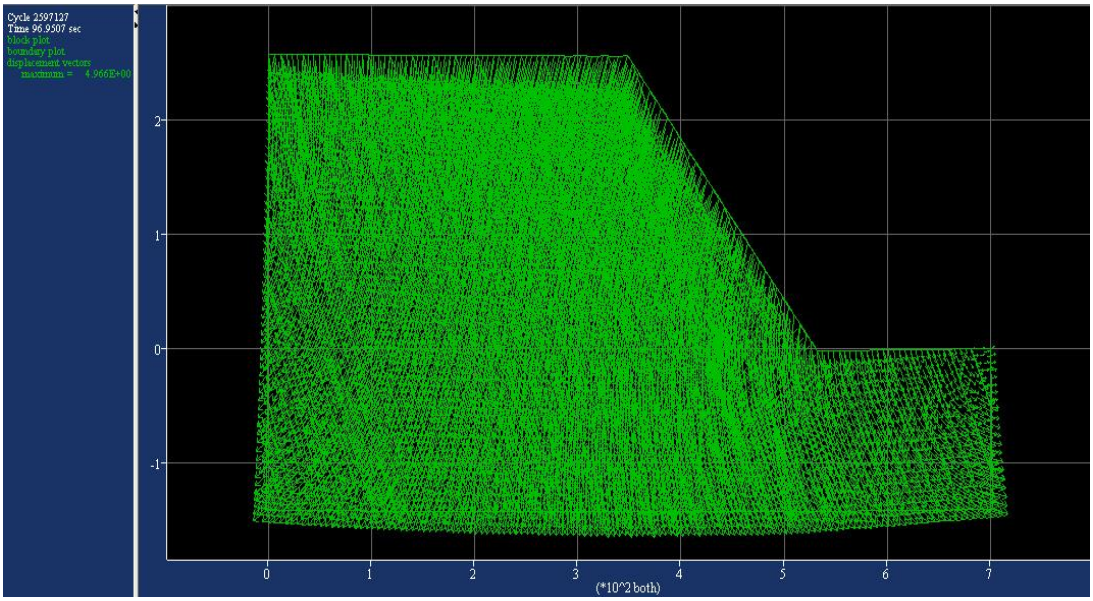

Fig. 4.25: displacement plot after 3 sec of seismic loading with joints dipping out of the plane

Fig. 4.25 shows the displacement plot of the slope after 3 second of seismic loading. The maximum displacement has found out to be 4.966 m while the increase in displacement (Δd) from the previous case is 1.93 m.

d) After 5 sec from the start of seismic loading:

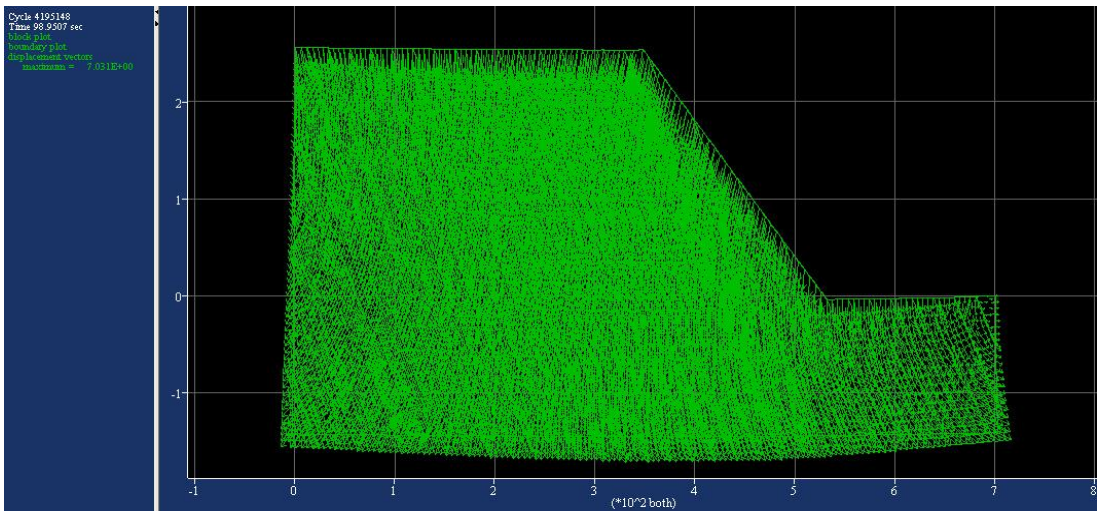

Fig. 4.26: displacement plot after 5 sec of seismic loading with joints dipping out of the plane

Fig. 4.26 shows the displacement plot of the slope after 5 second of seismic loading. The maximum displacement has found out to be 7.031 m while the increase in displacement (Δd) from the previous case is 2.065 m.

e) After 7 sec from the start of seismic loading:

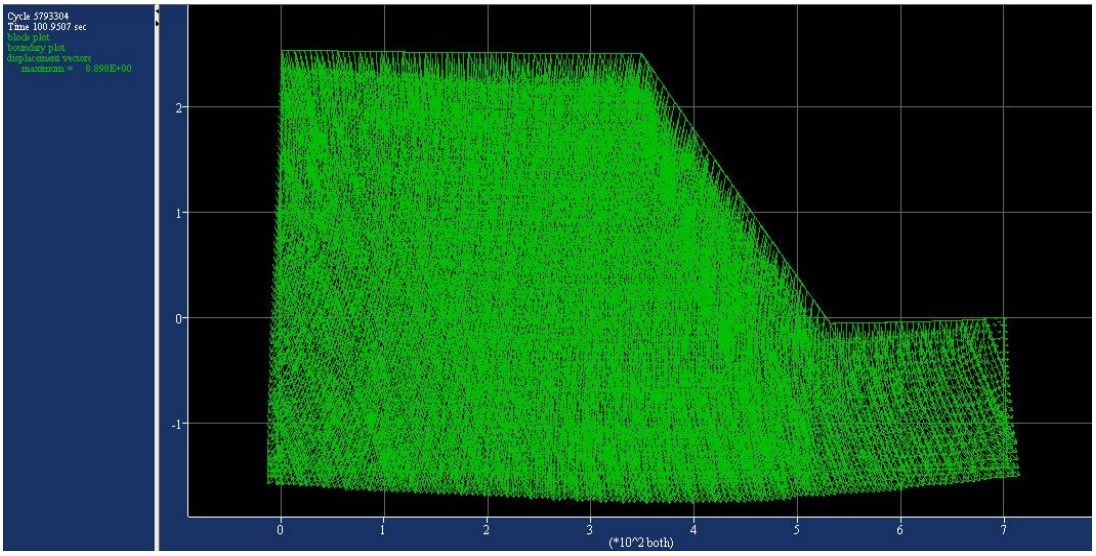

Fig. 4.27: displacement plot after 7 sec of seismic loading with joints dipping out of the plane

Fig. 4.27 shows the displacement plot of the slope after 7 second of seismic loading. The maximum displacement has found out to be 8.898 m while the increase in displacement (Δd) from the previous case is 1.867 m.

f) After 9 sec from the start of seismic loading:

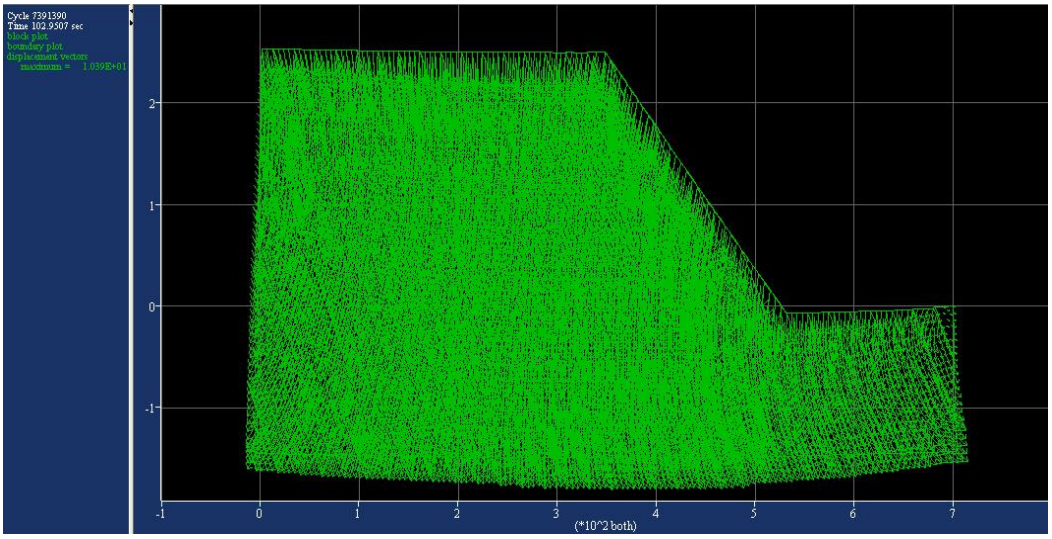

Fig. 4.28: displacement plot after 9 sec of seismic loading with joints dipping out of the plane

Fig. 4.28 shows the displacement plot of the slope after 9 second of seismic loading. The maximum displacement has found out to be 10.39 m while the increase in displacement (Δd) from the previous case is 1.492 m.

g) Displacement plot after 11 sec from the start of seismic loading:

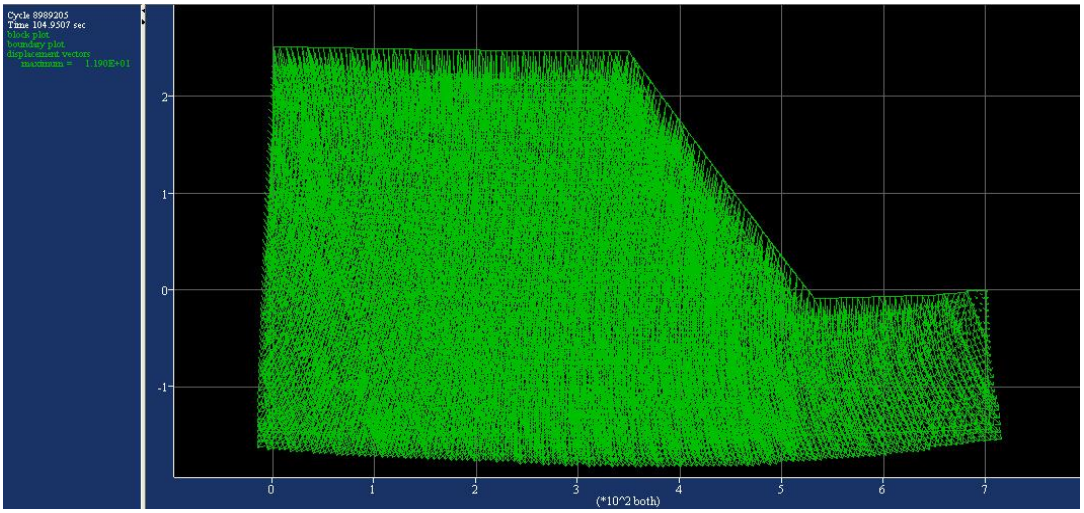

Fig. 4.29: displacement plot after 11 sec of seismic loading with joints dipping out of plane

Fig. 4.29 shows the displacement plot of the slope after 11 second of seismic loading. The maximum displacement has found out to be 11.90 m while the increase in displacement (Δd) from the previous case is 1.51 m.

f) After 11.259 sec of from the start seismic loading (slope failed):

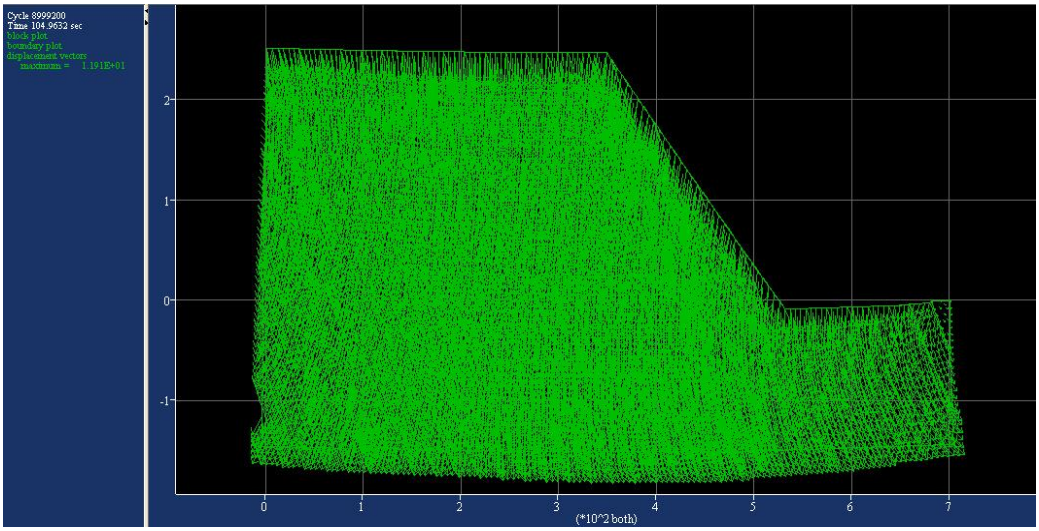

Fig. 4.30: displacement plot after 11.26sec of seismic loading with joints dipping out of plane

Fig. 4.30 shows the displacement plot of the slope after 11.259 second of seismic loading. The maximum displacement has found out to be 11.91 m while the increase in displacement (Δd) from the previous case is 0.01 m. In this case, the penetration of one block into another has become so large that the slope has failed.

Results: Table 4.5 shows the results in a tabular form.

Table 4.5: Seismic results for one joint set dipping 70° out of plane

Time Duration (sec)	Max. Total Displacement (m)	Max. Shear Displacement (m)	Block Rotation (m)
Gravity Loading	2.253	0.210	0.305
After 1 sec	3.036	0.238	0.365
After 3 sec	4.966	0.351	0.780
After 5 sec	7.031	0.687	1.105
After 7 sec	8.898	1.026	1.396
After 9 sec	10.39	1.409	1.678
After 11 sec	11.90	1.670	1.997
After 11.259 sec (failed)	11.91	1.671	1.999

Observations and Discussions:

1) It can be seen from Table 4.5, that in the seismic case, the total and shear displacement has increased from gravity loading. The slope fails after 11 sec.

2) At 11.259 sec when the slope failed we can see from the results that the increment of shear displacements and block rotation is almost nil from the previous one. This is because too great contact overlap. This means that the penetration of one block into another is so great, that there is no displacement. This situation refers to the failure of slope.

4.7.3 Joints Dipping Into the Plane

In this case, one joint set is considered. The joint set is having a dip inclination (ψ_p) of 70° into the plane with 20 m spacing. First the static in-situ analysis is done. After

that the sinusoidal shear stress wave is applied at the base of the model. The boundary conditions have been changed to free-field/viscous boundary to absorb the reflection of the wave into the model. The loading is applied gradually with time. Response of the slope has been measured with time. The following total displacement plots show the mechanism of failure. Total displacement is denoted by ‘d’ and incremental displacement is denoted by ‘Δd’.

a) Under gravity loading:

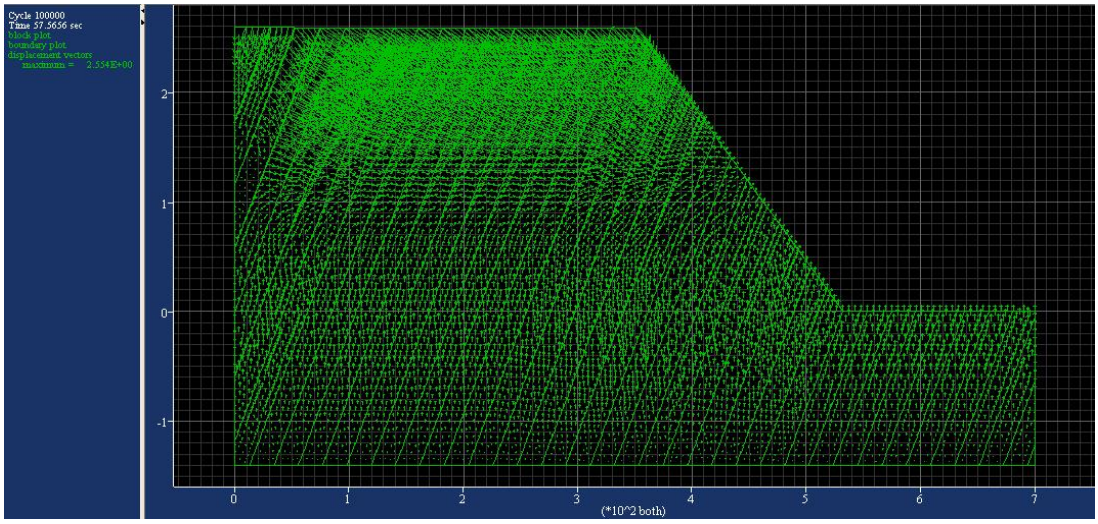

Fig. 4.31: Displacement plot at gravity loading for into the plane joints

Fig. 4.31 shows the plot of displacement vectors of the model under gravity loading. The maximum displacement under gravity loading is 2.554 m.

b) After 1 sec of seismic loading:

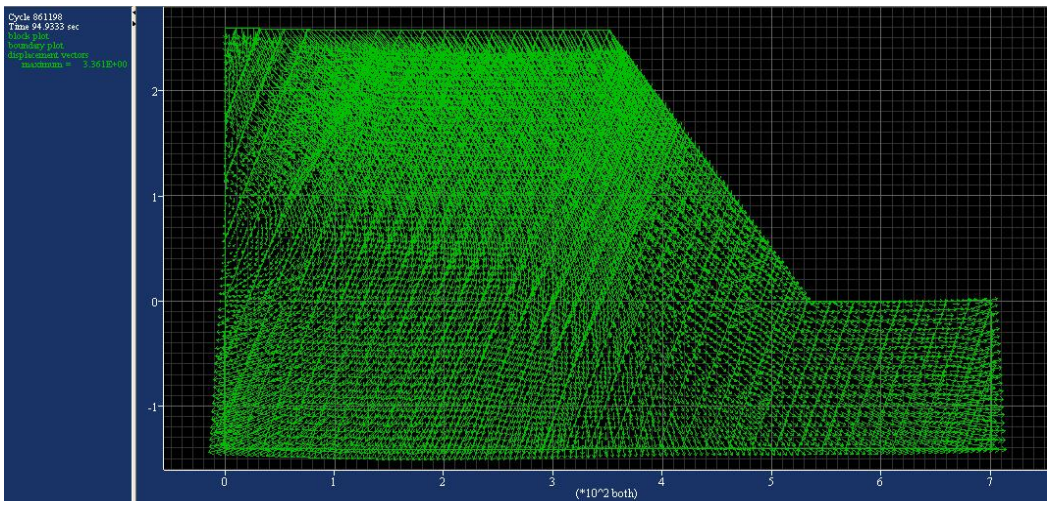

Fig. 4.32: displacement plot after 1 sec of seismic loading with joints dipping into the plane

Fig. 4.32 shows the displacement plot of the slope after 1 second of seismic loading. The maximum displacement has found out to be 3.361 m while the increase in displacement (Δd) from the previous case is 0.807 m.

c) After 3 sec of seismic loading:

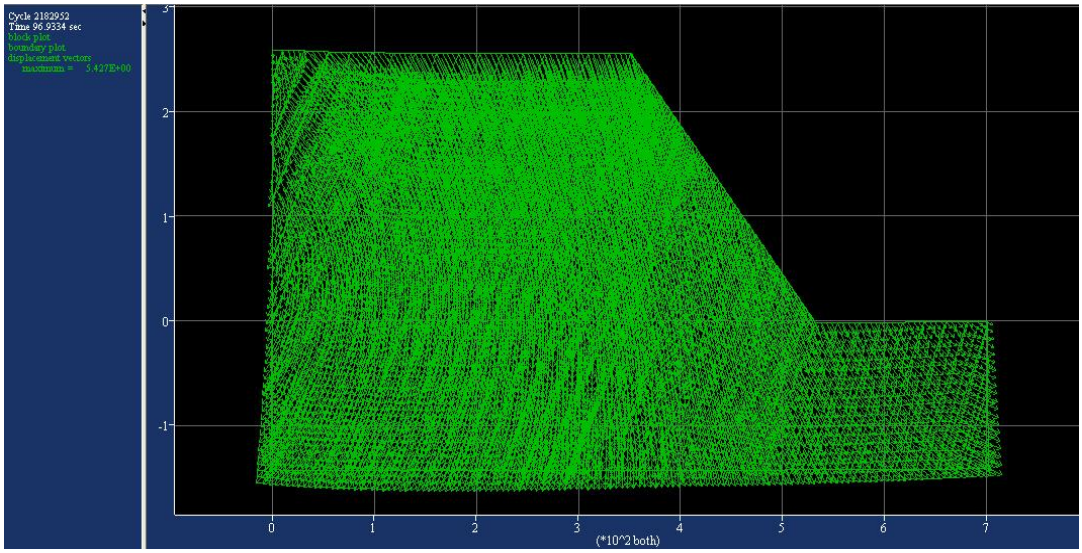

Fig. 4.33: displacement plot after 3 sec of seismic loading with joints dipping into the plane

Fig. 4.33 shows the displacement plot of the slope after 3 second of seismic loading. The maximum displacement has found out to be 5.427 m while the increase in displacement (Δd) from the previous case is 2.066 m.

d) After 5 sec from the start of seismic loading:

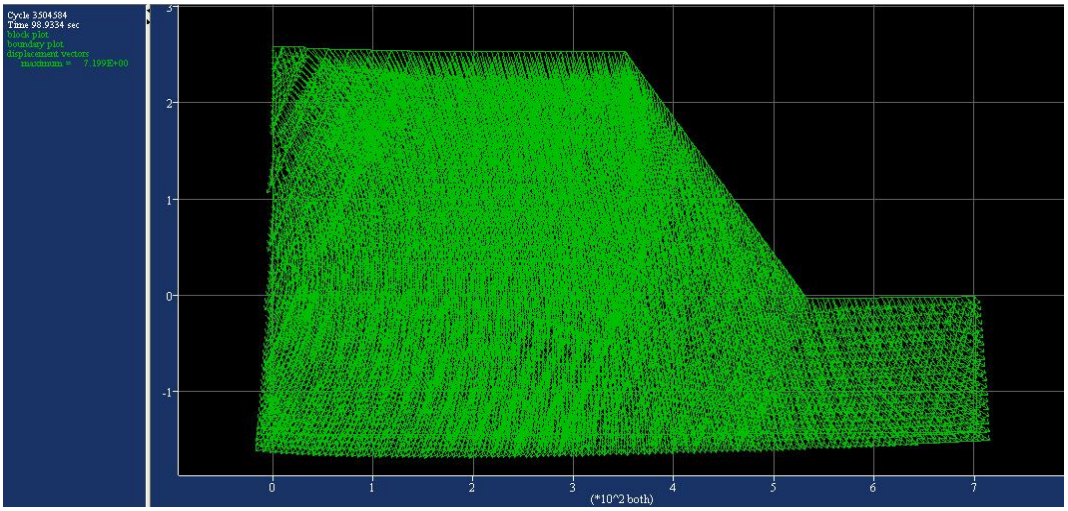

Fig. 4.34: displacement plot after 5 sec of seismic loading with joints dipping into the plane

Fig. 4.34 shows the displacement plot of the slope after 5 second of seismic loading. The maximum displacement has found out to be 7.2 m while the increase in displacement (Δd) from the previous case is 1.733 m.

e) After 7 sec from the start of seismic loading:

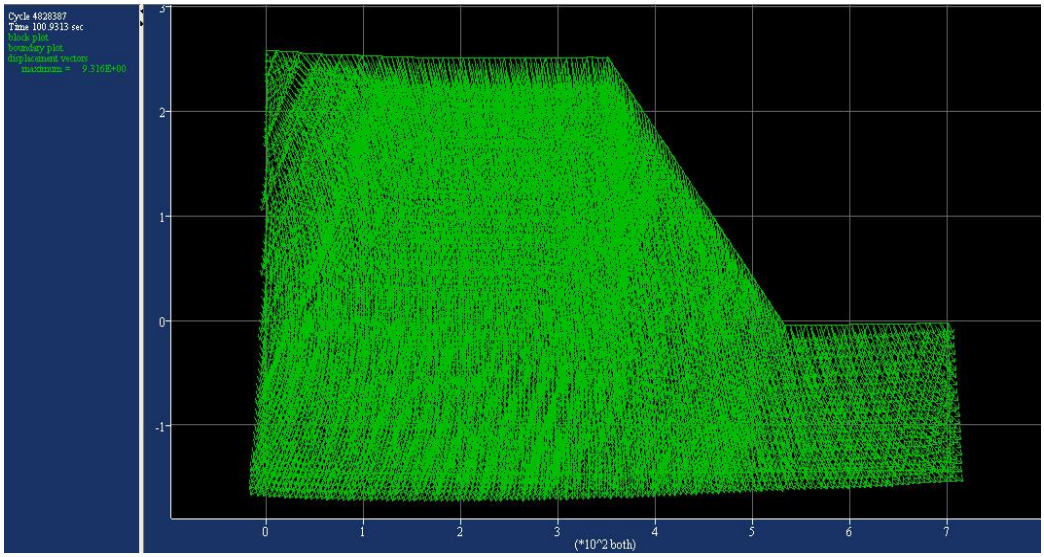

Fig. 4.35: displacement plot after 7 sec of seismic loading with joints dipping into the plane

Fig. 4.35 shows the displacement plot of the slope after 7 second of seismic loading. The maximum displacement has found out to be 9.316 m while the increase in displacement (Δd) from the previous case is 2.166 m.

f) After 9 sec from the start of seismic loading:

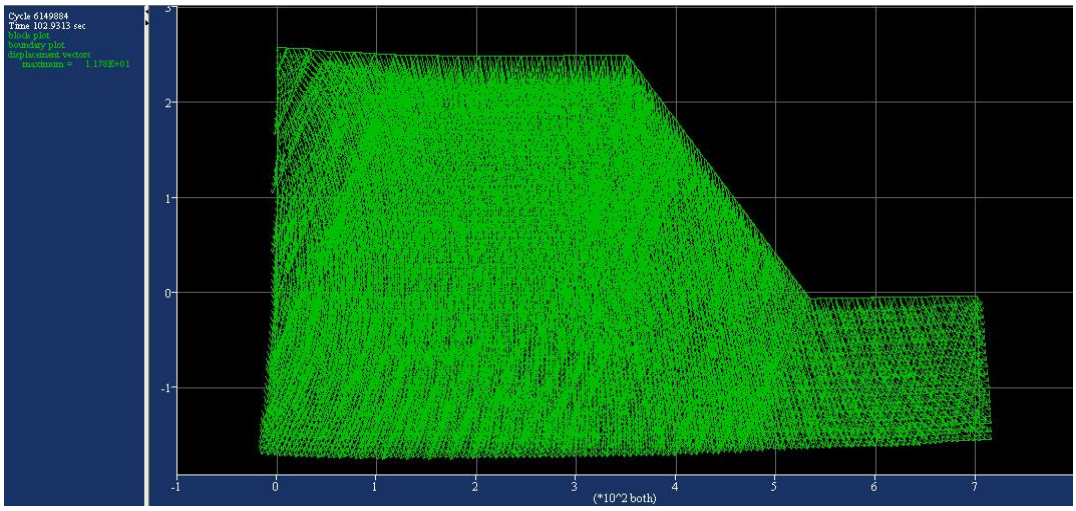

Fig. 4.36: displacement plot after 9 sec of seismic loading with joints dipping into the plane

Fig. 4.36 shows the displacement plot of the slope after 9 second of seismic loading. The maximum displacement has found out to be 11.78 m while the increase in displacement (Δd) from the previous case is 2.464 m.

g) After 11 sec from the start of seismic loading:

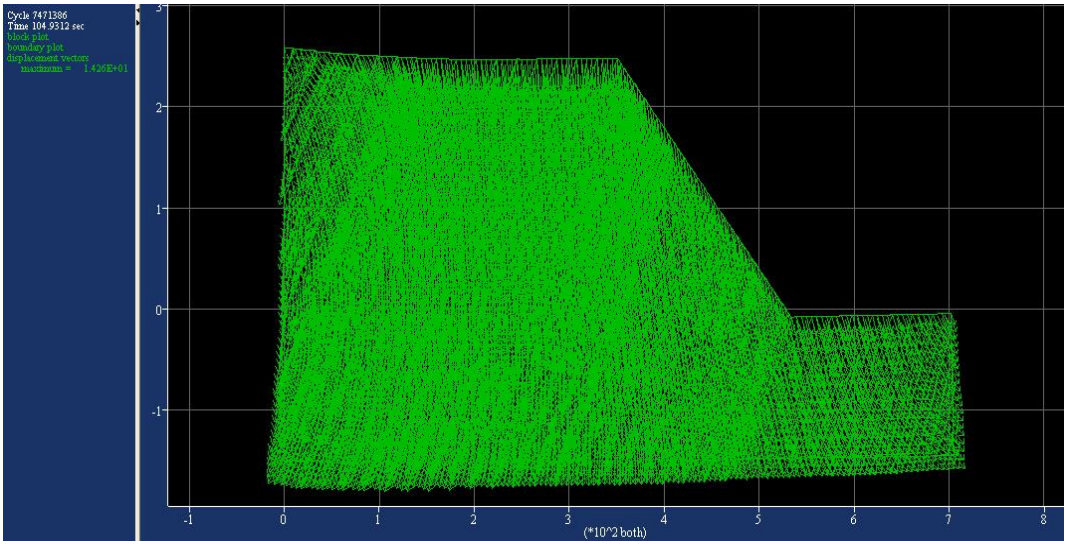

Fig. 4.37: displacement plot after 11 sec of seismic loading with joints dipping into the plane

Fig. 4.37 shows the displacement plot of the slope after 11 second of seismic loading. The maximum displacement has found out to be 14.26 m while the increase in displacement (Δd) from the previous case is 2.48 m.

h) After 13 sec from the start of seismic loading:

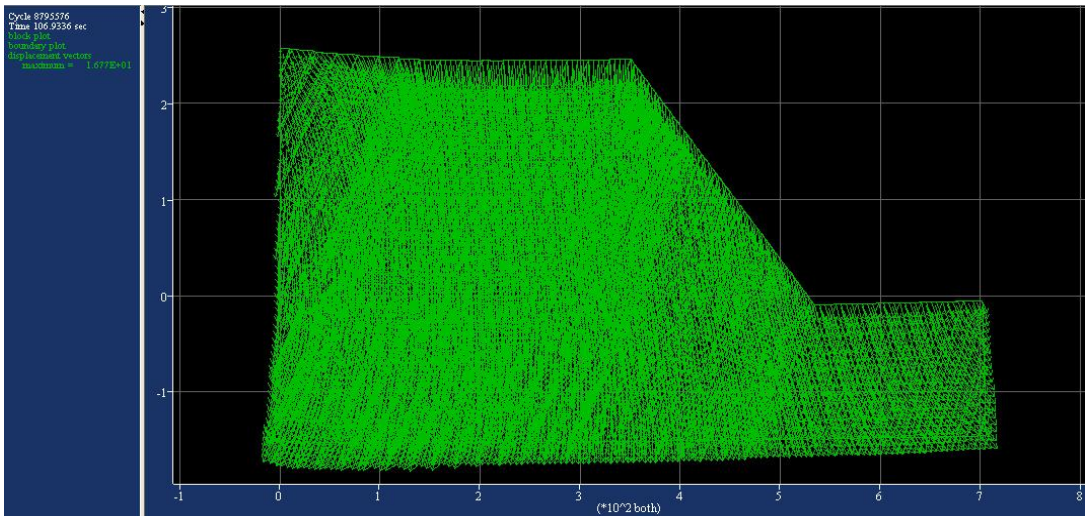

Fig. 4.38: displacement plot after 13 sec of seismic loading with joints dipping into the plane

Fig. 4.38 shows the displacement plot of the slope after 13 second of seismic loading. The maximum displacement has found out to be 16.77 m while the increase in displacement (Δd) from the previous case is 2.51 m.

Results: Table 4.6 shows the results in a tabular form

Table 4.6: Seismic results for one joint set dipping 70° into the plane

Time Duration (sec)	Max. Total Displacement (m)	Max. Shear Displacement (m)	Block Rotation (m)
Gravity Loading	2.554	0.220	0.580
After 1 sec	3.361	0.255	0.756
After 3 sec	5.427	0.262	1.315
After 5 sec	7.200	0.368	1.902
After 7 sec	9.316	0.671	2.133
After 9 sec	11.78	1.035	2.340
After 11 sec	14.26	1.494	2.585
After 13 sec	16.77	1.886	2.789

Observations and Discussions:

1) From Table 4.6, it is observed that the total and shear displacement have increased along with time after gravity loading. It is also observed that block rotation has also increased with time.

2) It is observed that the block rotation is higher in the case having joints dipping into the plane in comparison with joints dipping out of the plane (Table 4.5). Also the displacement plots have indicated that in the left portion of the slope, slabs of blocks are coming out. These observations confirm that when a slope has joint sets dipping into the plane, it undergoes toppling mode of failure.

3) It has also been observed that in this case, the slope remains stable even after 13 sec. It indicates that the slope having joint sets with inclination opposite to the dip of the slope angle ψ_f, is more stable than slopes having joint sets sub-parallel to the slope face.

For comparing the results obtained in section 4.7.2 and 4.7.3, two graphs have been plotted with the help of the results showed in Table 4.5 and 4.6. These two graphs help to understand the stability and failure of slopes having out of the plane and into the plane joint sets.

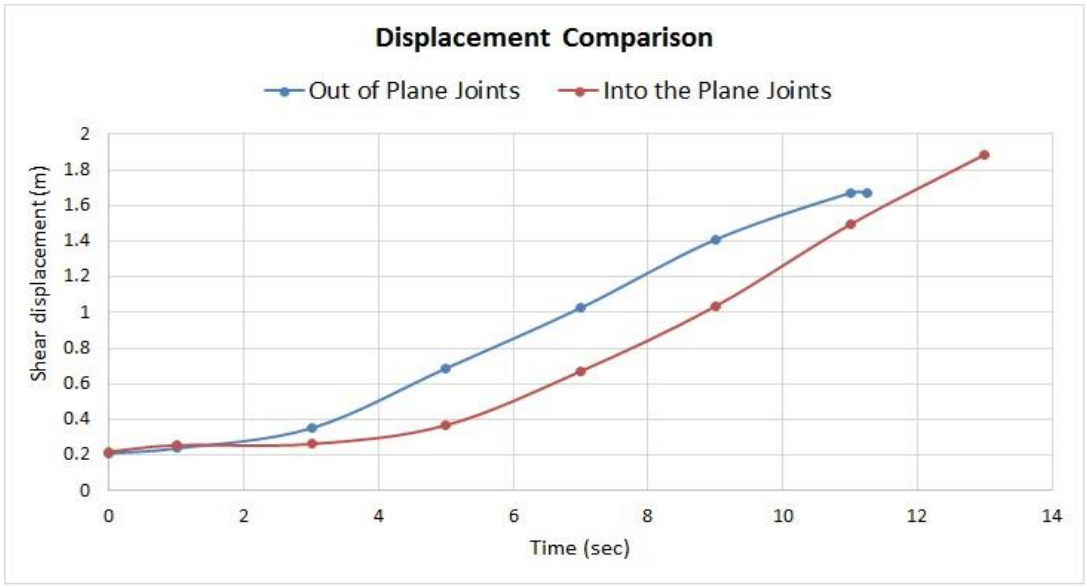

Fig. 4.39: displacement comparison between two joint orientations

From Fig. 4.39, it can be clearly noticed that the slope having joint sets orienting in out of plane direction, is less stable against shear failure in comparison to the slope having joint sets dipping in an into the plane direction. It is also observed that the slope having out of plane joint sets, fails in sliding, earlier than the other one.

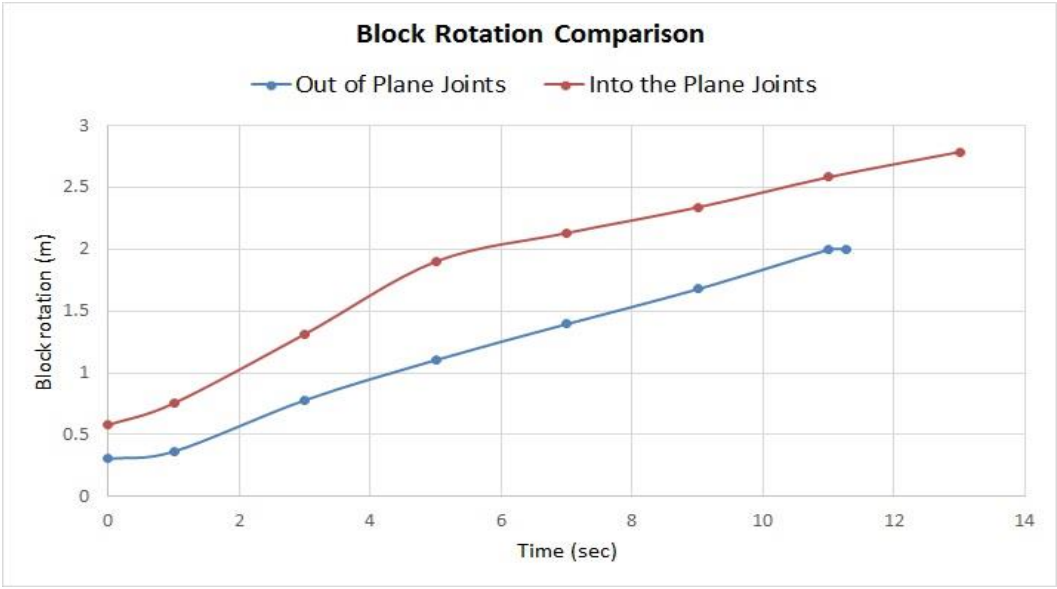

Fig. 4.40: block rotation comparison between two joint orientations

From Fig. 4.40, it can be clearly noticed that the slope having joint sets orienting in out of plane direction, is more stable against rotational failure in comparison to the slope having joint sets dipping in an into the plane direction. Block rotation is more in the into the plane case at all the time instants, in comparison to the other case.

4.7.4 Slope with Two Perpendicular Joints

In this case, two perpendicular joint sets are incorporated into the model. One joint set is having ψ_p of 70° into the plane and the other joint set is having ψ_p of 20° out of the plane. The spacing of the joints are 30 m and 20 m respectively. First the static in-situ analysis is done. After that the sinusoidal shear stress wave is applied at the base of the model. The boundary conditions have been changed to free-field/viscous boundary to absorb the reflection of the wave into the model. The loading is applied gradually with time. Response of the slope has been measured until it fails. The following total displacement plots show the mechanism of failure. Total displacement is denoted by 'd' and incremental displacement is denoted by 'Δd'.

a) Under gravity loading:

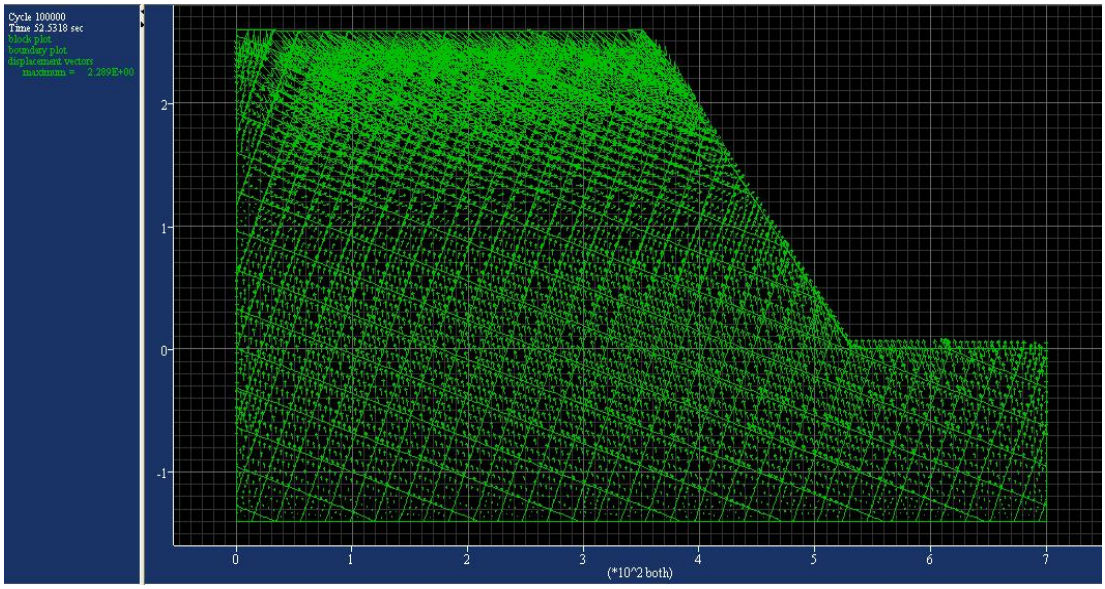

Fig. 4.41: Displacement plot at gravity loading for two joint sets

Fig. 4.41 shows the plot of displacement vectors of the model under gravity loading. The maximum displacement under gravity loading is 2.289 m.

b) After 1 sec of seismic loading:

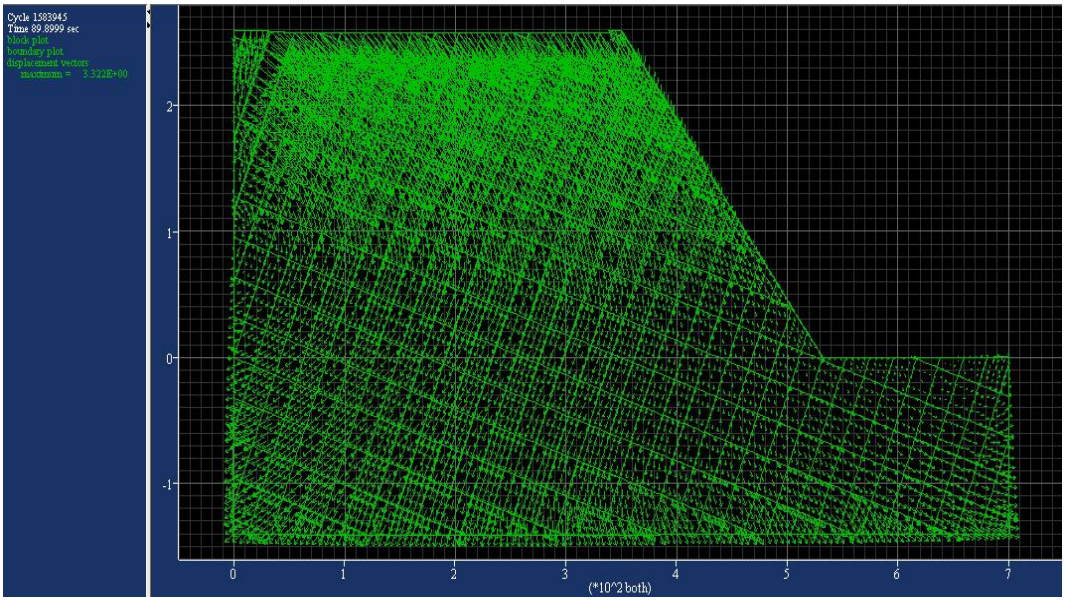

Fig. 4.42: Displacement plot after 1 sec of seismic loading for two joint sets

Fig. 4.42 shows the displacement plot of the slope after 1 second of seismic loading. The maximum displacement has found out to be 3.322 m while the increase in displacement (Δd) from the previous case is 1.033 m.

c) After 3 sec of seismic loading:

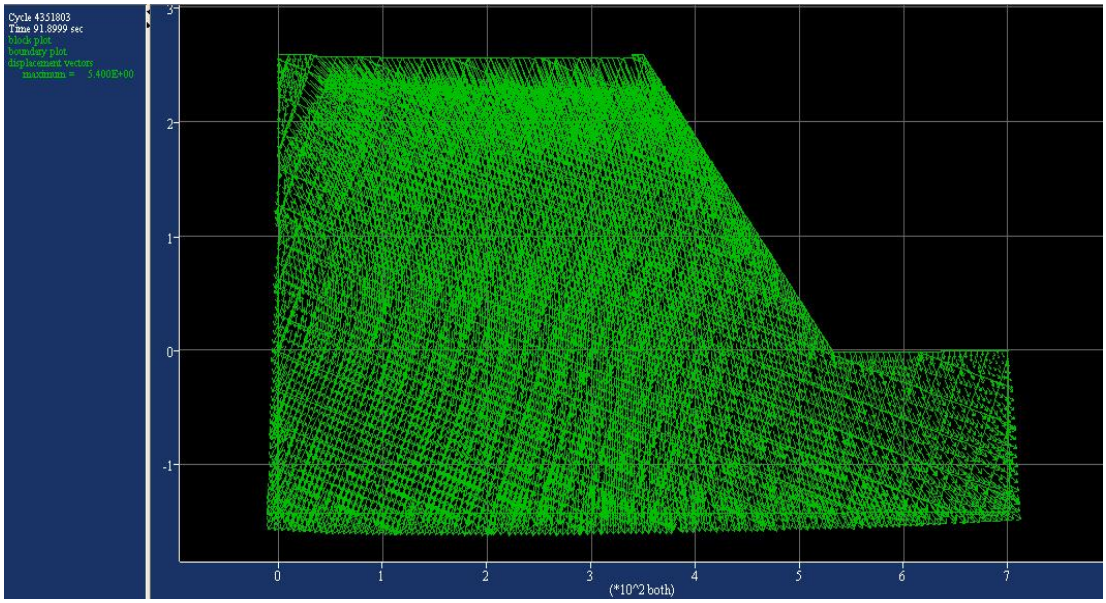

Fig. 4.43: Displacement plot after 3 sec of seismic loading for two joint sets

Fig. 4.43 shows the displacement plot of the slope after 3 second of seismic loading. The maximum displacement has found out to be 5.4 m while the increase in displacement (Δd) from the previous case is 2.078 m.

d) After 5 sec from the start of seismic loading:

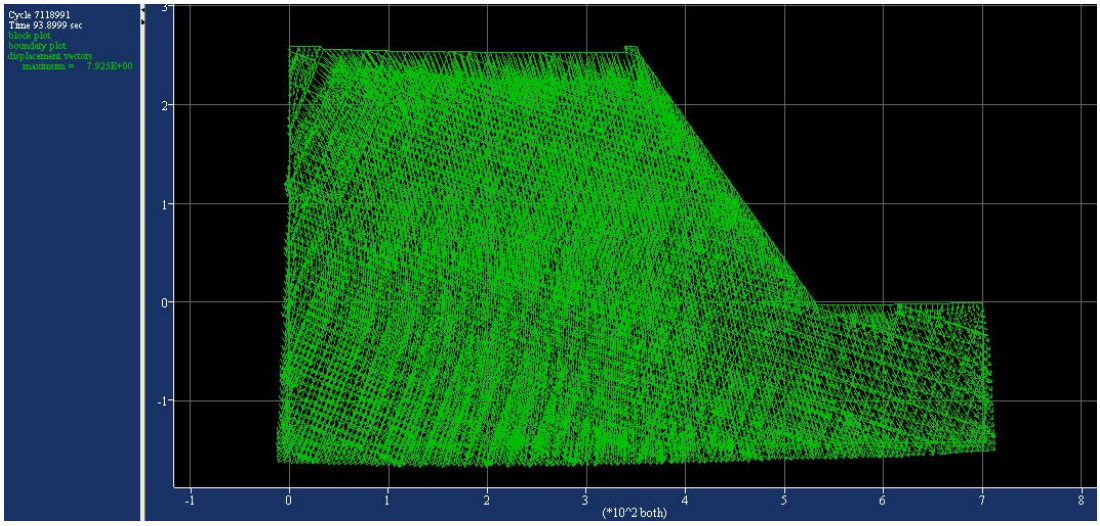

Fig. 4.44: Displacement plot after 5 sec of seismic loading for two joint sets

Fig. 4.44 shows the displacement plot of the slope after 5 second of seismic loading. The maximum displacement has found out to be 7.925 m while the increase in displacement (Δd) from the previous case is 2.525 m.

e) After 7 sec from the start of seismic loading:

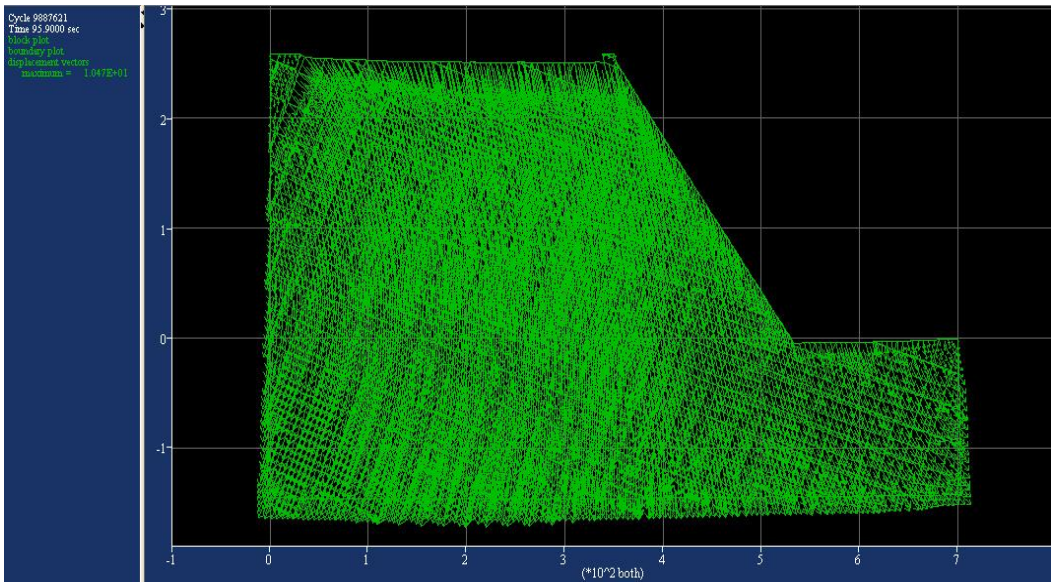

Fig. 4.45: Displacement plot after 7 sec of seismic loading for two joint sets

Fig. 4.45 shows the displacement plot of the slope after 7 second of seismic loading. The maximum displacement has found out to be 10.47 m while the increase in displacement (Δd) from the previous case is 2.545 m.

f) After 7.772 sec from the start of seismic loading (slope failed):

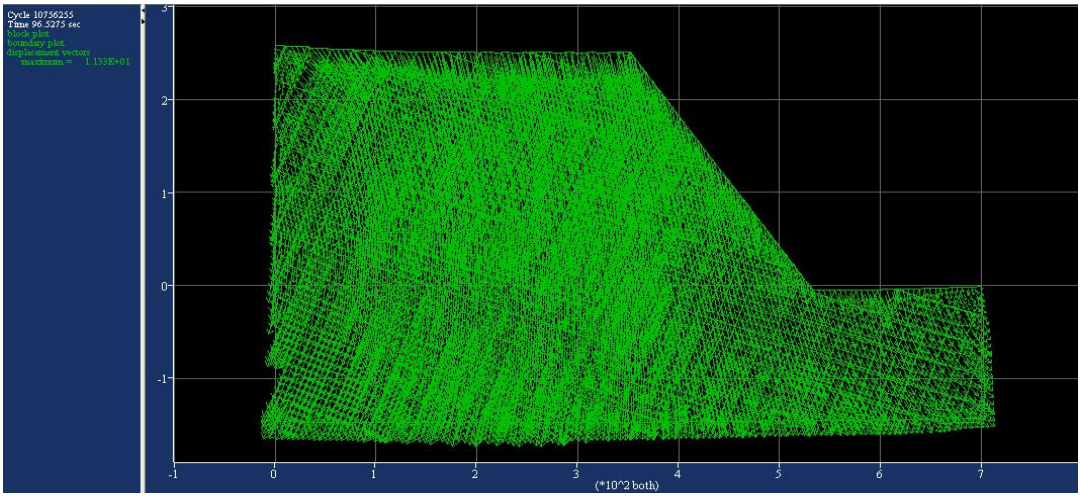

Fig. 4.46: Displacement plot at failure under seismic loading for two joint sets

Fig. 4.46 shows the displacement plot of the slope at failure under seismic loading. The maximum displacement has found out to be 11.33 m while the increase in displacement (Δd) from the previous case is 0.86 m.

Results: Table 4.7 shows the results in a tabular form.

Table 4.7: Results of seismic loading for two perpendicular joint sets

Time Duration (sec)	Max. Total Displacement (m)	Max. Shear Displacement (m)	Block Rotation (m)
Gravity Loading	2.289	0.8745	0.759
After 1 sec	3.322	1.656	1.393
After 3 sec	5.400	2.834	1.638
After 5 sec	7.925	4.449	1.840
After 7 sec	10.470	5.763	2.410
After 7.772 sec (Failed)	11.330	0.683	2.394

Observations and Discussions:

1) It can be seen from Table 4.7 that in the seismic case, the total and shear displacement has increased from the gravity loading.
2) It is observed that after 7.772 sec from the commencement of the seismic loading, the slope failed. This is because one block penetrates deeper into another block. From Table 4.7 we can also observe that at the point of failure, the shear displacement is very low. This situation demonstrates that due to high penetration between blocks, the shear displacement decreases.
3) From Table 4.7, we can also see that the block rotation increases with time up to 7 seconds. But at the time of failure, the block rotation has decreased from the previous case. This situation also says that as the block penetration occurs, the rotation of the blocks get reduced.
4) In comparison with the cases described in section 4.7.2 and 4.7.3, it has been observed that the slope fails earlier than the two cases. The reason behind that is as the slope becomes more fragmented due to two sets of joints, it becomes more prone to failure.

4.8 Concluding Remarks

1) A 260 m high rock slope with a face angle of 55° has been analysed under three types of loading conditions. In the static gravity analysis and the analysis under rainfall condition, the Mohr-Coulomb constitutive model has been idealised and in the dynamic analysis, elastic, isotropic model has been idealised for the material.
2) In the static gravity analysis, it has been observed that when the joint set dips in the out of the plane direction, a plane and sliding failure occurs. As the dip inclination of the joint set (ψ_p) gets stepper, the slope becomes more stable against sliding. When ψ_p dips into the plane, then sliding is not the failure pattern.
3) To simulate the rainfall effects, two cases have been considered. In one case the slope is having joint sets, dipping out of the plane while in the other case, the joints sets dip into the plane. It has been observed that the second case is more stable against sliding failure.
4) In the seismic analysis, sinusoidal shear stress wave has been applied into the model. Three case have been investigated. It has been observed that the block rotation

is more and the shear displacement is less in the case of slope having joint sets dipping into the plane in comparison to the case where joint sets dip out of the plane. Also where two perpendicular joint sets are present in the slope, the slope becomes more fragmented and it fails much earlier than other cases.

CHAPTER – 5

SUMMARY AND CONCLUSIONS

5.1 Summary

In this work, first the review of literature has been done for the methods available for the slope stability analysis. For the slope stability analyses, limit equilibrium method, finite element method and distinct element method have been discussed. Four case studies of distinct element method has also been discussed briefly. Also the newly emerging probabilistic method has been discussed briefly.

Two types of slopes have been analysed. Natural hill slopes and rock slopes. Under the category of natural hill slopes, two slopes of Uttarakhand state of India, Mussoorie slope and Nainital slope, have been analysed. The modelling and analysis of the slopes has been done by using Geostudio 2012 software products. The slopes have been modelled by using previously available field test data from the literature and with the help of shear wave velocity ranges. Two types of analysis has been done. In the limit equilibrium analysis, the slopes are analysed by using SLOPE/W software. Factor of safety values for both static and pseudostatic cases have been computed by applying different limit equilibrium methods. For the pseudostatic case, horizontal seismic coefficient of Sikkim earthquake (2011) is used. A comparative study between the different methods have also been done. In the finite element analysis, two finite element software, SIGMA/W and QUAKE/W are used for the static and dynamic analyses. For the dynamic analysis, time history data of Sikkim earthquake (2011) is incorporated into the model. Stress-deformation analysis is done in this case.

Analysis of rock slopes have also been performed. In this case, a jointed rock slope is analysed under different loading conditions and with different joint orientations and alignments. Three types of analyses are done. Firstly, in the static gravity analysis, four types of joint orientations are simulated. Secondly, under rainfall situation, two types of joint orientations are performed. Thirdly, under seismic environment, three types of joint alignments have been investigated. In this case, sinusoidal shear stress wave of Uttarkashi earthquake is incorporated at the base of the model. For the first

two cases, Mohr-Coulomb plasticity model is taken and the results are drawn in the form of factor of safety and shear displacement. For the last case, elastic, isotropic model is considered and results are drawn in the form of total displacement, shear displacement and block rotation. UDEC 4.0 software is used for the analyses of rock slope.

5.2 Conclusions

From the analyses, the following conclusions are drawn:

1. In the natural slopes, limit equilibrium and finite element analyses are done. In the limit equilibrium analyses, the static and pseudostatic factor of safety values have been obtained by different methods. It has been observed that the pseudostatic factor of safety value is less than the static ones, computed by all the methods. This observation shows that a slope becomes unstable under seismic loading. Also different methods have predicted different factor of safety values. The main difference between the methods are due to the consideration of interslice forces. Morgenstern-Price method gives the most appropriate factor of safety measurement since it takes both the interslice shear and normal forces into account and also satisfies both the moment and force equilibrium for determining factor of safety.
2. In the finite element analyses of the slopes, stress and deformation of the slopes has been obtained for both the static and dynamic cases. It has been observed that displacement increases in the dynamic cases whereas in the static case there were no displacement. But for both static and dynamic analyses, the displacement decreases with increase in depth. Also it has been observed that the stresses increase with depth for both the slopes. But the stresses is observed to be reduce a little in the dynamic case from the static case. This occurs because as the displacement of the slopes increases in both horizontal and vertical direction, the confinement of the slopes gets loosen up resulting in a small decrease in the stresses.
3. In the analyses of rock slopes, for the static gravity analyses, it has been observed that when the joint dips in the out of plane direction, it possesses sliding failure and the shear displacement is large while when joints dip into the face, shear displacement is very small and it undergoes rotational failure.

4) It has also been observed that slope becomes more stable when the dip of the joint gets stepper in the out of plane direction.

5) In the analyses under rainfall condition, it has been observed that the slope becomes prone to failure when the joint friction angle is reduced. Also it has been observed that when the joint set dip out of the plane it fails in sliding while for the out of the plane joints, toppling failure occurs.

6) In the seismic analyses, it has been observed that, for joints dipping into the plane, toppling failure occurs due to higher block rotation while for joints dipping out of the plane, sliding due to shear displacement occurs. When two joint sets are present in the slope, the slope becomes more fragmented and it fails much earlier than the other cases.

5.3 Recommendations for Future Work

It can be said that for the analysis of different types of slopes, different types of methods can be used. Limit equilibrium methods give a preliminary understanding about the behaviour of slopes. Finite element method can be applied for the analysis of almost all types of slopes while distinct element method can be used for highly fractured or jointed rock slopes. Effort should be given to see the suitability of application of these methods depending upon the types of slopes. In rock slope analysis, the failure pattern of different types of slopes should be investigated more. Different types of stabilisation techniques are available these days. The economic and practical feasibility of applying these methods should be checked. New methods in both deterministic (like material point method, extended finite element method etc.) and probabilistic approaches are also emerging. These methods are at the early stages. Feasibility of applying these methods should also be checked.

REFERENCES

1. APPC- Properties of soil (Appendix C), http://www.scribd.com/doc/196923062/APPC- Soil-Properties-pdf.

2. Bhasin, R., Kaynia, A. M., (2004), "Static and dynamic simulation of a 700-m high rock slope in western Norway", Journal of Engineering Geology 71, pp. 213-226.

3. Bishop, A. W., (1955), "The use of slip circle in the stability analysis of slopes" Geotechnique, Vol., 5, pp. 7-17.

4. Borcherdt, R. D., (1994), "Estimation of Site-Dependent Response Spectra for Design", (methodology and justification) earthquake spectrum 10, pp. 617-653.

5. Bray, J. D., Travasarou, T., (2007), "Simplified procedure for estimating earthquake-induced deviatoric slope displacements", J Geotech Geoenviron Eng ASCE 133(4):381–392.

6. Bray et al., (1998), "Simplified seismic design procedure for lined solid-waste landfills", Geosyn Int. 5(1–2):203–235.

7. Cundall, P. A., (1971), "A Computer Model for Simulating Progressive Large Scale Movements in Blocky Rock Systems", in Proceedings of the Symposium of the International Society of Rock Mechanics (Nancy, France, 1971), Vol., 1, Paper No. II-8.

8. Cundall, P. A., (1980), "UDEC-A Generalised Distinct Element Programme for Modelling Jointed Rock", Peter Cundall Associates, Report PCAR-1-80; European Research Office, U.S. Army, Contract DAJA37-79-C-0548.

9. Cundal, P.A., O. D. L. Strack., (1979), "A Discrete Numerical Model for Granular Assemblies", Geotechnique, Vol., 29, pp. 47-65.

10. Duncan, C. W., Mah, C. W., (2004), "Rock Slope Engineering", Spoon Press, pp. 129-213.

11. Felleinus, W., (1936), "Calculation of Stability of Earth Dams", in Proceedings of the Second Congress of Large Dams, Vol., 4, pp. 445-463.

12. Fredlund, D. G., Krahn, J., (1977), "Comparison of Slope Stability Methods of Analysis", Canadian Geotechnical Journal, Vol., 14, No. 3, pp. 429-439.

13. Geol615,https://www.academia.edu/4986952/Some_Useful_Numbers_on_the_Engineering_Properties_of_Materials_Geologic_and_Otherwise_GEOL_615.

14. Geo-slope International Ltd. (2012), "Stability Modelling with SLOPE/W", 2012 edition.

15. Hammah, R. E., et al., (2007), "Analysis of blocky rock slopes with finite element shear strength reduction analysis", in Proceedings of the 1st Canada-US Rock Mechanics Symposium, pp. 329-334.

16. Hunter, J. A., Motezedian, D., "Shear wave velocity measurements for soft soil earthquake response evaluation in the eastern Ottawa region, Ontario, Canada", in Proceedings of the 19th EEGS Symposium on the Application of Geophysics to Engineering and Environmental Problems. 2006.

17. Itasca Consulting Group, Inc. (1996), "UDEC Theory and Background", Version 4.0.

18. Janbu, N., (1954), "Applications of Composite Slip Surfaces for Stability Analysis", in Proceedings of the European Conference on the Stability of Earth Slopes, Stockholm, Vol., 3, pp. 39-43.

19. Jibson, R. W., (2007), "Regression Models for Estimating Coseismic Landslide Displacement", Journal of Engineering Geology, Vol., 91, pp. 209-218.

20. Kainthola et al., (2012), "Distinct Element Modelling of Mahabaleshwar Road Cut Hill Slope", Geomaterials, Vol., 2, No. 4, pp. 105-113.

21. Kaynia et al. (2011), "Real-time mapping of earthquake-induced landslides", Bull Earthquake Eng, Vol., 9, pp. 955–973.

22. Kramer, S. L., (2009), "Geotechnical Earthquake Engineering", Prentice-Hall, pp. 423-462.

23. Lemos et al., (1985), "A Generalized Distinct Element Programme for Modelling Jointed Rock Mass (A Keynote Lecture)", in Proceedings of the International Symposium on Fundamentals of Rock Joints (Bjorkliden, September 1985)", pp. 335-343.

24. Morgenstern, N. R., Price, V. E., (1965), "The Analysis of the Stability of General Slip Surfaces", Geotechnique, Vol., 15, pp. 79-93.

25. Noorzad, A., et al., (2008), "Seismic Slope Stability Analysis of Jointed Rock Masses on the Northern Abutment of Gotvand Dam, Iran", in Proceedings of the 14th World Conference on Earthquake Engineering (14WCEE), Bejing, China.

26. Pal et al., (2012), "Earthquake Stability Analysis of Rock Slopes: A Case Study", Journal of Rock Mech Rock Engg, Vol. 45, pp. 205-215.

27. Rathje, E. M., Saygili, G., (2009), "Probabilistic assessment of earthquake-induced sliding displacements of natural slopes", Bull New Zealand Soc Earthq Eng, Vol. 42, No.1, pp. 18–27.

28. Saygili, G., Rathje, E. M., (2008), "Empirical predictive models for earthquake-induced sliding displacements of slopes", J Geotech Geoenviron Eng ASCE, Vol. 134, No. 6, pp. 790–803.

29. Singh, A., (2014), "Seismic Slope Stability Analysis for Earthquake Induced Landslides (master's thesis)", Indian Institute of Technology Roorkee, Roorkee, India.

30. Sorkhabi, R., (2012), "GeoEducation: Know Your Faults, Part I", GeoExpro, Vol. 9, No. 5, pp. 64-68.

31. Spencer, E. (1967), "A Method of Analysis of Embankments Assuming Parallel Inter-slice Forces", Geotechnique, Vol., 17, No. 1, pp. 11-26.

32. Walton et al., (1988), "Particle-Dynamics Calcultions of Gravity Flows of Inelastic, Frictional Spheres", in Micromechanics of Granular Material, pp. 153-161.

33. Watson-Lamprey, J., Abrahamson, N., (2006), "Selection of ground motion time series and limits on scaling", Soil Dyn Earthq Eng, Vol. 26, No. 5, pp. 477–482.